Fall 2009

A multidimensional Eulerian-Lagrangian model to predict organism distribution

Yushi Wang
University of Iowa

A MULTIDIMENSIONAL EULERIAN-LAGRANGIAN MODEL TO PREDICT ORGANISM DISTRIBUTION

by

Yushi Wang

A thesis submitted in partial fulfillment
of the requirements for the Master of
Science degree in Civil and Environmental Engineering
in the Graduate College of
The University of Iowa

December 2009

Thesis Supervisors: Adjunct Assistant Professor Marcela Politano
Professor Larry J. Weber

Graduate College
The University of Iowa
Iowa City, Iowa

CERTIFICATE OF APPROVAL

_____

MASTER'S THESIS

_____

This is to certify that the Master's thesis of

Yushi Wang

has been approved by the Examining Committee
for the thesis requirement for the Master of Science degree
in Civil and Environmental Engineering at the December 2009 graduation.

Thesis Committee: _____
Marcela S. Politano, Thesis Co-supervisor

_____
Larry J. Weber, Thesis Co-supervisor

_____
Jacob Odgaard

ACKNOWLEDGMENTS

The author wishes to thank several individuals who made the completion of this research possible. First and foremost, I would like to thank my advisor Dr. Larry Weber and co-advisor Dr. Marcela Politano. I would not be where I am today without their assistance and support. Thanks, moreover, are due to Dr. Politano for her kindness, patience and guidance in my research and thesis.

Secondly I would like to thank Dr. Jacob Odgaard and my thesis committee. I greatly appreciate all of the committee's constrictive criticism and comments.

I would also like to thank the IIHR - Hydroscience & Engineering faculty, staff, and students for the special assistance which they have provided towards the completion of my research. The support provided by IIHR - Hydroscience & Engineering staff Brian Miller and Dan Daly is appreciatively acknowledged.

A special thank is due to my parents and family for always believing in me and encouraging my research and study. I also want to thank my girlfriend Yue; she has been there to motivate and support me through the entire process.

Lastly, I would like to thank Dr. Pablo Carrica for his assistance in the completion of my thesis.

TABLE OF CONTENTS

LIST OF TABLES

LIST OF FIGURES

CHAPTER I

INTRODUCTION

1.1 Motivation

The Columbia River basin is one of the most productive hydropower sources in the United States. Dams constructed since 1900 in the Columbia River basin provide power to homes and industry, control floodwaters, and irrigate farmlands. More than 400 hydraulic structures of varied size have been built on the mainstem Columbia River, Snake River and their tributaries to enhance navigation, irrigation, and produce hydroelectric power. The generating capacity of the Columbia basin is estimated at 2.1 million kilowatts. On the other hand, the dams also have negative impacts on the environment and contribute to the decline of fish, snail and freshwater mussel populations in this area. Studies show native aquatic species may be harmed through habitat changes in velocity, surface elevation, hydraulic strain, water temperature, or other conditions modified by hydraulic structures. Dams change discharge, flowrate, pool elevation, channel morphology, and block spatial connections in rivers. Aquatic life significantly declines, especially during migration and reproduction intervals, due to the loss of natural habitat. U.S. Fish and Wildlife Service (USFWS) list more than 10 aquatic organisms in the Mid-Snake River as endangered or threatened. Federal and State governments have long noted changes in river conditions due to dams and they are trying to find solutions for these problems.

Regulations and laws have been proposed to restrict the construction and operation of hydraulic structures. Dam owners must meet ecological standards to be licensed by the Federal Energy Regulatory Commission (FERC) subject to periodic renewal. Under the Federal Columbia River Power System (FCRPS) Biological Option, 96 percent of the juvenile fish that migrate through dams in the spring and 93 percent of the summer migrants on the Snake River must survive. Besides passing through dams,

aquatic organisms are also protected in the process of migration through the reservoirs and river reach. In 1980, Congress passed the Northwest Power Planning and Conservation (NPCC) Act to develop a program in protecting, mitigating, and enhancing fish and wildlife resources that have been adversely affected by the construction and operation of regional hydroelectric projects in the Columbia Basin. The Columbia Basin Fish and Wildlife program, as it is called, focuses on anadromous fish, emphasizing a comprehensive system-wide approach to rebuild fish and wildlife resources in the Columbia River basin.

1.2 Idaho Power and Bliss Dam

Bliss dam is a concrete, gravity-type hydroelectric dam. Construction began in 1948 and was completed in 1950 near Bliss, Idaho. It is located at River Mile (RM) 560.3 on the Snake River. The dam is composed of a power house with three generators and boosts a total nameplate generating capacity of 80,000 kilowatts. An aerial view of Bliss Dam is shown in Figure 1-1.

Bliss Dam is part of the Mid-Snake Projects, along with the Upper Salmon Falls, Lower Salmon Falls, and 14 other hydropower projects that Idaho Power Company (IPC) owns and operates on the Snake River and its tributaries. The Mid-Snake Projects have a nameplate capacity of 169.5 MW. When customer demand for electricity, or load, is high, Bliss dam is operated in a limited, load-following capacity. Other times Idaho Power operates the dam as a run-of-river facility. This means the volume of water coming in equals the volume of water leaving the dam in a given 24 hour period. Variations in discharge, velocity, and water surface elevation due to the dam operation have a potential to impact the downstream environment and aquatic organisms.

Several hydroelectric projects along the Snake River have been involved in re-licensing since 1990. The FERC has granted new licenses to Idaho Power to continue operating the Mid-Snake Project while protect the endangered species on the Snake

River. In such circumstances, IPC is required to give equal consideration to power development and environmental protection. They must study project operation effects on federally listed threatened and endangered snail species near the hydraulic structures and submit a protection plan to the commission. The license also calls for protection of fish species, such as the White Sturgeon, which the State of Idaho classifies as a species of special concern, on the Snake River.

According to the officials, the federal plan to protect and recover endangered fish will ensure the viability of the listed species through an array of protection measures, including:

- Installation of multi-million dollars, fish slides at dams to improve fish passage and survival
- Targeting fish and wildlife funds for habitat improvements
- Reforming hatcheries to boost natural spawning runs in key areas

To achieve these goals, Idaho Power has funded scientific field and laboratory research to discern relationships between hydraulic and environmental conditions and aquatic species habitats. This effort aims at the development of a numerical tool to evaluate the river hydraulic impacts on snail and fish egg movements. The results of this study will help to locate and improve the snail habitats and fish hatcheries and determine the best means to mitigate potential negative dam operating impacts to these areas.

Most fish prefer to stay in pools during the day. Sturgeons particularly like deep pools. The White Sturgeon habitat below Bliss Dam to the C.J Strike river section is the largest and deepest pool directly below the rapids in the Mid-Snake River reach. It is estimated that 50 percent of the high quality, constant, clean, and cool (59^{o}F) spring flow along the Snake River at the Milner Dam and Bliss Reservoir is utilized for fish production (Idaho Water Plan, 1996). The reach also covers the U.S. Fish and Wildlife Service's Recovery Plan for threatened snail species at Mid-Snake River. This recovery plan is keyed to improving water quality, maintaining or increasing spring flows in river

reach, and establishing minimum flows to improve habitat for all riverine species. Due to the importance of this area, this thesis focuses on a two mile reach of the downstream Mid-Snake River, just below the Bliss Dam, which is a crucial habitat for Bliss Rapids snails and spawning White Sturgeon. This location is shown in Figure 1-2.

1.3 Bliss Rapids Snail and White Sturgeon in the Snake River

Fish and snail populations are extremely dependent upon the characteristics of their aquatic habitat. The transformation of Snake River from a free-flowing, cold water, riverine habitat into an impounded, slower, and warmer water habitat has been shown to be the leading cause of aquatic species declines. The White Sturgeon and Bliss Rapids Snail populations have declined significantly due to the construction of hydraulic structures. USFWS defines the overall recovery area for these species as extending from the C.J. Strike Reservoir (RM 518) upstream to American Falls Dam (RM 714) (USFWS, 1995).

1.3.1 Bliss Rapids Snails

The Bliss Rapids snail (Taylorconcha serpenticola) is one of five snail species endemic to the Mid-Snake River and that was listed as threatened under the Endangered Species Act (57 FR 59244) by USFWS in 1992. The Bliss Rapids snail has a very small turbinate shell. The average base width of this shell is about 0.056 in (1.42 mm) and the height is about 0.071 in (1.81 mm). Their average weight is about 2.52 mg (Figure 1-3). The average lifespan of the Bliss Rapids snail is about one year. Base on live collections, the species currently exists as discontinuous population within its historic range (Taylor, 1982). This is shown in Figure 1-4, as the area between point A and B. It is believed to be one of the few snails to survive prehistoric Lake Idaho, which existed about 3.5 million years ago. The species are currently impacted by continued adverse habitat modification

from hydroelectric development and peak-loading effects of existing hydroelectric project operations on the Snake River.

Studies show that aquatic organisms residing in shallow habitats may be impacted by frequent water stage fluctuations due to dam operations. Bliss Rapids snails are found at various depths in the Snake River, including shallows subject to frequent stage fluctuation (Clark et al., 2007). Several studies have addressed this issue to comply with Information Need IB in the settlement offer "River Stage Height and Snail Distribution" (Idaho Power Company and U.S Fish and Wildlife Service, 2004). An accurate numerical model of snail distribution as a function of water stage fluctuations is needed to complement the research plan.

1.3.2 White Sturgeon Eggs

White Sturgeon (Acipenser Transmontanus), an endangered fish in the Columbia River and Mid-Snake River, is important for recreation and commerce. It is the largest fresh water fish in North America and can reach a weight of 1795.2 lbs (816 kg) and a length of 20 ft (6.1 m) (Figure 1-5). The White Sturgeon historically migrated between estuaries along the pacific coast and the large inland river systems. From north to south, these include the Fraser, Columbia, San Joaquin, and Sacramento Rivers. The longest of these is the Columbia River, which drains about 100,360 mi^2 (260,000 km^2). Its largest tributary, the Snake River, runs from Wyoming, through Idaho to join the Columbia River in the state of Washington (Jager et al., 2000).

White Sturgeon produce one hundred thousand to four million eggs when they spawn once every eight years. The eggs have a spherical shape and average around 0.138 in (3.5 mm) in diameter (figure 1-6). Many studies have focused on White Sturgeon populations decline due to obstacles to their upstream migration by dams on the Columbia basin. Problems for downstream migration of fish and the fate of fish eggs over the river reach after spawning have not been as well studied or fully considered.

Downstream migration problems may cause a major factor affecting anadromous or catadromous fish stocks.

Fish eggs depend upon certain flow conditions for their safety and migration. Streamflow velocities equal to or greater than 3.28 ft/s (1.0 m/s) are thought to greatly reduce or eliminate predation on white sturgeon eggs (Barton et al., 2006). The appropriate water temperatures during spawning periods range from 50-59^{o}F (11-15^{o}C) (Paragamian et al., 2001). Snake River reach below Hells Canyon and Bliss dams are reported as ideal hatcheries by these criteria. A sizable population and evidence of recent reproduction behaviors have been found in these areas (Cochnauer et al., 1985). Further research to determine the fish egg distributions over the river reach is important for the protection of the fish eggs and juveniles.

1.4 Objectives

The four main objectives of this study are:

- To develop a three-dimensional (3D) Computational Fluid Dynamic (CFD) model to predict hydrodynamics and White Sturgeon egg and Bliss Rapids snail distributions in the Mid-Snake River.
- To model, implement, and simulate interactions between the river bed and White Sturgeon eggs and Bliss Rapids snails.
- To determine the effects of various turbulence models on White Sturgeon egg and Bliss Rapids snail distributions.
- To explore various operational conditions effects on the White Sturgeon egg and Bliss Rapids snail distributions.

1.5 Thesis Overview

Chapter II provides a literature review of numerical modeling projects relevant to this study.

Chapter III outlines mathematical and computational methodologies for the numerical model.

Chapter IV introduces the grid generation. Simulation conditions are explained in detail.

Chapter V discusses results of the CFD numerical model simulations.

Chapter VI provides a summary, draws conclusions, and makes recommendations for future work.

Figure 1-1 Bliss Dam Aerial View.

Source: Google Earth

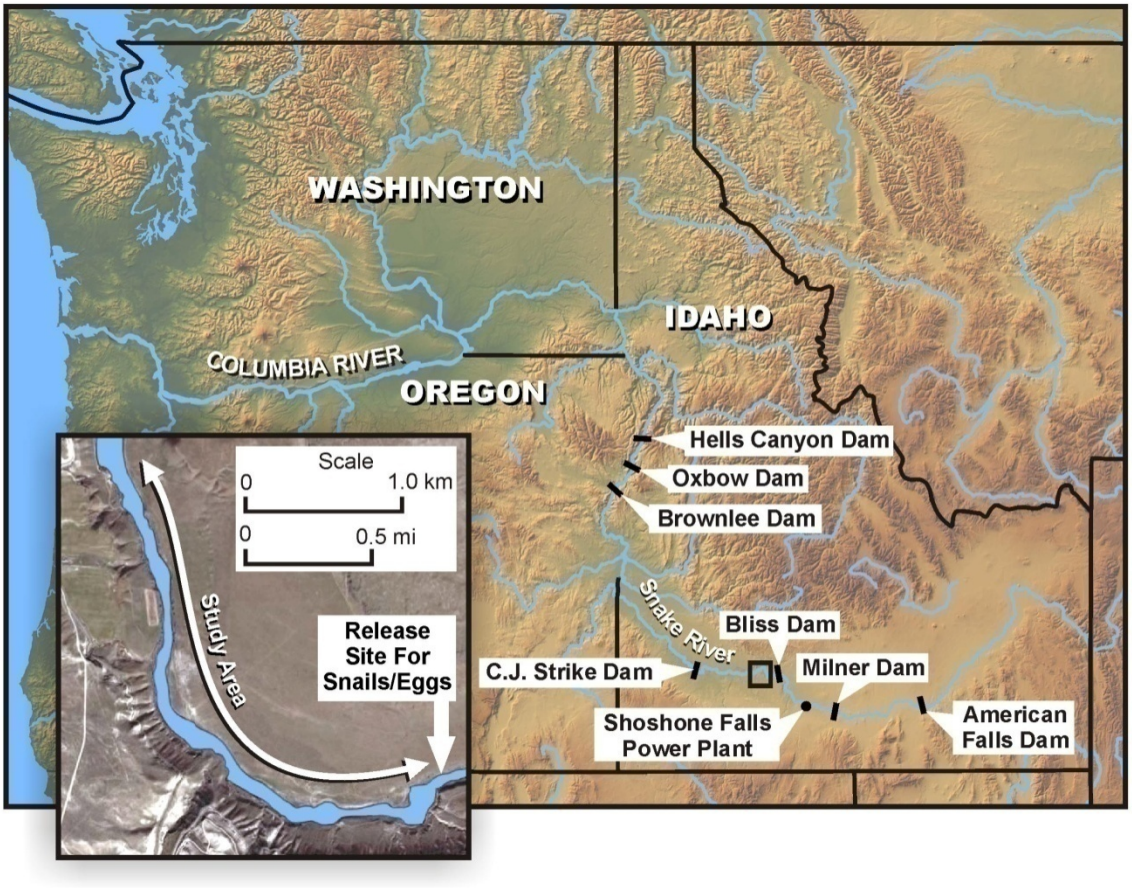

Figure 1-2 Study Area.

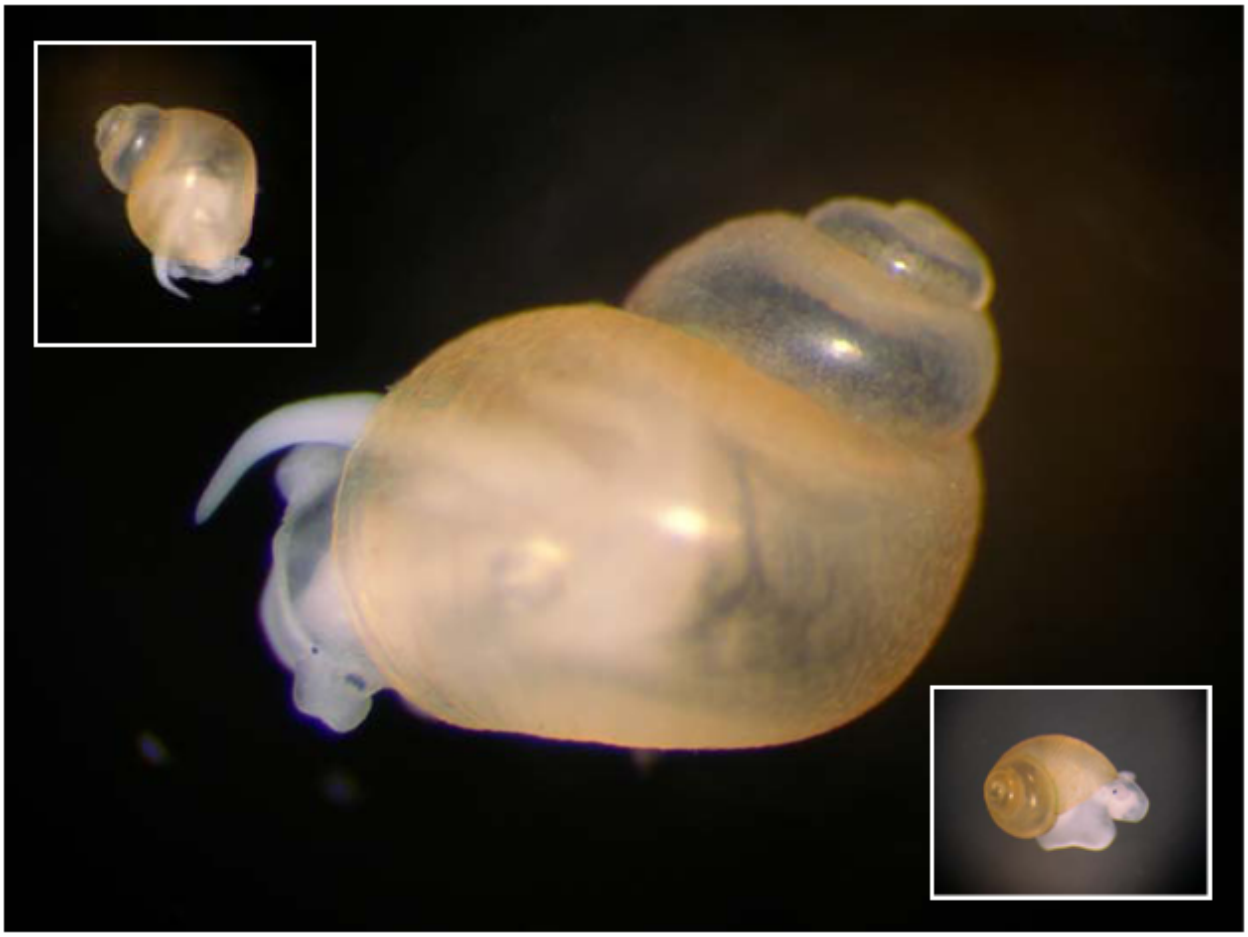

Figure 1-3 Bliss Rapids Snails.

Source: USFWS

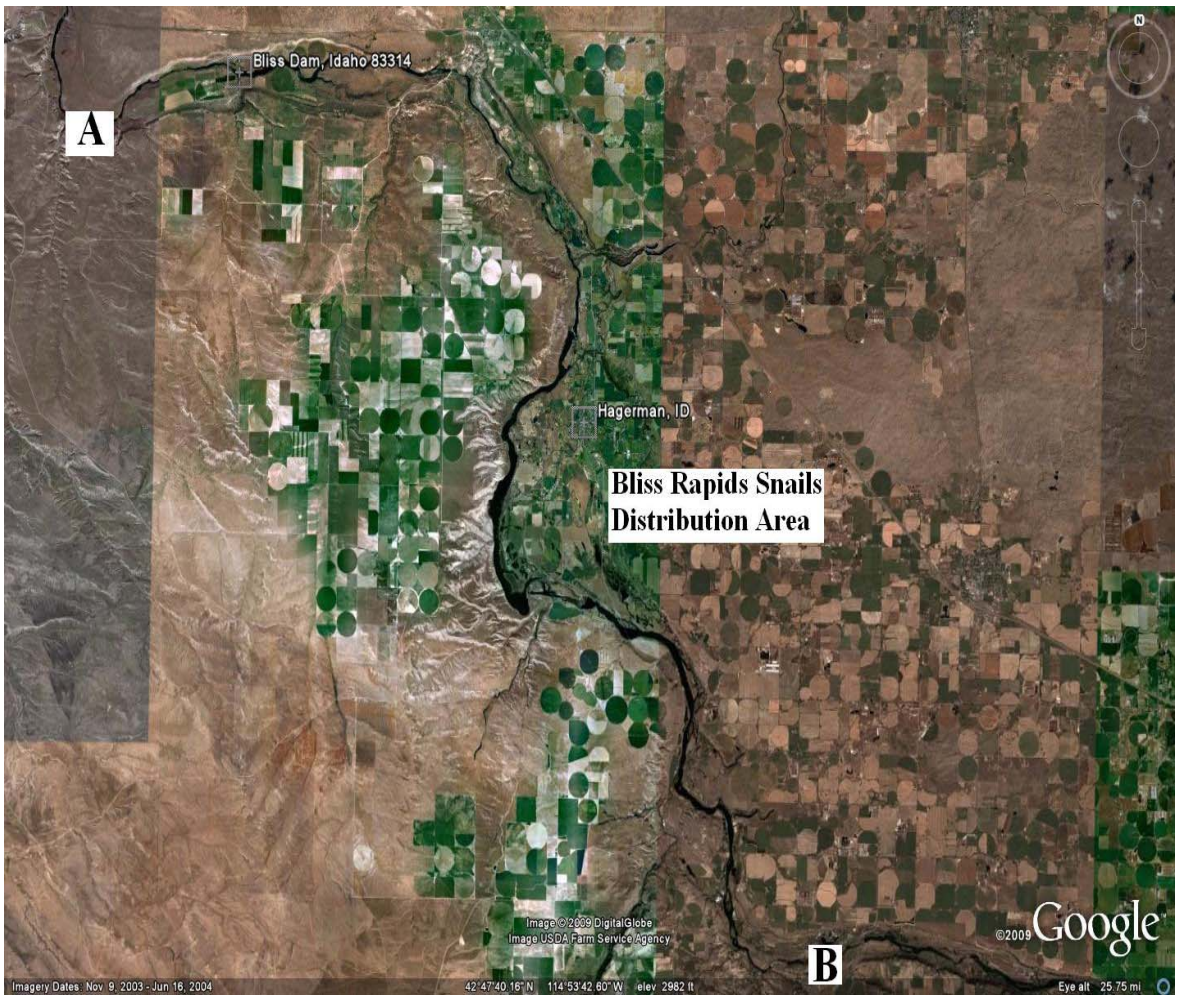

Figure 1-4 Bliss Rapids Snails Distribution Area.

Source: Google Earth

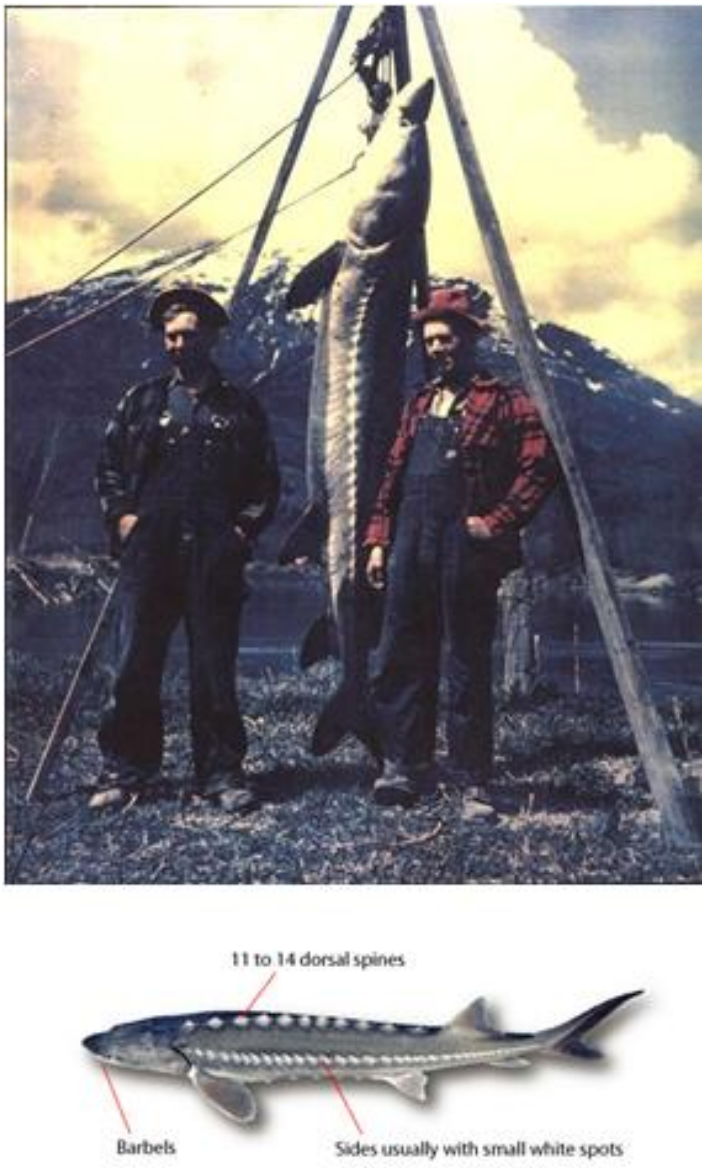

Figure 1-5 White Sturgeon.

Source: B.C. Government Home
http://www.env.gov.bc.ca/fw/fish/sport_fish/images/WhiteSturgeon_desc.jpg

Figure 1-6 White Sturgeon Eggs.

Source: USBR
http://www.usbr.gov/pmts/tech_services/tracy_research/photos/sturgeon/SturgeonFigure2.jpg

CHAPTER II

LITERATURE REVIEW

The prediction of flow patterns within a river reach is of significant interest to researchers and engineers. Studies validating CFD models demonstrate that numerical models can resolve most flow features observed in the field or laboratory. This literature review focuses on flow simulations in natural river geometries which relate to this thesis.

2.1 Three-Dimensional CFD Models

Anderson (2009) tells us "Computational fluid dynamics is the art of replacing the governing partial differential equations of fluid flow with numbers, and advancing these numbers in space and/or time to obtain a final numerical description of the complete flow fluid of interest". Modern computational fluid dynamics evolved from the advent of digital computers in the early 1950's through the efforts of engineers and mathematicians are utilized to solve momentum, heat, and mass transfer problems. One of the important applications of modern CFD is numerical river flow simulation.

According to Ingham (2005), numerical simulation is playing an increasingly important role in research and engineering applications compared to more traditional methods of field and laboratory measurement. Natural river flow structures are inherently complex due to the effects of irregular bank and bed topographies. Presently, appropriate representation of the complex river flow condition in the CFD model is the major issue of river flow modeling, which raises issues in grid resolution, grid dependence, representation of wall roughness, appropriate turbulence model, and other areas. CFD simulation may shed considerable light on flow structures with the appropriate numerical model and well chosen boundary conditions.

The most common approach to model turbulent river flows is to solve Reynolds-Averaged Navier-Stoke (RANS) equations incorporating a turbulence model. Simulations

based on standard RANS models using the rigid-lid method are widely applied to simulate river flows.

Wright et al. (2004) investigated on the capability of commercial CFD packages to correctly predict complex phenomena in open channel flow. They compared predicted hydraulic parameters for five different turbulence models with high quality flume measurements obtained for a trapezoidal channel. The results reveal distinct differences in secondary flow characteristics, though bulk flow features for all models are nearly identical. The accuracy of the predictions increases with the level of complexity of the turbulence model used.

Modenesi et al. (2004) presented a new 3D river simulation model that required less time and performed better. They represent the river with half channel of uniform elliptical cross section. The Navier-Stoker equations were derived for the elliptical system. Their results show good agreement with experimental data obtained from REPLAN (PETROBRAS refining unit) on the Atibaia River in São Paulo, Brazil.

Booker et al. (2004) used a 3D hydraulic-bioenergetic model to predict physical habitat quality for drift feeding juvenile salmonids in a 50m reach of Bere Stream, Dorset, UK. They assume that feeding fish prefer areas of high energy gain, moving to areas of lower velocity when resting. Their simulation employed a 3D CFD model and resulting hydrodynamics were combined with a bioenergetic model. Navier-Stoke equations with two k-epsilon turbulence closure equations utilized in the model enabled more realistic calculations of the foraging areas of fish. Their simulation results support the hypothesis of this paper.

Beyond the standard two-equation k-epsilon model, a higher level turbulent model Reynolds Stress Model (RSM), originally proposed by Launder (1975), is also widely utilized in simulating secondary currents. Kang and Choi (2005) preformed a numerical study of compound open channel flows with vegetation using the RSM. Their

simulation results were compared with measurements and a successfully simulated mean flow and turbulence structure was obtained in good agreement with experimental data.

CFD models have also been developed to simulate the hydrodynamics around hydraulic structures to aid in the design of fish passage alternatives. Turan et al. (2007) conducted a 3D numerical study to model the flow entrainment phenomena downstream of spillways. The RSM with an additional model to account for normal velocity fluctuation attenuations at the free surface was applied to ensure anisotropic closure for the two-phase mixture RANS equations with zero normal fluctuation at the free surface. The model was validated with experimental results from previous studies.

2.2 Lagrange Particle Tracking

Two phase flow phenomena has been extensively investigated and long been recognized as important to varied industrial and engineering applications. Two main methods are currently dominating two phase flows models, the Euler-Euler approach and the Euler-Lagrange approach.

In the Euler-Euler approach, both phases are treated within the Eulerian framework. A volume fraction for each phase is defined so the volume of one phase cannot be occupied by the other phase. These volume fractions are assumed to be continuous functions spatially and temporally with a sum equal to one. Averaged equations for conservation of mass, momentum, and energy for each phase, and a set of equations for the transfer of mass, momentum, and energy between phases, are solved.

CFD simulations based on the Euler-Euler approach have been applied to various fields of research, especially in nuclear engineering and the chemical industry. A complete review of the state-of-the-art for Eulerian two-phase flow modeling at the time is found in Jakobsen et al. (2005).

In contract to the successful applications in nuclear and chemical engineering, the Euler-Euler approach is not commonly used in hydraulic applications. Recent work by

Groll and Tropea (2005) presented a 2D, two-phase Euler-Euler model of a channel with backward-facing step geometry. They emphasized simulating turbulent diffusion, particle/fluid drag interaction, and particle collisions. Their simulation result was compared with experimental data and obtained good agreement.

Bakhtyar et al. (2009) developed a numerical Euler-Euler coupled two phase flow model to simulate fluid-sediment oscillatory sheet flow, advancing our mechanistic understanding of sediment transport under sheet flow conditions. RANS equations with a standard k-epsilon model were utilized to simulated turbulence. Resulting concentrations and sediment flux profiles were validated against experimental data.

The Euler-Lagrange approach is frequently used when the dispersed second phase occupies only a low volume fraction. In this method, the fluid phase is calculated as a continuum by solving the time-averaged Navier-Stokes equations. The dispersed phase is solved by applying external forces on the particle and tracking it through the calculated flow field. Particle trajectories are calculated individually during the fluid phase calculation.

Compared with Euler-Euler, the Euler-Lagrange approach is much more computationally efficient for calculating relatively small amount of particle loads. Only forces exerted on particles are solved. Complicated interfacial force terms between the continuity and discrete phases are ignored. This character makes Euler-Lagrange approach appropriate for a wide range of industrial and engineering applications.

Suzzi et al. (2009) presented a 3D numerical pharmaceutical bubble column reactor model to validate and evaluate the performance of Euler-Euler and Euler-Lagrange simulation approaches. The RANS transport equations were solved with the standard k-epsilon turbulent model to predict bubble column flow. The study reveals that the accuracy of simulation results by Euler-Lagrange approach is impacted by the near wall treatment. Simulation results by Euler-Euler approach are demonstrated to be more dependent on the turbulence model used.

Lagrangian CFD models were also used to study aquatic species migrations and inhabitations. Results were used to locate habitats and help protect aquatic species movements through hydraulic structures. Goodwin et al. (2006) developed a 3D Lagrangian model to predict juvenile salmon downstream migration as well as their response to different bypass structures and operational conditions. The model utilized simulated hydrodynamic data to model fish movements within the flow field. Model results were used to help in the design of fish bypass in dams. The model predicted fish passage survival rate were validated with field data.

Daraio et al. (2004) developed their numerical Mussel Dynamic Model to simulate mussel population dynamics in response to alternative management strategies for exotic and native mussel species in Upper Mississippi River. A 3D hydrodynamic model was coupled with an individual-based population dynamic model for various simulation conditions. Good agreement was obtained between the model and observations made in previous studies.

2.3 Particle-Boundary Interactions

Particle interactions with walls are critical to the prediction of the settling and accumulation locations of fish eggs and snails. The simplest boundary condition is a trap condition, which assumes a particle loses all momentum upon contact with the boundary layer. The trajectory calculations are terminated and the particle is reported as trapped once it encounters a wall. German and Kant (1998) performed a numerical study for particle movement and settlement in a storm water detention pond using the trap condition as a boundary. Their simulation results were compared with experimental data. An over-predicted deposition rate was obtained using this boundary condition.

A better result is possible using Bed Shear Stress (BSS) to determine particle fates after hitting walls. BSS is frequently used to estimate particle transport and deposit in hydraulic and mechanical engineering applications. Stovin and Saul (2000), Adamsson et

al (2003), and Dufresne et al (2008) have employed BSS to analyze sediment deposition in 3D sewer detention tanks. They assumed that when BSS was below a critical value, particles reaching the bottom will settle. Particles are reflected back into the flow if the local shear stress is above the critical value. Simulation results compared with experimental data obtained a similar sediment deposition pattern. Further comparisons between trap and BSS boundary conditions show that BSS better captures sediment distribution patterns than does trap condition.

2.4 Summary

CFD studies related to river flow simulation, particle tracking, and bed shear stress applications have been discussed. Past successful applications demonstrate the capabilities of current models and provide a theoretical basis for this thesis.

CHAPTER III

COMPUTATIONAL METHODOLOGY

In this chapter, numerical models and governing equations employed in this study are described.

3.1 Numerical Model

Numerical simulations of the river hydrodynamics and distributions of fish eggs and snails were performed by solving an Eulerian-Lagrangian model. The commercial CFD code Fluent, based on a control-volume finite element method, was employed in this study. Fluent is a general purpose CFD code with broad applications for a wide array of industrial and research functions.

3.1.1 Continuous Phase

The liquid phase hydrodynamics are solved with the standard Reynolds-averaged Navier-Stokes (RANS) equations. An additional turbulence model is incorporated to solve the turbulent field. The RANS equations of motion for an incompressible Newtonian fluid are

$$\frac{\partial(\rho\bar{u}_i)}{\partial x_i} = 0 \tag{1}$$

$$\frac{\partial(\rho\bar{u}_i)}{\partial t} + \frac{\partial(\rho\bar{u}_i\bar{u}_j)}{\partial x_j} = -\frac{\partial\bar{p}}{\partial x_i} + \frac{\partial}{\partial x_i}\left(\mu\frac{\partial\bar{u}_i}{\partial x_j} - \rho\overline{u'_i u'_j}\right) \tag{2}$$

where $\bar{u}_i$ and $\bar{u}_j$ are components of mean (time-averaged) velocities, u'_i and u'_j are fluctuating velocity components, $\bar{p}$ is mean pressure, ρ is fluid density, and μ is viscosity.

Turbulence modeling is crucial to appropriately model the Reynolds stresses term, $\rho\overline{u'_i u'_j}$. Based on the Boussinesq assumption, Reynolds stresses are related to mean velocity gradients by

$$-\rho\overline{u'_i u'_j} = \mu_t\left(\frac{\partial \bar{u}_i}{\partial x_j} + \frac{\partial \bar{u}_j}{\partial x_i}\right) - \frac{2}{3}\rho k\delta_{ij} \quad (3)$$

Turbulent viscosity, or eddy viscosity, μ_t is modeled as

$$\mu_t = \rho C_\mu \frac{k^2}{\varepsilon}. \quad (4)$$

For this study, performance of two turbulence models to solve flow fields and particle distributions were studied.

One turbulence model applied the standard two equations, k-epsilon method. Turbulent kinetic energy k, and turbulent dissipation ε, were solved with two transport equations to represent the turbulent flow properties. The transport equation for turbulent kinetic energy k is represented by

$$\frac{\partial}{\partial t}(\rho k) + \frac{\partial}{\partial x_i}(\rho k u_i) = \frac{\partial}{\partial x_j}\left[\left(\mu + \frac{\mu_t}{\sigma_k}\right)\frac{\partial k}{\partial x_j}\right] + P_k - \rho\varepsilon \quad (5)$$

Dissipation ε is given by

$$\frac{\partial}{\partial t}(\rho \varepsilon) + \frac{\partial}{\partial x_i}(\rho \varepsilon u_i) = \frac{\partial}{\partial x_j}\left[\left(\mu + \frac{\mu_t}{\sigma_\varepsilon}\right)\frac{\partial \varepsilon}{\partial x_j}\right] + C_{1\varepsilon}\frac{\varepsilon}{k}P_k - C_{2\varepsilon}\rho\frac{\varepsilon^2}{k} \quad (6)$$

In these equations, P_k represents turbulence kinetic energy generation due to mean velocity gradients, calculated by

$$P_k = -\rho\rho\overline{u'_i u'_j}\frac{\partial u_j}{\partial x_i} \quad (7)$$

σ_k and σ_ε are turbulent Prandtl numbers for k and ε, respectively.

For this study, default k-epsilon model coefficients $C_{1\varepsilon} = 1.44, C_{2\varepsilon} = 1.92, C_\mu = 0.09, \sigma_k = 1.0, \sigma_\varepsilon = 1.3$ were used.

The other turbulence model used to obtain closure of the Reynolds-averaged momentum equation is the Reynolds Stress Model (RSM). Individual Reynolds stresses, $\rho\overline{u'_i u'_j}$, are calculated using differential transport equations

$$\frac{\partial}{\partial t}\left(\rho\overline{u'_i u'_j}\right)+\frac{\partial}{\partial x_k}\left(\rho u_k\overline{u'_i u'_j}\right)$$

$$=\frac{\partial}{\partial x_k}\left[\left(\mu+\frac{\mu_t}{\sigma_k}\right)\frac{\partial\overline{u'_i u'_j}}{\partial x_k}\right]-\rho\left(\overline{u'_i u'_k}\frac{\partial u_j}{\partial x_k}+\overline{u'_j u'_k}\frac{\partial u_i}{\partial x_k}\right)+\phi_{ij}-\rho\varepsilon_{ij} \tag{8}$$

In the above equation, ϕ_{ij} represents the pressure strain, which can be written as

$$\phi_{ij}=\overline{p\left(\frac{\partial u'_i}{\partial x_j}+\frac{\partial u'_j}{\partial x_i}\right)} \tag{9}$$

Turbulent flows are significantly affected by the presence of walls. Special treatment is required to solve the flow fields near a wall boundary. For this study, the standard wall functions first proposed by Launder and Spalding were used. The velocity profile was estimated with the log law

$$u^*=\frac{1}{\kappa}\ln(Ey^*) \tag{10}$$

and is valid for $30<y^*<300$, where

$$u^*\equiv\frac{u_p c_\mu^{1/4}k_p^{1/2}}{\tau_w/\rho} \tag{11}$$

$$y^*=\frac{\rho c_\mu^{1/4}k_p^{1/2}y_p}{\mu} \tag{12}$$

κ is the Von Kármán constant, E=9.793 is an empirical constant, u_p is mean fluid velocity and k_p, the turbulence kinetic energy for grid point p at wall-adjacent cells. y_p is the distance from point p to the wall. y^* quantities are approximately equal to y^+ in equilibrium turbulent boundary layers. y^+ is represented by

$$y^+\equiv\frac{\rho u_\tau y}{\mu} \tag{13}$$

where u_τ is the friction velocity at the nearest wall, defined by

$$u_\tau\equiv\sqrt{\frac{\tau_w}{\rho}} \tag{14}$$

and τ_w is wall shear stress and y is the distance to the nearest wall.

Under the local equilibrium hypothesis, the production of k and its dissipation rate ε are assumed equal in the wall-adjacent control volume. Production of kinetic energy, G_k, is obtained from

$$G_k = \tau_w \frac{\tau_w c_\mu^{1/4} k_p^{1/2} y_p}{\kappa \rho} \tag{15}$$

Dissipation rate, ε is obtained from

$$\varepsilon_p = \frac{c_\mu^{3/4} k_p^{3/2}}{\kappa y_p} \tag{16}$$

The near wall Reynolds stress values required by the RSM are presented under a local coordinate system, with τ the tangential coordinate, η the normal coordinate, and λ the binormal coordinate, as

$$\frac{\overline{u'^2_\tau}}{k} = 1.098, \frac{\overline{u'^2_\eta}}{k} = 0.247, \frac{\overline{u'^2_\lambda}}{k} = 0.655, \frac{\overline{u_\tau u_\eta}}{k} = 0.255 \tag{17}$$

3.1.2 Discrete Phase

A Lagrangian model is employed to obtain particle trajectories and distributions within the computational domain. A discrete phase particle trajectory is predicted by integrating the force on the particle within a Lagrangian reference frame. The Newton law of motion can be written in Cartesian coordinates as

$$\frac{du_p}{dt} = F_D + \frac{g(\rho_p - \rho)}{\rho_p} \tag{18}$$

where u is fluid phase velocity, u_p is particle velocity, ρ_p is particle density, F_D represents the drag force per unit particle mass, and the latest term on the right hand side represents the buoyancy force.

Fluid turbulence effects on particle dispersion were accounted for through a simple stochastic approach, the Random Walk Model (RWM). Instead of using mean

phase velocity $\bar{u}$ to calculate a trajectory, instantaneous fluid velocity, $\bar{u} + u'$ is used to account for the random turbulence effects on the particle dispersion. u' represents fluctuating velocity components. The RWM assumes that u' conforms to a Gaussian probability distribution. Values for u', v', and w' are obtained from

$$\sqrt{\overline{u'^2}} = \sqrt{\overline{v'^2}} = \sqrt{\overline{w'^2}} = \sqrt{2k/3} \tag{19}$$

for the k-epsilon model (assuming isotropy). RSM incorporates the nonisotropy of stresses into the derivations of the velocity fluctuations (Zhou et al. 1991)

$$u' = \zeta\sqrt{\overline{u'^2}}, v' = \zeta\sqrt{\overline{v'^2}}, w' = \zeta\sqrt{\overline{w'^2}} \tag{20}$$

where ζ is a normally distributed random number.

Values of the fluctuating velocity components are maintained constant throughout a succession of turbulent eddy. Particle trajectories are integrated over this period. The integral time T_L is approximated as

$$T_L = 0.15\frac{k}{\epsilon} \tag{21}$$

for the standard k-epsilon model, and

$$T_L = 0.3\frac{k}{\epsilon} \tag{22}$$

for the RSM. The particle dispersion rate is proportional to T_L. Large T_L value indicates greater turbulent motions in the flow and greater particle turbulent dispersion.

3.1.2.1 Drag Force

The drag force per unit mass is obtained from

$$F_D = -\frac{1}{2}\frac{\rho}{\rho_p}\frac{A}{V}C_D(u_p - u)\left|u_p - u\right| \tag{23}$$

where *A* and *V* are the cross-sectional area and volume of the particle. C_D represents the drag coefficient of the particle.

For a spherical particle, the drag force per unit particle mass can be written as

$$F_D = -\frac{3}{8}\frac{\rho}{\rho_p}C_D(u_p - u)|u_p - u| \tag{24}$$

The drag coefficient, C_D, depends on the flow regime. For a spherical particle, it is given by

$$C_D \begin{cases} \dfrac{24}{Re} & \text{Re} < 0.1 \\ a_1 + \dfrac{a_2}{Re} + \dfrac{a_3}{Re^2} & 0.1 < Re < 10000 \\ 0.4 & \text{Re} > 10000 \end{cases} \tag{25}$$

where Re is the particle Reynolds number defined as

$$Re \equiv \frac{\rho d_p |u_p - u|}{\mu} \tag{26}$$

Constants a_1, a_2, and a_3 depend upon the particle Reynolds number.

Since Bliss Rapids snails have a cone shaped shell and do not approximate a sphere, a nonspherical law was imposed to compute their drag force. In Fluent, the non-sphericity is taken into account through the drag coefficient, C_D. It was taken from (Morsi and Alexander, 1972)

$$C_D = \frac{24}{Re_{sph}}\left(1 + b_1 {Re_{sph}}^{b_2}\right) + \frac{b_3 Re_{sph}}{b_4 + Re_{sph}} \tag{27}$$

where

$$b_1 = exp(2.3288 - 6.4581\emptyset + 2.4486\emptyset^2) \tag{28}$$

$$b_2 = 0.0964 + 0.5565\emptyset \tag{29}$$

$$b_3 = exp(4.905 - 13.8944\emptyset + 18.4222\emptyset^2 - 10.2599\emptyset^3) \tag{30}$$

$$b_4 = exp(1.4681 + 12.2584\emptyset - 20.7322\emptyset^2 + 15.8855\emptyset^3) \quad (31)$$

The shape factor, $\emptyset$, is defined as

$$\emptyset = \frac{s}{S} \quad (32)$$

where s is the surface area of a sphere having the same volume as the particle, and S is the actual surface area of the particle. The relationship between shape factor $\emptyset$ and drag coefficient C_D is shown in figure 3-1. Reynolds number Re_{sph} is computed using equation (26) with the diameter of a sphere with the same volume as the particle.

3.2 Boundary Conditions

Boundary conditions for the two-phase simulation are described in the following sections.

3.2.1 Continuous Phase Boundary Conditions

A total of five boundary conditions were used for the fluid, they are periodic, inlet, outflow, free surface, and wall. Each continuous phase boundary condition will be outlined and discussed in following sections. Further detail is found in the Fluent User's Guide (2006).

3.2.1.1 Periodic

Additional simulations using periodic boundary conditions were performed to obtain a fully developed solution for the upstream inflow. The river reach anterior to the inflow boundary is considered as a straight channel. River bathymetry at the inflow cross section is used as the river bed shape for the straight channel. Evenly distributed mass flows, corresponding to low flow and high flow conditions, are imposed normally to the upstream straight channel. A symmetry boundary condition was imposed as the free surface and a no-slip (zero velocity) surface boundary condition was applied to the

channel bottom. A fully developed flow field is obtained from the simulation and implemented at the inflow boundary to improve simulation quality and reduce boundary effects.

3.2.1.2 Inlet

A single inlet boundary condition was used at the upstream cross section of the river. A mass flow rate was imposed at the inflow boundary. Velocity distributions and profiles obtained from the periodic boundary were also imposed. Two flowrate conditions were investigated for this study. Figure 3-2 shows the 2007 daily mean flowrate measured at Snake River below Bliss Dam. 7,700 cfs represents average early summer flows at Mid Snake River, when White Sturgeon is spawning. 51,500 cfs represents the 100 year flow based on the Log-Pearson III method.

3.2.1.3 Outflow

Outflow boundary conditions were used to regulate flow exits at the computational domain. At the outflow boundary, Fluent applies a zero diffusion flux for all flow variables and an overall mass balance correction to control outflow. Outflow plane information is extrapolated from the interior. A flow rate weighting of 1 was used to ensure the mass conservation over the numerical domain.

3.2.1.4 Free Surface

Free surfaces of the computational domains were modeled with a Rigid-Lid approximation. Fixed smooth surfaces were imposed as the free surface. Pressure, turbulence quantities, and tangential velocity components at the free surface are extrapolated from the interior while the normal velocity is fixed at zero. A symmetry boundary condition was used for the k-epsilon model at the free surface. The water surface shape was prescribed based on a one-dimensional simulation provided by IPC. Zero normal velocity and zero normal gradients for all turbulent variables at the

symmetry plane were applied under a standard k-epsilon model. Under the RSM, to account for the attenuation of the normal velocity fluctuation at the free surface, the anisotropy model developed by Turan et al. (2007) was used.

3.2.1.5 Wall

A no-slip (zero velocity) surface boundary condition was applied to the solid surface of the grid. Although this study does not take boundary roughness into consideration, previous research by Meselhe and Odgaard (1998) prove this approach to be satisfactory for large scale river reaches with deep, low velocity and a wide roughness variations.

3.2.2 Discrete Phase Boundary Conditions

Particles are tracked through the flow field until they come into contact with flow domain boundaries. Boundary conditions are very important for this study.

To study the fish eggs and snails distributions, a total of five boundary conditions were utilized for the particles (discrete phase): escape, reflect, trap, Shear Stress Reflect (SSR), and Shear Stress Resuspend (SSS). Each discrete phase boundary condition is outlined and discussed in the following sections.

3.2.2.1 Outflow

An escape boundary condition was applied at the inflow and outflow boundary planes. Trajectory calculations for the discrete phase are terminated when a tracked particle encounters those boundary planes.

3.2.2.2 Free surface

A reflect boundary, in which a particle is reflected back into the flow upon reaching the boundary plane, was imposed at the free surface. An elastic collision is assumed in this study, where the particle retains all normal and tangential momentum after rebounding.

3.2.2.3 Wall

Particle interactions with the wall can significantly change their paths in the fluid and distribution over the river bed. None of the Fluent currently available boundary condition adequately represents fish eggs and snails behaviors. These can become resuspended after initial deposition in response to the turbulence or velocity fluctuations. Two boundary conditions based on local shear stress were therefore incorporated into this study. One allows particles to reenter the flow field after settling, responding to continuous phase turbulence or a random factor. The other does not allow for resuspension.

These additional boundary conditions were implemented into Fluent using User Defined Functions (UDFs). A UDF is a subroutine in C++ programming language that can be dynamically loaded with the Fluent solver for a specific user purpose.

Previous studies have defined a critical bed shear stress for deposition such that particles are trapped if the local bed shear stress is below the critical bed shear stress. Otherwise particles are reflected. This can be represented as

$$boundary\ condition\ at\ river\ bed \begin{cases} \tau < critical\ shear\ stress \rightarrow trap \\ \tau \geq critical\ shear\ stress \rightarrow reflect \end{cases}$$

where τ is the local shear stress.

The critical shear stress is determined as the shear stress to initiate the motion of particle. Its value for different materials can be obtained experimentally. Since quartz and snails are similar in density, the critical value of quartz sediment in water as a function of grain size was used in this study (figure 3-3).

The Rouse number is usually used as a non-dimensional number in fluid dynamics to determine how sediment is transported in a flowing fluid. It is defined as

$$Rouse = \frac{w_s}{ku_*} \tag{33}$$

where w_s is the sediment fall velocity and u_* is the shear velocity. To obtain the equivalent diameter for fish eggs, the Rouse number for fish eggs and quartz are assumed to be the same.

Observations have established that the initiation of motion appears to be random in both time and space when shear stress nears the critical value. So the initiation of motion process is statistical in nature and should not be set as a solid threshold (Vanoni, 1977). For the new bed shear stress boundary condition, instead of automatically trapping the particle when local shear is below critical shear stress, a probability function is applied which causes particle trapping become a function of the local bed shear stress. Due to a lack of required research and data for organism deposition process, a simple linear relationship was employed for this study. The number of reflections is proportional to the local bed shear stress (figure 3-4).

1) Wall-Trap

A default trap boundary used by Fluent was applied at walls. Trajectory calculations are terminated when particles encounter a solid surface. Fish eggs are considered unlikely to be easily suspended and likely to deposit within a relatively short distance from the spawning location (Barton et al., 2005). The trap condition was utilized to model this situation. Particle distributions under this boundary condition are compared with BSS boundary condition distributions to evaluate bed shear stress effects on particle behaviors.

2) Wall-Shear Stress Reflect

The SSR boundary condition used at walls determines fates of particle based on local shear stress. Discrete phase particle deposition rate is a function of local bed shear stress. Particles are considered more likely to reflect within high bed shear stress regions and settle within low shear stress areas. This boundary condition assumes that particles are not subject to re-suspension after deposition. Trajectory calculations for the discrete phase are terminated when particles are determined to be trapped.

3) Wall-Shear Resuspend

The SSS boundary condition used at walls traps particles as a function of local bed share stress. This condition assumes that particles can re-enter the flow field after their initial deposition. Particles can be resuspended due to the turbulence or velocity fluctuation. All trajectories are recorded for particles within the computational domain.

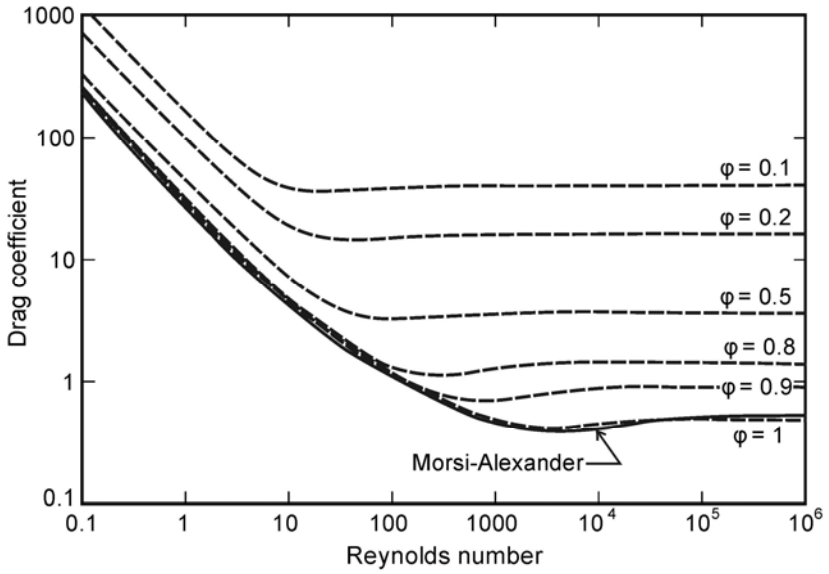

Figure 3-1 Drag coefficients for nonspherical particles

Source: Fluent User's Guide 2006

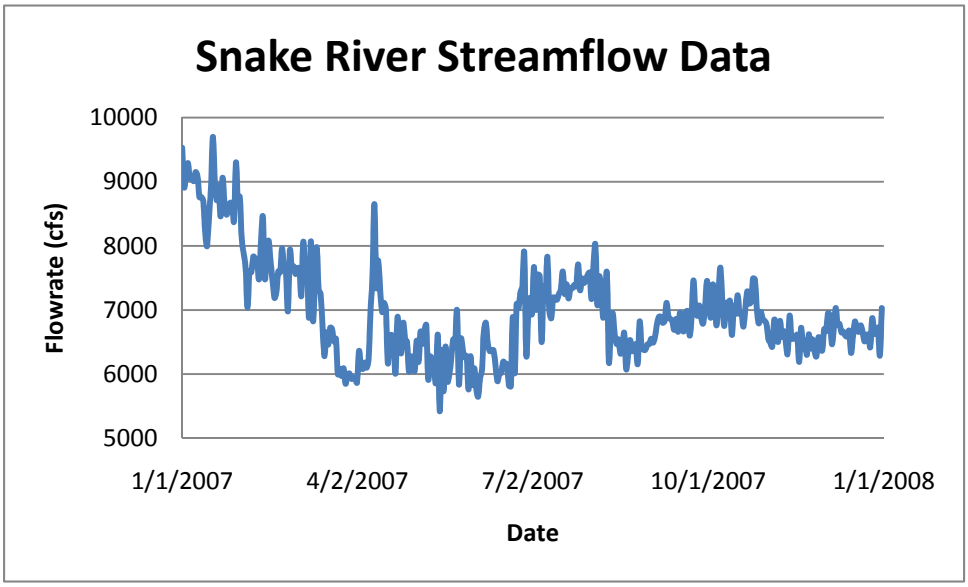

Figure 3-2 Averaged daily flowrate profile at Mid Snake River for year 2007

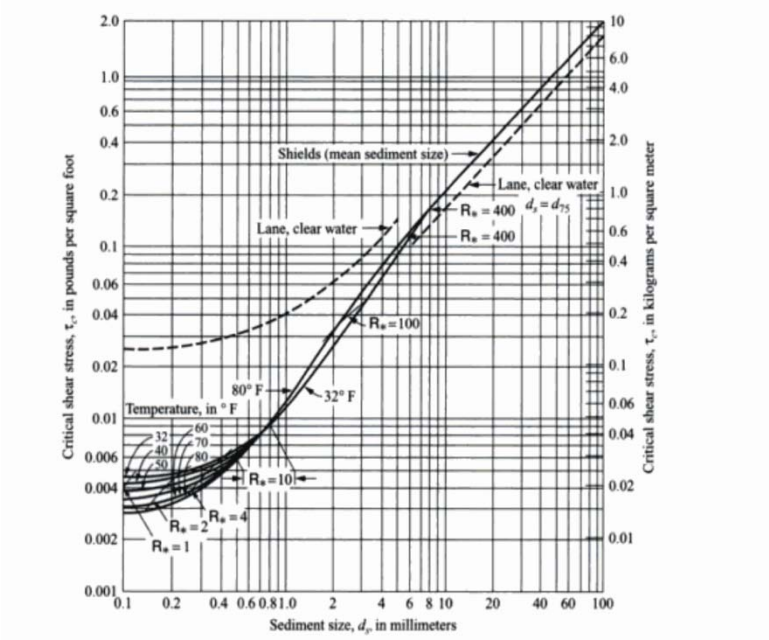

Figure 3-3 Critical Shear Stress for Quartz in water as function of particle size (Shields, 1936 and Lane, 1955)

Source: Vito A. Vernoni, *Sedimentation Engineering,* 1977, New York

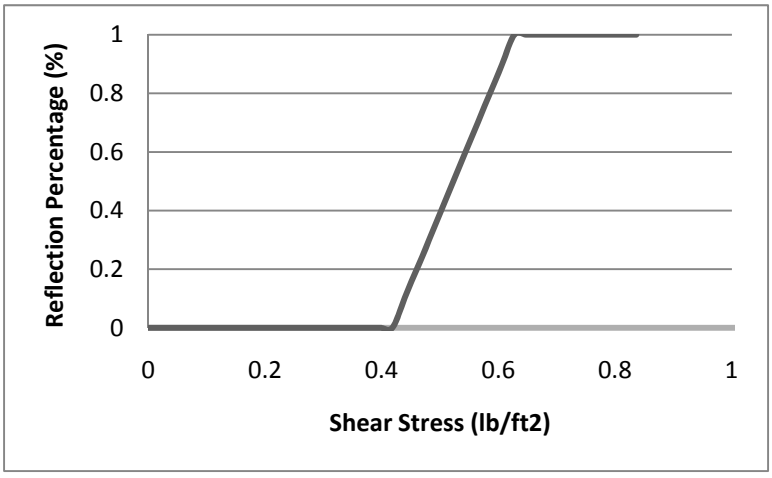

Figure 3-4 Bliss Rapids Snails reflection percentage as a function of local bed shear stress

CHAPTER IV

MIDDLE SNAKE RIVER FISH EGGS AND SNAILS TRACKING MODEL

4.1 Grid Generation

The commercial grid generator Gridgen was used to create numerical grids for these simulations. Gridgen is a complete meshing toolkit for generation of 3D, multiple block grids for complex geometries in a production environment. It has been applied for meshing by engineers and scientists worldwide for decades and is proven as a reliable high quality grid generator. Gridgen provides tools to check numerical mesh quality, which is used in this study to ensure meshes are appropriate to easily converge with the selected solver.

Water surface elevations based on previous 1D simulation provided by IPC and river bathymetry was employed to construct grids for the two mile Mid-Snake River reach between River Mile (RM) 556.2 and 554.2. Meshes were generated to simulate average and 100 year flow conditions. River bathymetry and bank lines varied with flowrates and free surface elevations. Plan views of the simulated domains with bathymetry are show in figures 4-1 and 4-2 for inflow rates of 7,700 and 51,500 cfs, respectively. Free surface elevations for the two flowrate conditions are shown in figures 4-3 and 4-4. The inflow increment caused surface elevations to rise. River depths for the high flow case increase an average of 15 ft on the main channel.

Due to the length and complexity of the geometry, the low flowrate grid contained 34 blocks and approximately one million grid points. The high flowrate grid consisted of 16 blocks and approximately 800,000 grid points. Shore lines for low flows are more complex than for high flows, requiring more dimensions for accurate simulation. A plan view of the Mid-Snake River low flow grid is shown in figure 4-5. Close up plan views of the channel grid are shown in figures 4-6 to 4-14. A 3D illustration of boundary conditions applied to the computational mesh is shown in figure 4-15.

Grid points were clustered and nodes were highly concentrated near the river bed to resolve flow fields near the wall and ensure a valid y^* for the standard wall law. Figure 4-16 shows a representative inflow cross section grid point clustering.

Two additional monoblock straight channel meshes were generated for periodic simulations. The river channel anterior to the flow inlet was assumed straight with a constant free surface at the inlet. The inflow cross section was extended 500 ft upstream from the inlet and served as a bathymetry template for the straight channel. About 100,000 grid points were used or both the low and high flowrate channels. Figures 4-17 and 4-18 show plan and 3D close up views of the extended straight channels for low and high flow cases, respectively.

4.2 Simulation Conditions

For this study, 5 simulation cases were performed to resolve the hydrodynamics and fish egg and snail distributions. The simulation conditions are described in the following sections.

4.2.1 Physical Properties

Clean water was used to simulate the river hydrodynamics. Physical properties of White Sturgeon eggs and Bliss Rapids snails were taken into account for the discrete phase. Details of these properties are found in tables 4-1 and table 4-2. Discrete phase particles were injected 196.85 ft downstream from the inflow domain to avoid possible boundary effects. They are evenly distributed over the first 6.56 ft below the free surface. Following Stovin (1996), 10,000 particles were injected to ensure that the simulated data was representative of the results obtained from an infinite number of simulations.

4.2.2 Description of Simulated Cases

A standard rigid-lid, 3D unsteady simulation was performed with the standard k-epsilon and RSM turbulent model in case 1. Hydrodynamic results from the two turbulent models were obtained and studied.

In case 2, variation in organism distributions for White Sturgeon eggs and Bliss Rapids snails over the river bed in response to river discharge and turbulent models used are studied.

The random walk model, included in case 3, studies the effects of turbulent dispersion on particle trajectories and distributions over the river reach.

The UDF SSR boundary conditions, implemented in case 4, evaluated the impacts of local bed shear stress on aquatic organism distributions for the Mid-Snake River.

An analysis and comparison of SSR and SSS boundary conditions was performed in case 5. A sensitivity analysis of the selected critical shear stress value was performed and studied in this section.

Table 4-3 shows an abbreviated description of these 5 cases.

Table 4-1: Properties for Bliss Rapids Snails

Individual	Base Width (mm)	Height (Length) (mm)	Weight (mg)
1	1.63	2.06	2.8
2	1.64	2.36	4.2
3	1.54	1.91	2.7
4	1.44	1.83	2.7
5	1.27	1.58	1.8
6	1.00	1.11	0.9

Table 4-2: Properties for White Sturgeon Eggs

	Average Radius (mm)	Average Density (kg/m3)
Sturgeon Eggs	1.77	1051

Table 4-3: Description of All Cases Run

Simulation Cases	Description	Fish eggs	Snails
Hydrodynamic Simulations	Hydrodynamic simulation for flow condition of 7,700 and 51,500 cfs	no	no
Turbulence Model Comparison	DPM analysis for k-epsilon and RSM	yes	yes
Random Walk Model Effect	Particle tracking with turbulent dispersion	yes	no
SSR Boundary Condition	Particle tracking with SSR boundary conditions	yes	yes
Analysis of SSR and SSS Boundary Conditions	Comparison and Sensitivity analysis of SSR and SSS boundary conditions	no	yes

4.3 Numerical Method

The commercial code Fluent 6.2 was used as the CFD model in this study. Continuity and momentum equations (1) and (2) are solved for the hydrodynamics. The turbulent field is solved by equations (5) and (6) for k-epsilon model or (8) for RSM. The

SIMPLE (Semi-Implicit Method for Pressure-Linked Equations) algorithm is used to couple pressure and velocity. The Standard discretization method is applied to pressure and the first order upwind method is used for momentum and turbulent variables. Unsteady solutions for the hydrodynamics are obtained using a fixed time-step of 1 s. Steady solutions are obtained approximated in 2 hours flow time. 20 hours flow time was ran to ensure a full converged solution. The particle trajectory is then calculated by integrating the force balance equation (18) using hydrodynamic data from the Eulerian model. Implicit and Trapezoidal schemes are chosen as the low and high order schemes for the discrete phase model. They will switch between each other based on Fluent default accuracy requirement and the stability range for each scheme. Discrete phase particle trajectories and distributions are obtained by a steady solver. The number of time steps was set at 50,000, large enough to ensure that tracking particles reach the river bottom or outlet. SSR and SSS boundary conditions are programmed using UDFs and used at the river bed.

4.4 Summary

This chapter details 3D numerical girds generation and the numerical simulation strategies for this thesis. A complete description and figures for the Mid-Snake River computational domain has been presented. Physical and numerical conditions for the simulations are listed and tabled in this chapter. The commercial CFD code Fluent was used in this study and the numerical method has been thoroughly described.

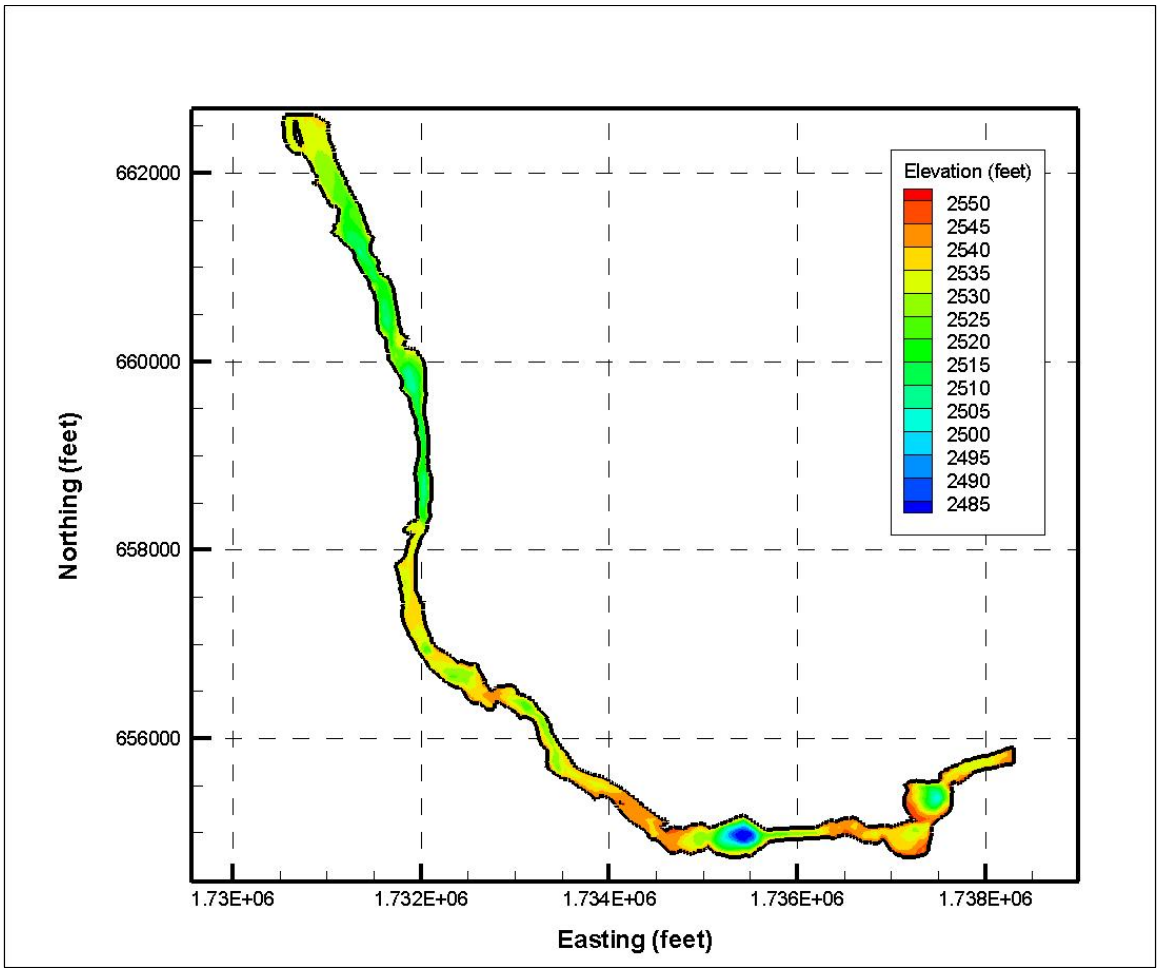

Figure 4-1 Numerical model bathymetry for low flow condition at Mid-Snake River

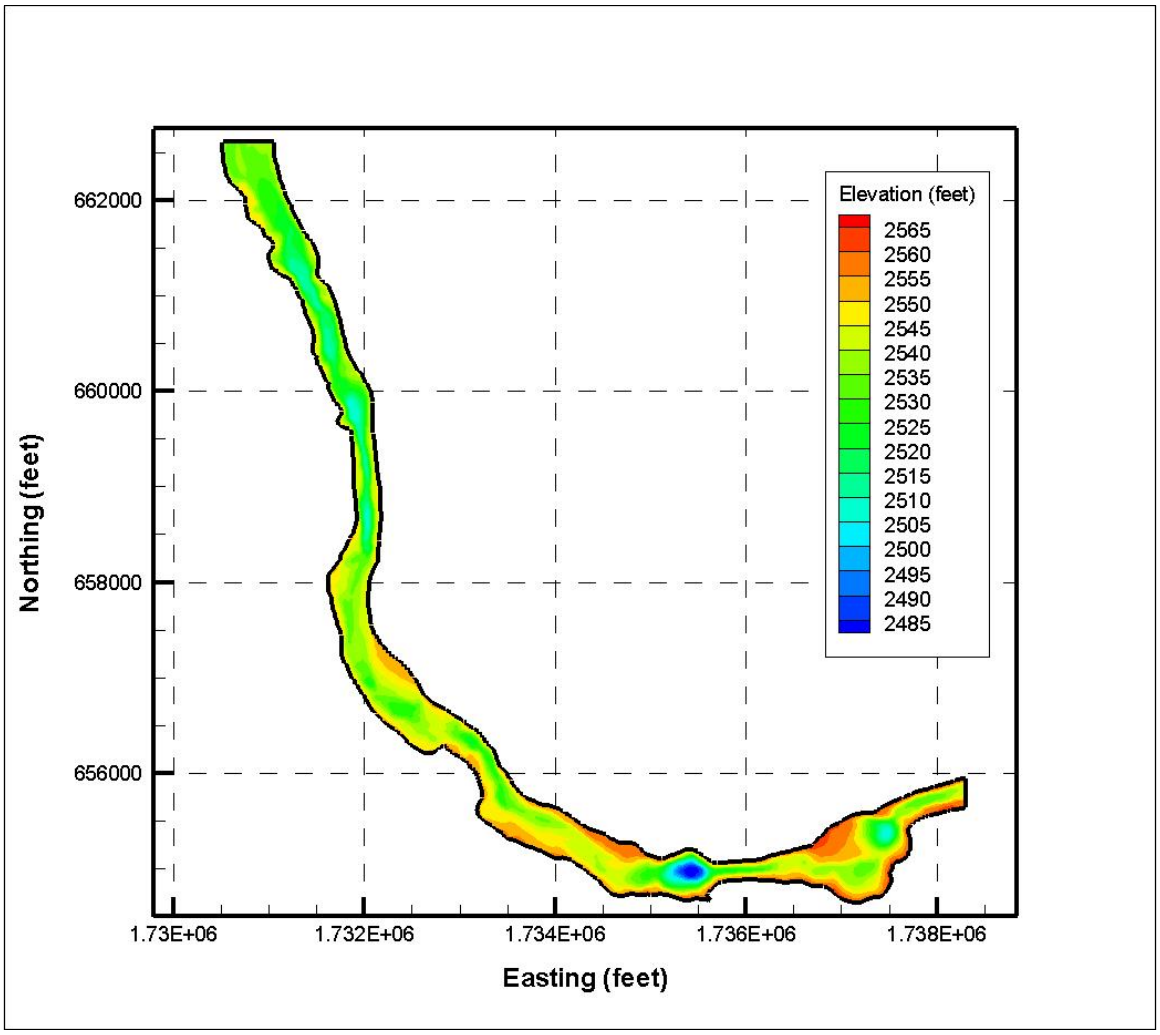

Figure 4-2 Numerical model bathymetry for high flow condition at Mid-Snake River

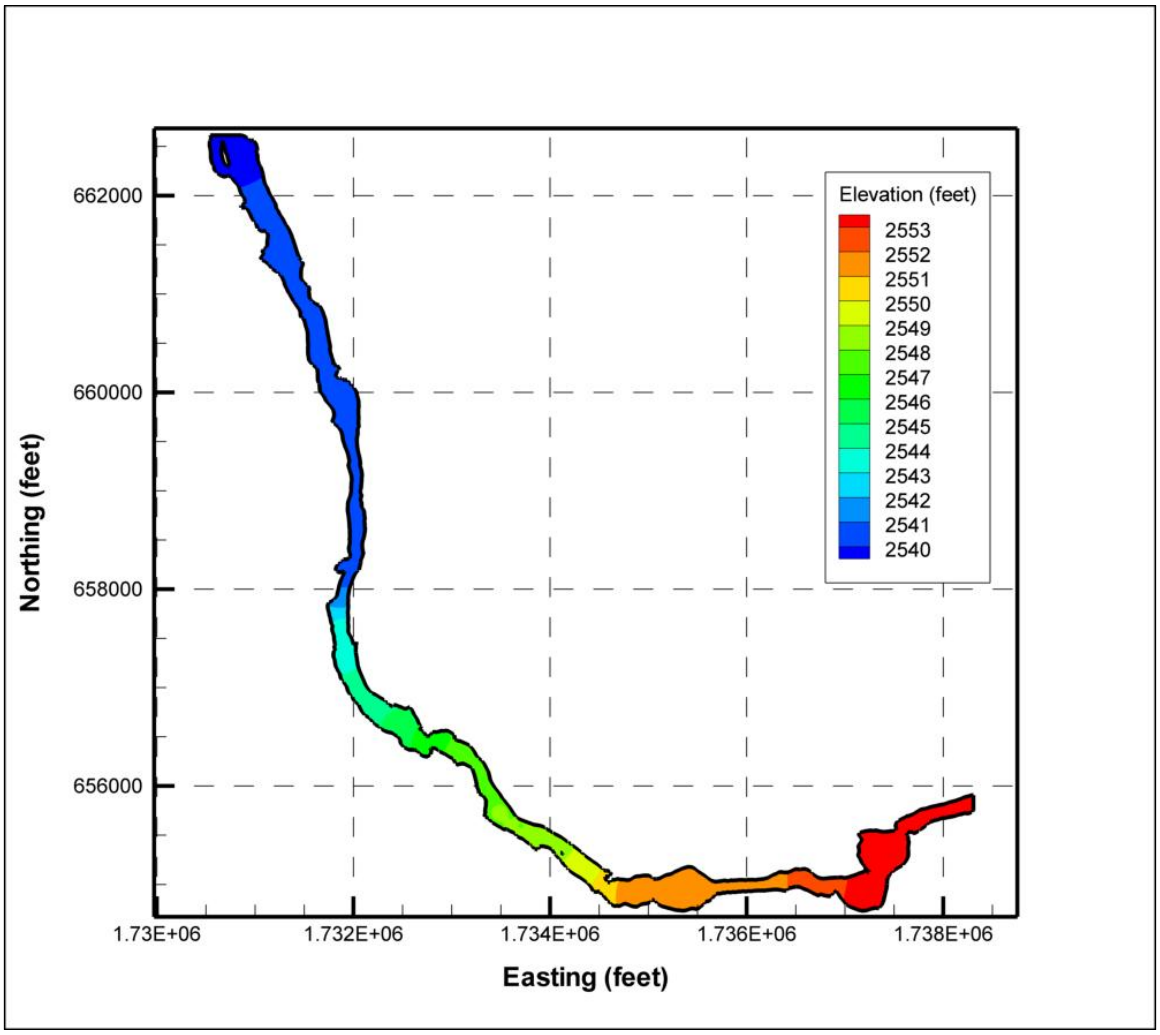

Figure 4-3 Free surface elevation contours for low flow condition at Mid-Snake River

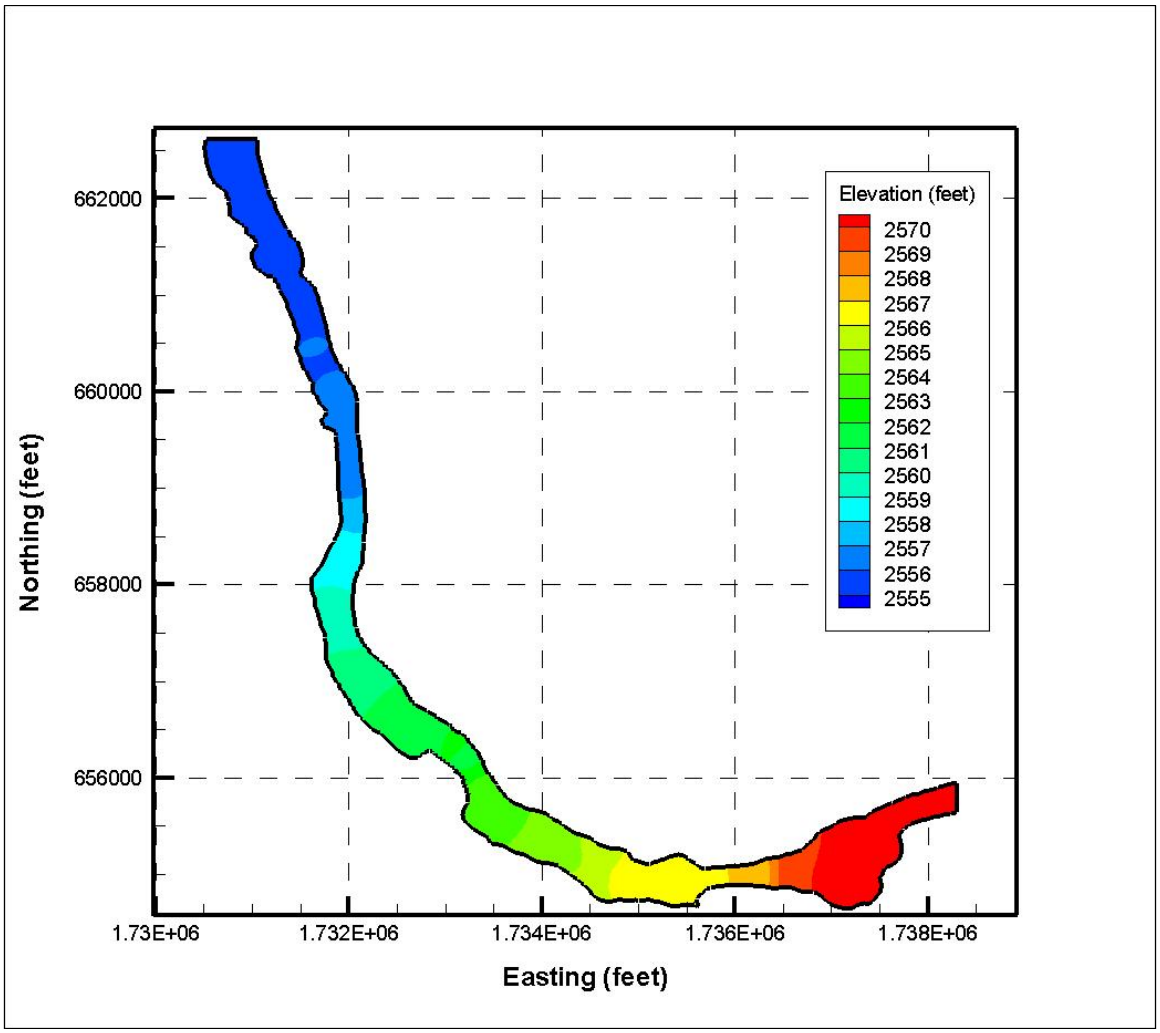

Figure 4-4 Free surface elevation contours for high flow condition at Mid-Snake River

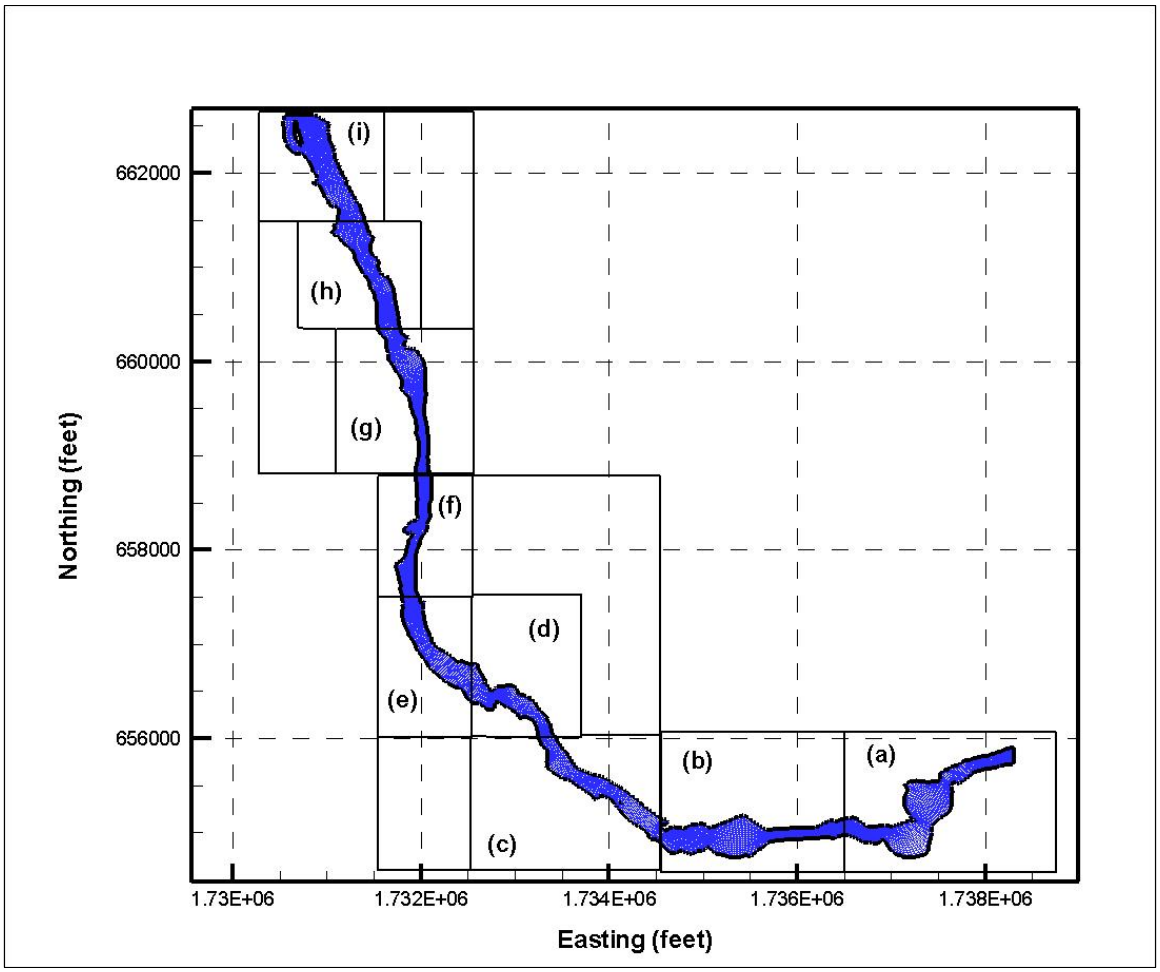

Figure 4-5 Plan view of Mid-Snake River grid at free surface for low flow condition

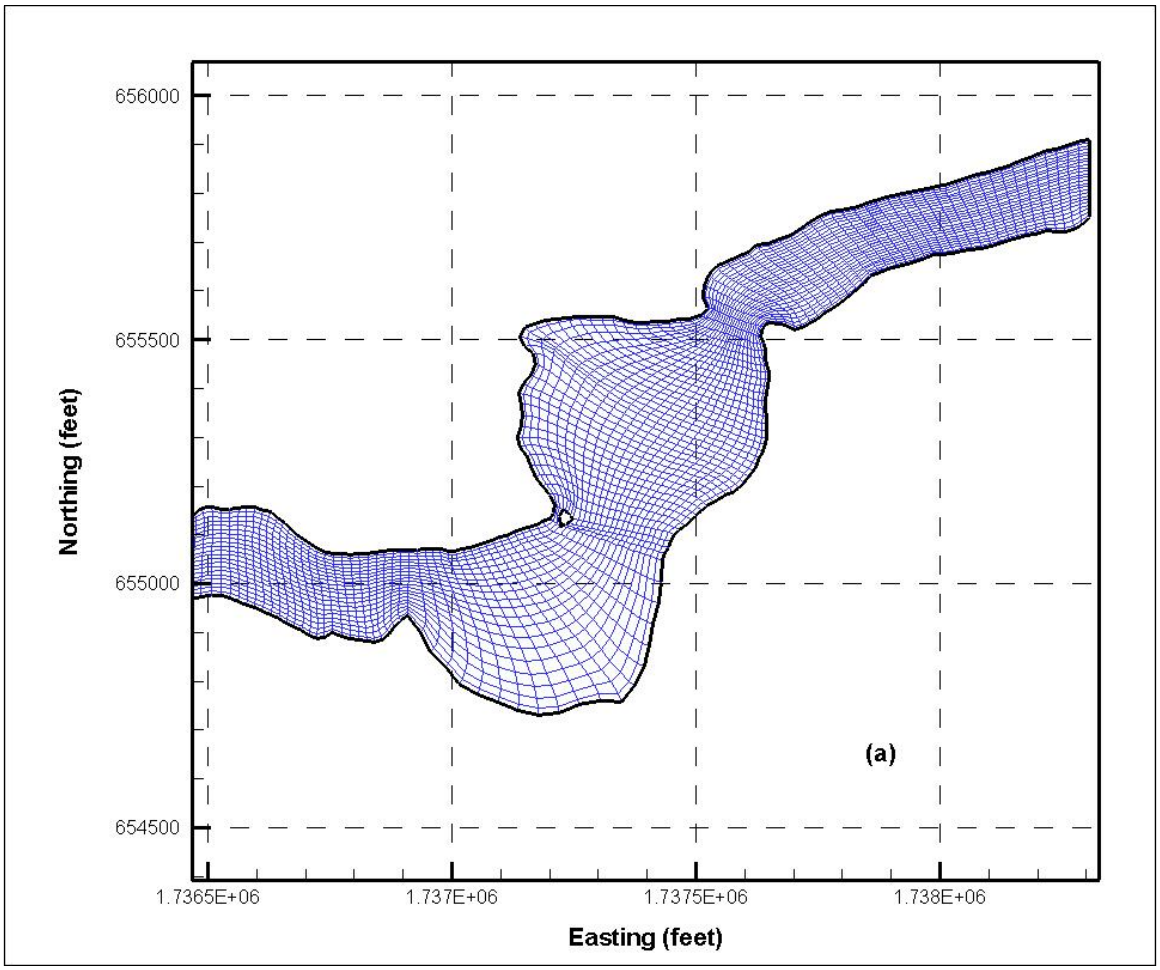

Figure 4-6 Close-up Mid-Snake River grid showing detail (a) (figure 4-5)

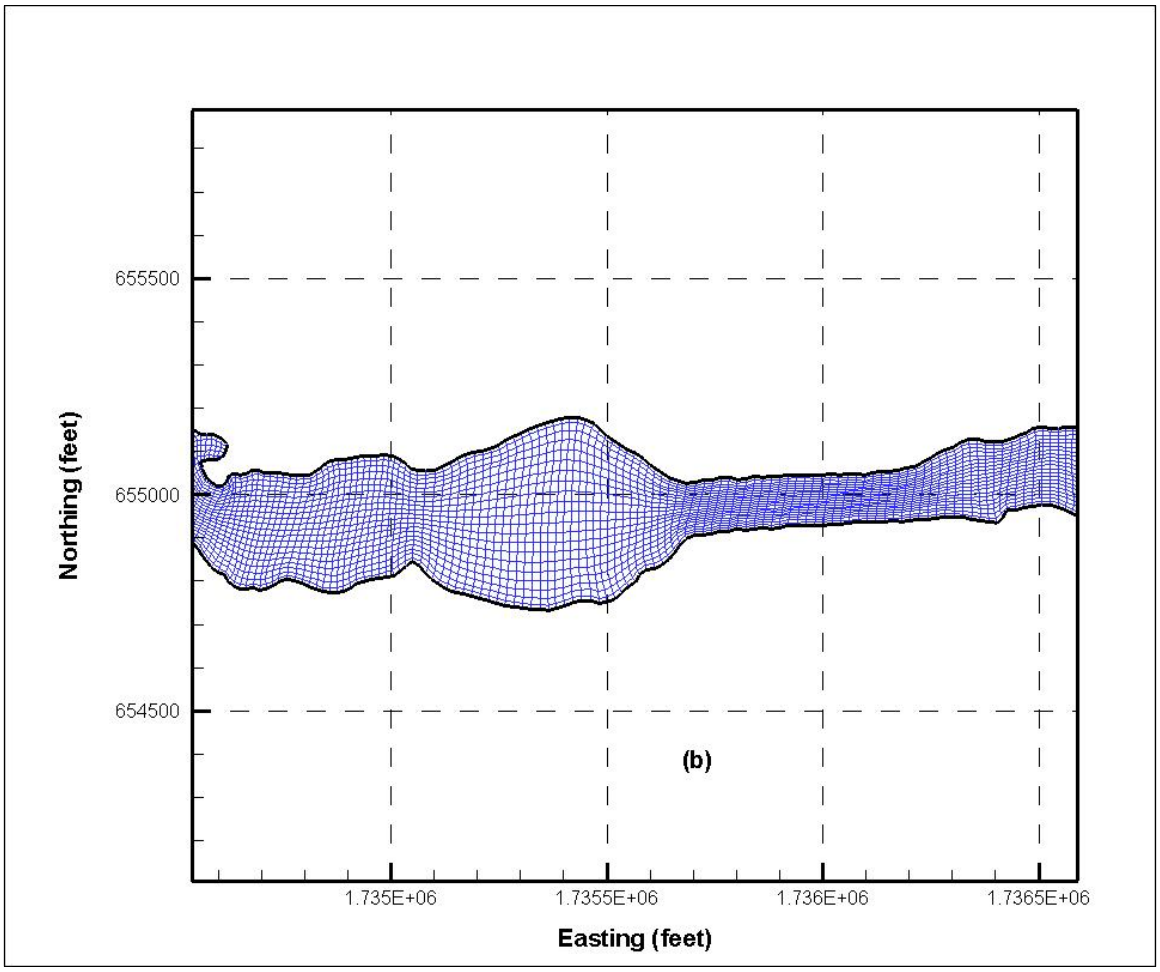

Figure 4-7 Close-up Mid-Snake River grid showing detail (b) (figure 4-5)

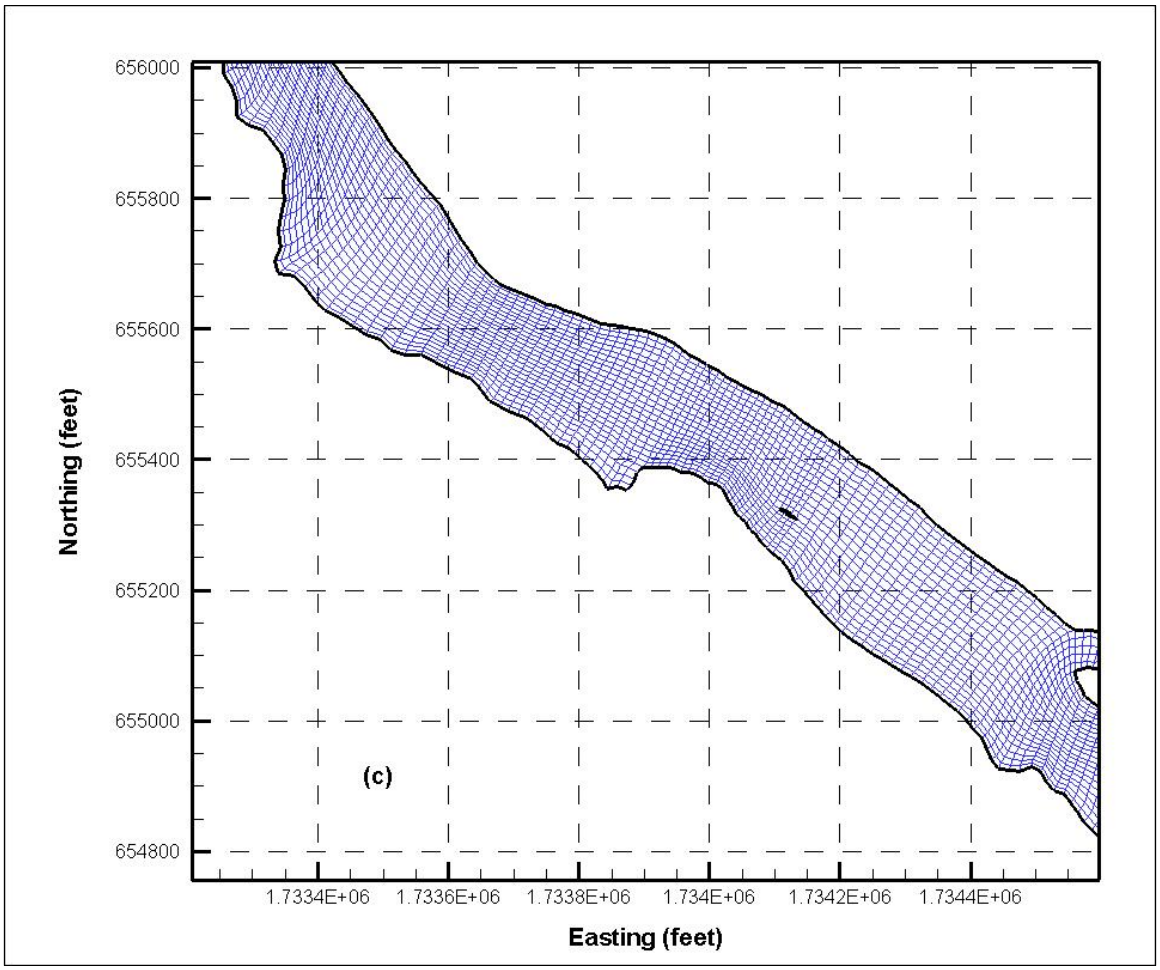

Figure 4-8 Close-up Mid-Snake River grid showing detail (c) (figure 4-5)

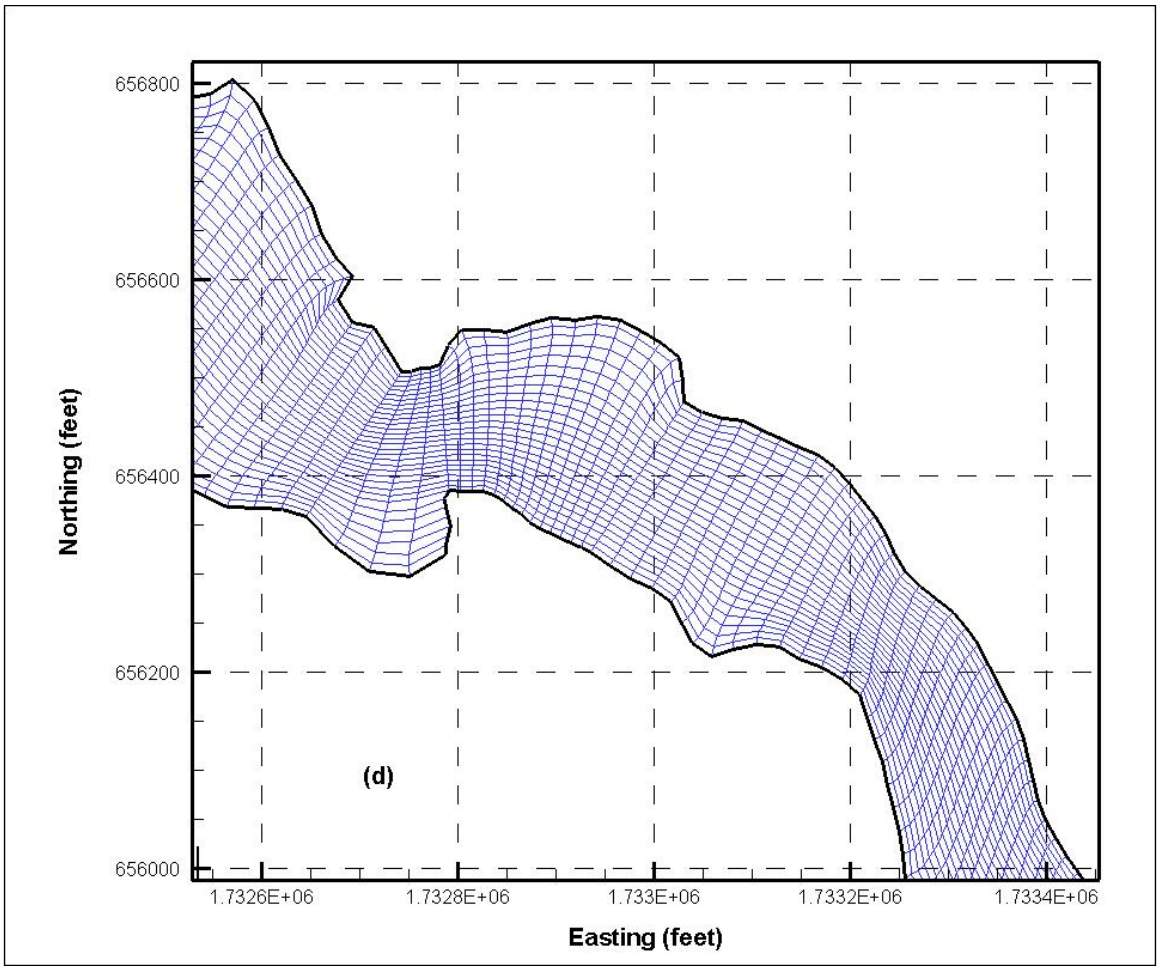

Figure 4-9 Close-up Mid-Snake River grid showing detail (d) (figure 4-5)

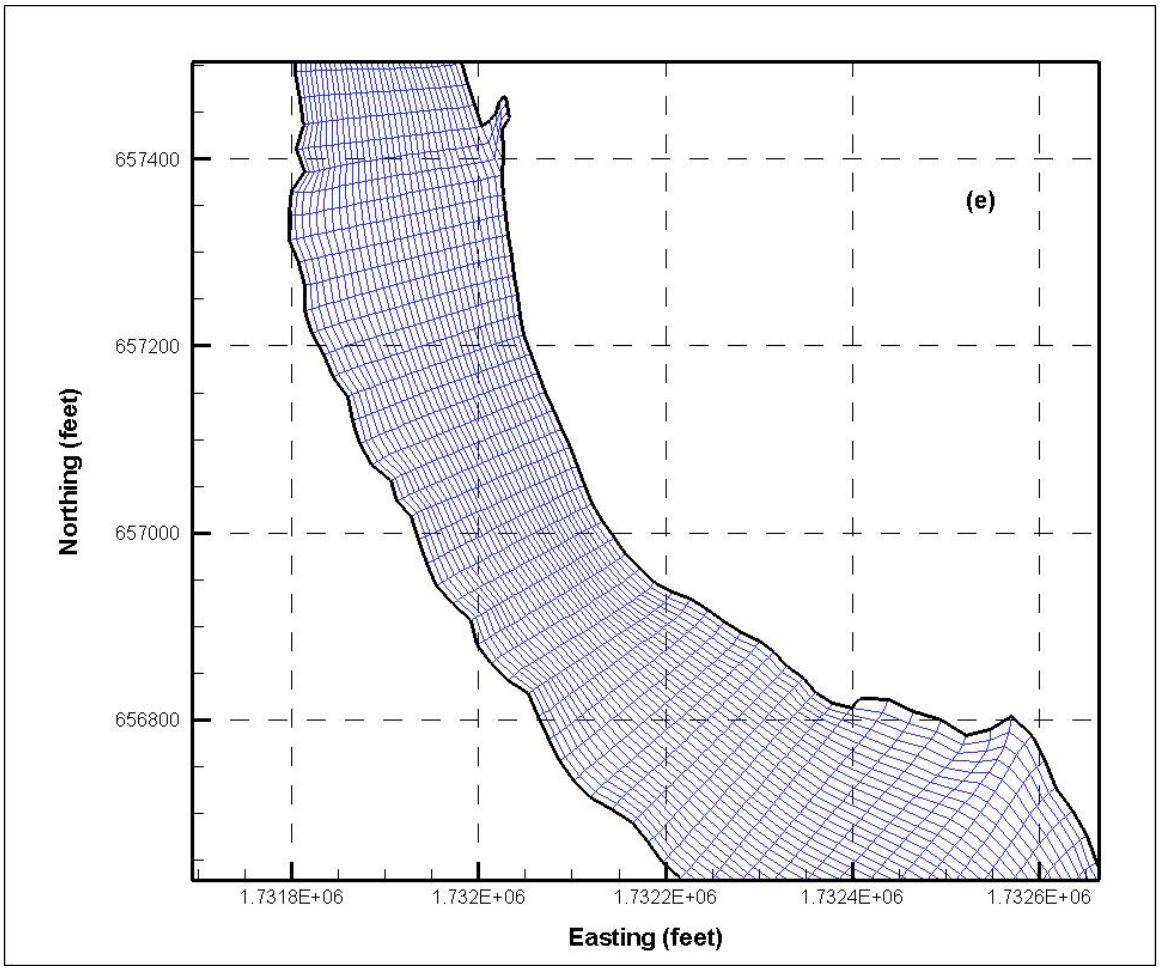

Figure 4-10 Close-up Mid-Snake River grid showing detail (e) (figure 4-5)

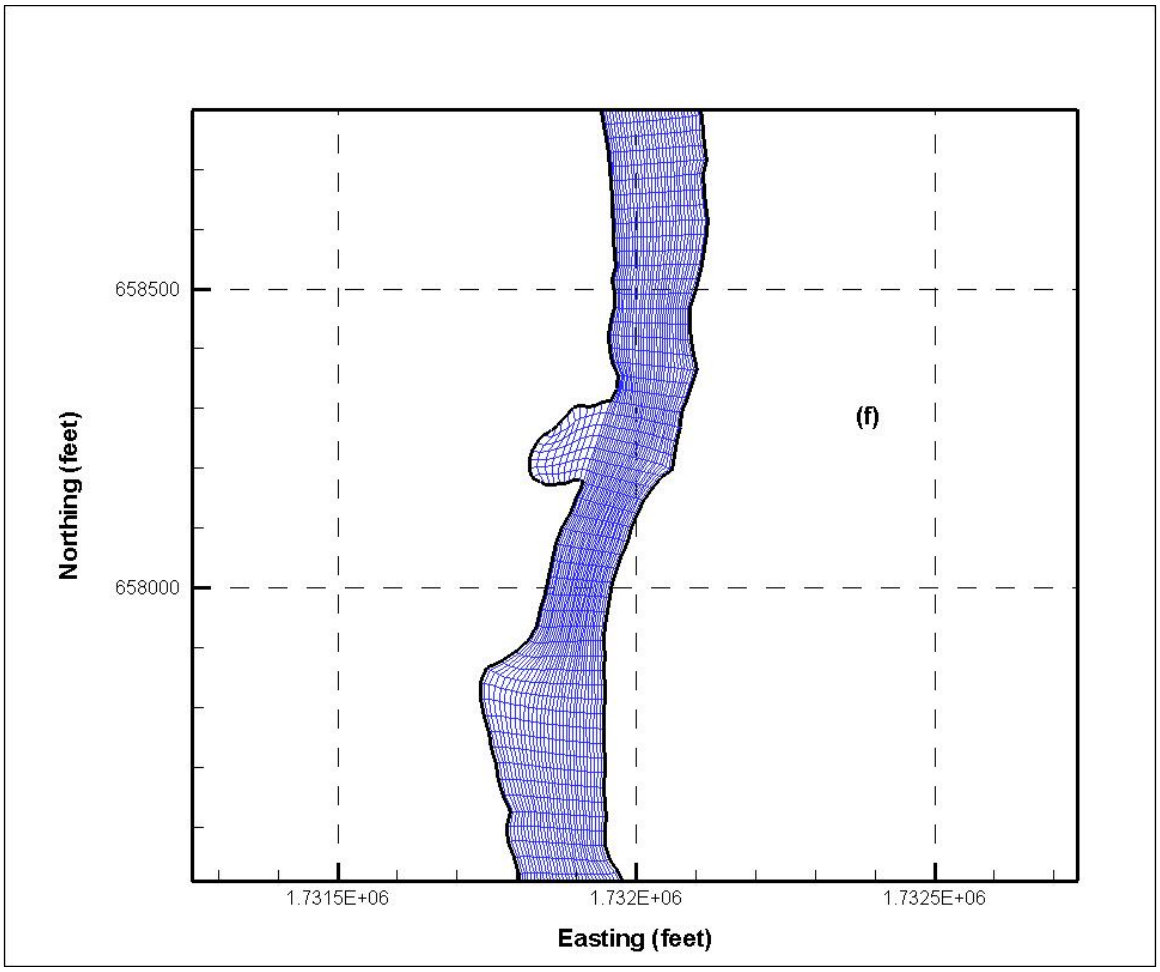

Figure 4-11 Close-up Mid-Snake River grid showing detail (f) (figure 4-5)

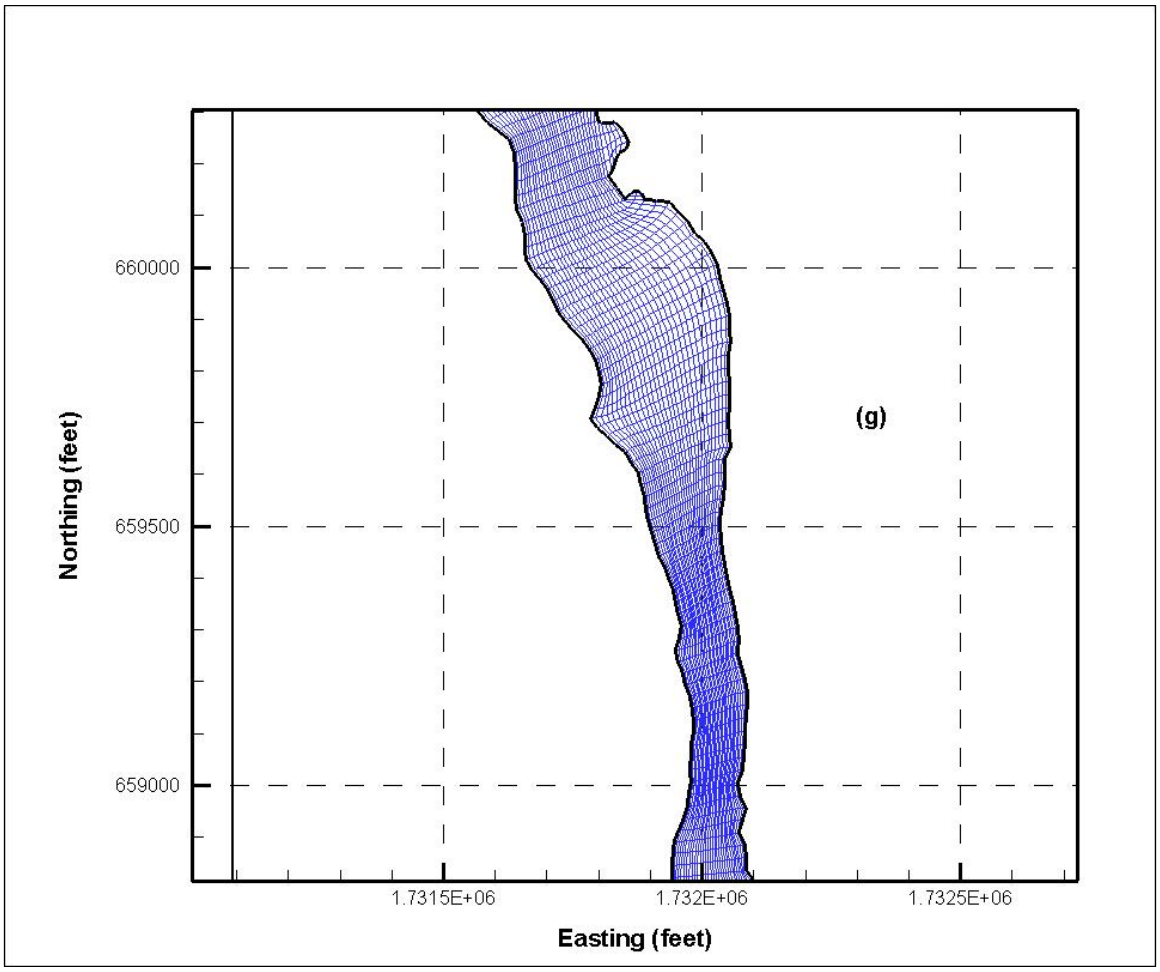

Figure 4-12 Close-up Mid-Snake River grid showing detail (g) (figure 4-5)

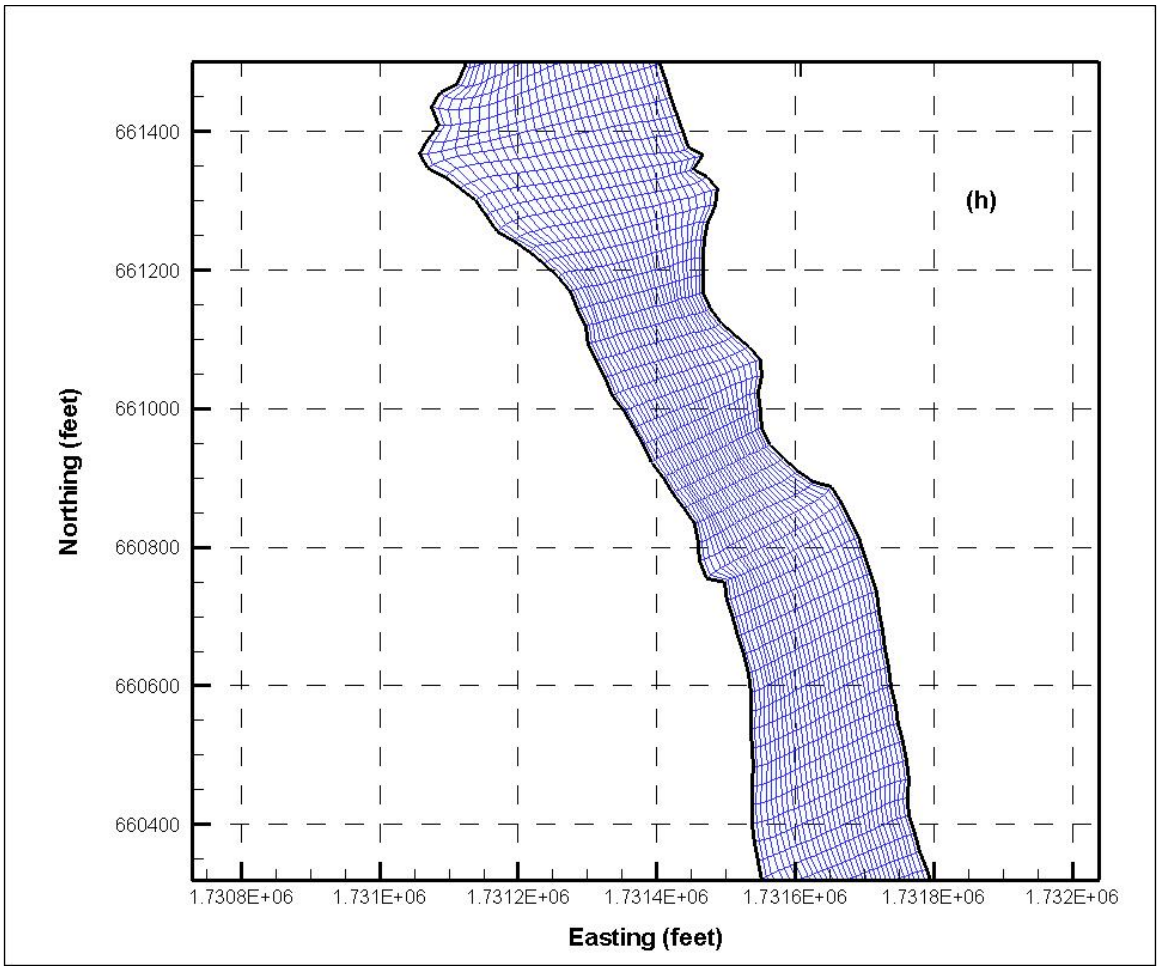

Figure 4-13 Close-up Mid-Snake River grid showing detail (h) (figure 4-5)

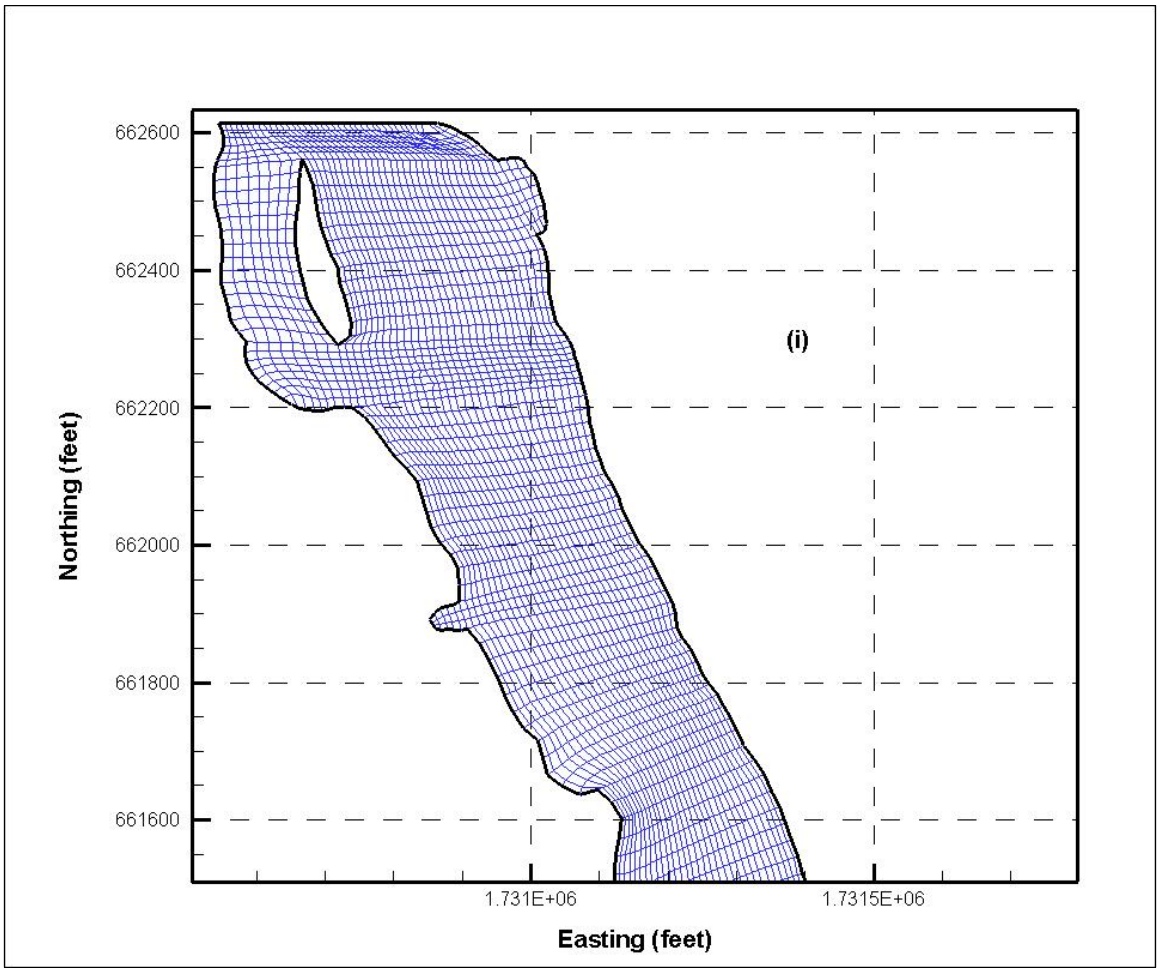

Figure 4-14 Close-up Mid-Snake River grid showing detail (i) (figure 4-5)

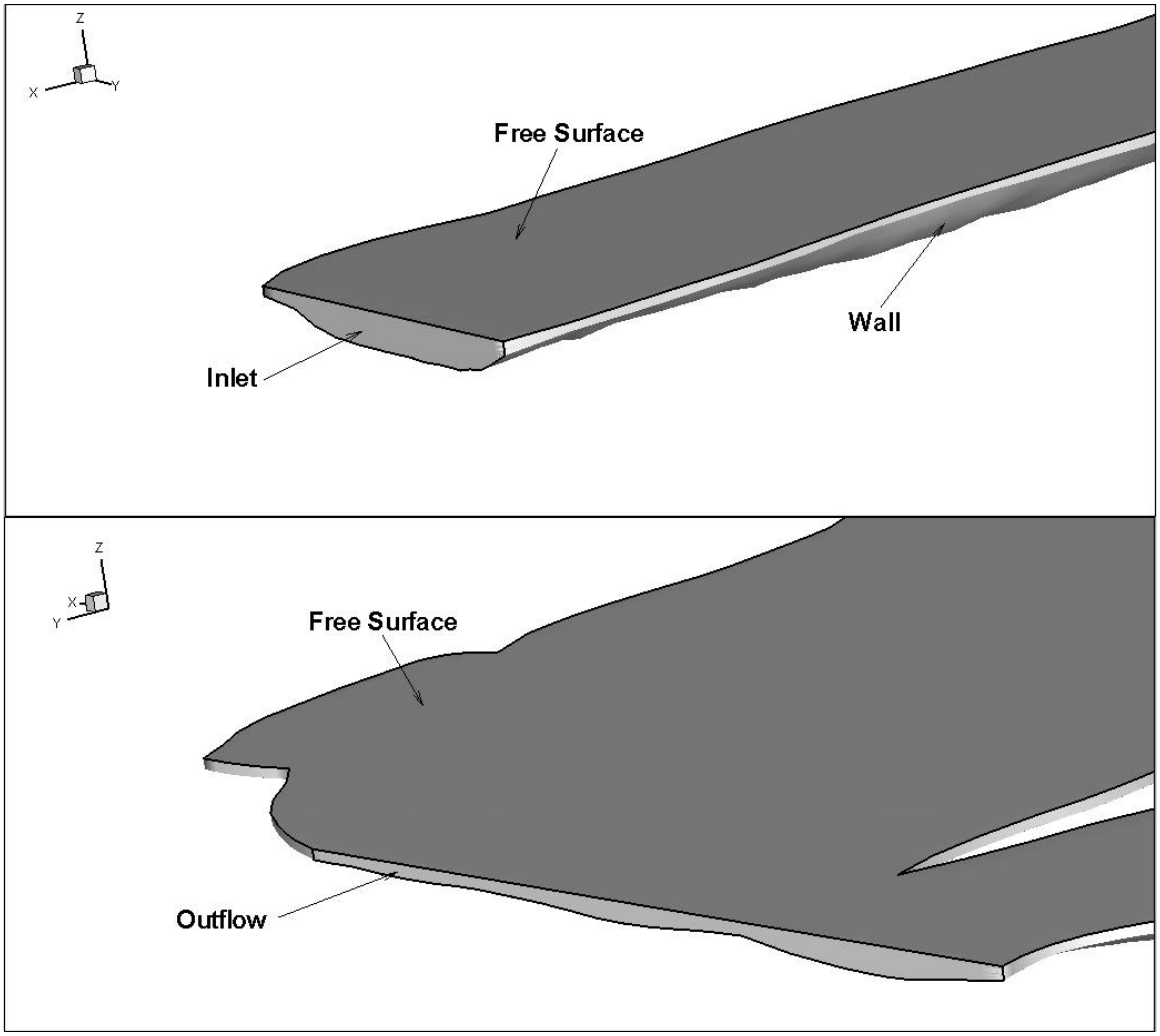

Figure 4-15 Mid-Snake River inflow and outflow domain 3D view showing boundary conditions

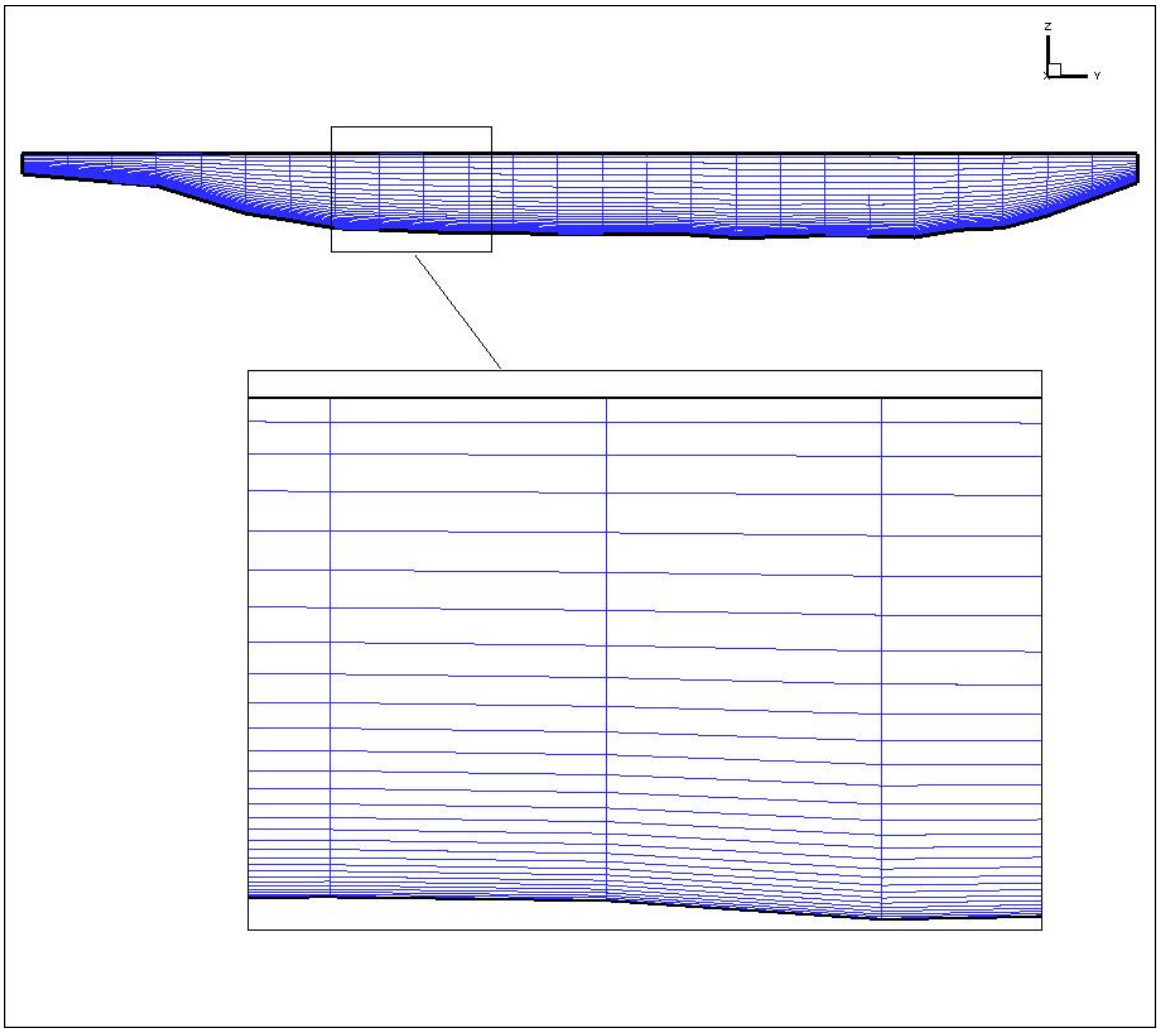

Figure 4-16 Close-up view of inflow cross-section of Mid-Snake River illustrating grid clustering near the river bottom

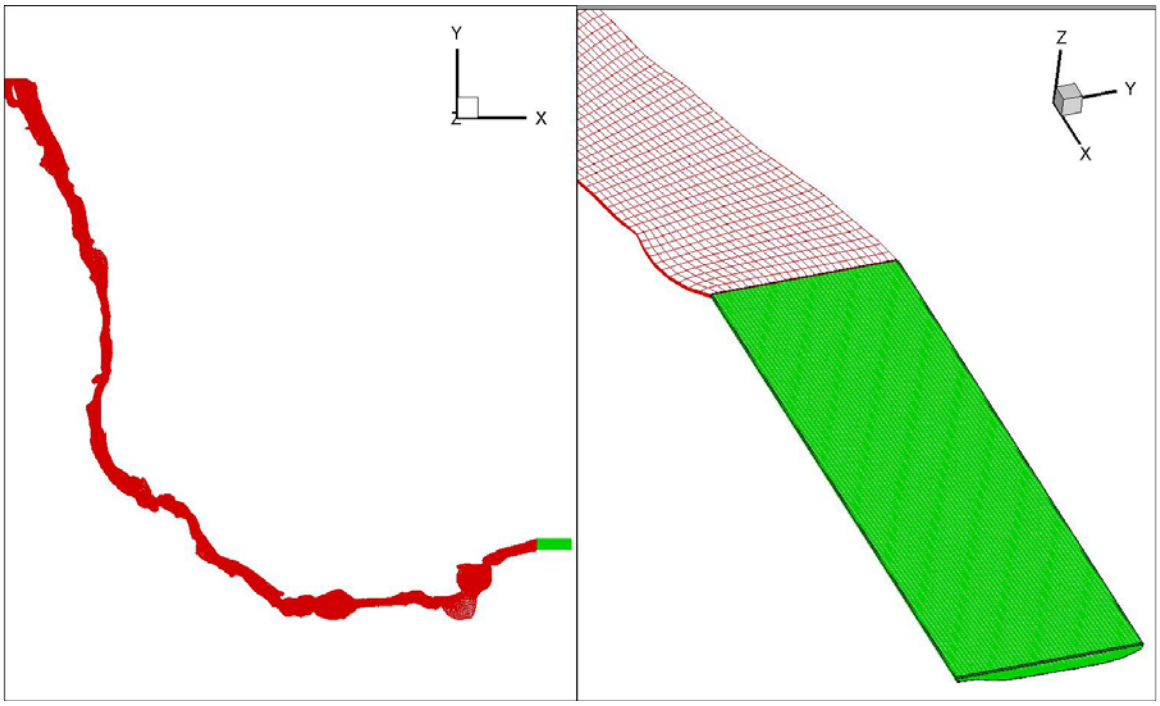

Figure 4-17 3D illustration of straight channel for periodic boundary condition at the inlet for low flow condition

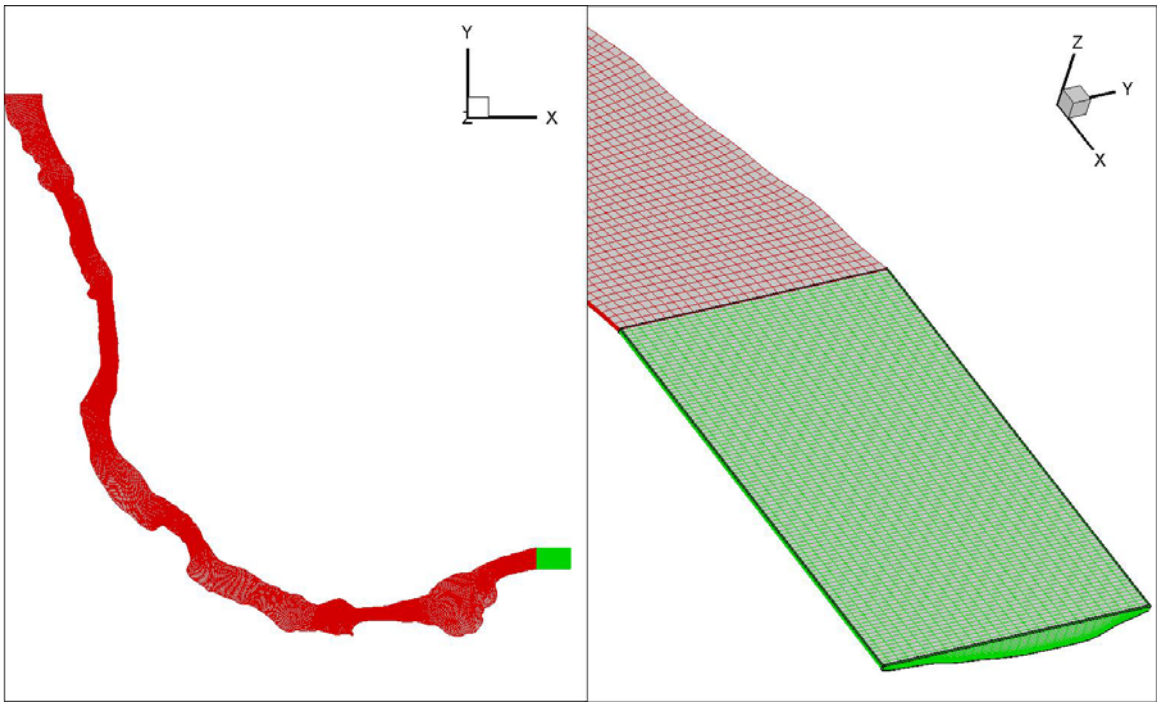

Figure 4-18 3D illustration of straight channel for periodic boundary condition at the inlet for high flow condition

CHAPTER V

RESULTS AND DISCUSSIONS

5.1 Hydrodynamic Solution

The first numerical modeling task was to solve the flow field for the entire domain. Hydrodynamic solutions from the model were then used to calculate organism distribution over the river reach.

Figure 5-1 is a plan view of the entire modeled area with velocity contours at the free surface for a flow rate of 7,700 cfs. The velocity distribution along the main stem varies from approximately 0.1 fps to about 10 fps. The river reach is then divided into three sections. Close up plan views of the streamtraces and river bed elevation contours for each sub-portion are shown in figure 5-2. Streamlines simulation results illustrate a complex flow field due to the irregular bathymetry and river bank. Several large vortices formed along the river reach which may capture fish eggs and snails. A large surface vortex found near the discrete phase particle release region may influence deposition patterns and particle distributions. A detailed view of features of vortices in the particle release and deposit region is shown in figure 5-3.

Figures 5-4 to 5-6 show corresponding velocity contours and streamtraces at the free surface for a flow rate of 51,500 cfs. The maximum velocity increases by approximately 2 fps from the low to high flow conditions, as shown in figure 5-4. The streamlines for the high flowrate condition shows a pattern similar on the main channel to that of the low flow condition, as shown in figure 5-5. A change in the flow field was found near the river bank due to shore line shape differences for the two cases. No major vortex was found near the particle release and deposit area, as is illustrated in figure 5-6.

5.2 Turbulence Model Comparison

Particle dispersion is a function of turbulence level. Turbulent viscosity varies due to inflow conditions and the turbulence models used in the study. The standard k-epsilon model and RSM were used to evaluate turbulence model effects on the flow field.

Figure 5-7 is a plan view of turbulent viscosity 6.56 ft below the free surface using the standard k-epsilon turbulence model. A high turbulence viscosity area, approximately 135 lb/ft s, was found near the vortex, close to area A. Less turbulent viscosity was predicted using RSM, as illustrated in figure 5-8. The predicted turbulent viscosity variation between the two models was as much as 55 lb/ft s.

To evaluate effects of the turbulence anisotropy, ww Reynolds stresses, calculated with the two turbulent models, were studied for both flow conditions. ww Reynolds stress predicted with the k-epsilon model can be estimated under the isotropy assumption by $ww = \frac{2}{3}k$. A vertical cross-section of ww Reynolds stress contours for the low flowrate condition, using the standard k-epsilon and RSM, is shown in figure 5-9. The cross-section is 60 ft downstream of the inflow domain, close to the White Sturgeon eggs and Bliss Rapids snails predicted deposition area (figure 5-7). Two high ww Reynolds stress regions are found. One is on the main stem and the other is close to the southern bank. Comparing the above simulations reveals ww Reynolds stresses much lower under RSM than with the standard k-epsilon model.

Corresponding turbulent viscosity and vertical Reynolds stress contours are plotted for the standard k-epsilon and RSM at the high flow condition in figures 5-10 to 5-12. Patterns found in these figures match those for the low flow condition. In river channel flows, vertical velocity fluctuation w' and vertical Reynolds stress ww are lower than their corresponding horizontal components. Therefore, turbulent viscosity predicted by the k-epsilon model is over-estimated for river channel flow compared to RSM predictions. Turbulent dispersion is consequently lower when RSM is used rather than the k-epsilon model. The above comparisons suggest that particle trajectory and

distribution predictions, which depend upon the turbulence, might be affected by the choice of turbulence model.

5.2.1 Fish Eggs Simulation

To study their distribution over the river reach, White Sturgeon egg trajectories and distributions were calculated.

Differences in deposition point and residence time due to varied inflow condition are studied. Figures 5-13 and 5-14 show final settled positions and residence times for particles under low and high flow conditions. Differences in distance traveled are caused by variations in flow velocity magnitude, as illustrated in figures 5-1 and 5-4. Particles released close to the river bank generally settled early, due to the shallower waters near the river shore. Particles settling near the southern bank became trapped by the eddies described earlier.

An analysis of different residence times and travelling distances was performed using the two turbulence models. Plan views of particle deposition positions and residence times predicted by the turbulence models are shown in figures 5-15 and 5-16. The different distances traveled are caused by the varied turbulent viscosities predicted by the two turbulent models. As mentioned above, particles tend to travel farther when turbulent dispersion is higher.

5.2.2 Snail Simulation

Trajectories and deposition locations for Bliss Rapids snails were calculated. Final settled positions are illustrated in figures 5-17 and 5-18 for low and high flow conditions. Snails have a higher density than sturgeon eggs therefore travel less distance under a given flow condition. Simulated results of the distances traveled by snails for both flow conditions with the two different turbulence models were analyzed. Histograms for travel distance versus deposition percentage are shown in figures 5-19 to 5-20. The deposition peak near the particle release area is the result of shallower waters near the

bank and vortices near the release region, which trap particles. The general deposit patterns are similar for the k-epsilon model and RSM. Notable differences in particle distribution were captured by the two turbulent models. The difference in the overall travel distance is suspected to be a function of the varied turbulent viscosities predicted by the two turbulent models. According to Wright et al. (2004), the accuracy of the predictions increases with the level of complexity of the turbulence model used, the RSM is assumed more accurately simulated turbulent viscosity and was applied to the following simulation cases.

5.3 Random Walk Model Effect

Turbulent dispersion effects on White Sturgeon egg distributions were evaluated. Deposition positions under RSM for low flow and high flow conditions are shown in figures 5-21 and figure 5-22. Contours show velocity magnitudes close to the river bed. Particle distribution over the river bed is more even when turbulent dispersion is taken into account. The RWM includes a random coefficient to calculate velocity fluctuation when integrated the trajectory. Turbulence effects on particle trajectories have greater statistical and realistic meaning and are therefore included in the following simulation cases.

5.4 SSR Boundary Condition

Effects of SSR boundary condition on the spatial distribution of fish eggs and snails are evaluated. Low flow conditions are used for the following cases.

A plan view of deposition position with the bed shear stress magnitude contour is shown in figure 5-23. Particles in black represent fish eggs settled positions under trap boundary condition. Particles in white represent fish eggs settled positions under SSR boundary condition. In contrast to the more evenly distributed Fluent default trap boundary condition results, fish eggs under SSR boundary condition settled in a pattern more concentrated near the low shear area. Particles traveled longer under SSR boundary

condition because they are reflected back to the flow when the local shear stress is high enough at the boundary layer. A histogram comparison of boundary conditions is shown in figure 5-24. The trap boundary condition predicted a relatively low deposition rate near the particle release area. Under the SSR condition, particles reflected in that region are trapped by the vortex and returned to their release area due to the presence of eddies. A low settling rate predicted by SSR condition over the main channel at a distance of 200 to 650 ft. It is caused by high shear stresses in this region. Particles are reflected back to the flow upon contact with high shear stress areas. The settling rate peak a on the histogram 5-24 is the result of a low shear area on the river bed at a distance of 700 ft, illustrated by area A in figure 5-23.

A similar settling distribution plan view for snails is shown in figure 5-25. The streamtrace plot, shown in figure 5-26, illustrates the eddy effects on the release region. A histogram of snails under different boundary conditions is shown in figure 5-27. Snail distributions over the river bed follow a pattern similar to those for fish eggs. Lower deposition percentages are predicted for SSR boundary versus trap conditions, if local shear is relatively high (Figure 5-25). Higher deposition percentages are predicted for the SSR condition if local bed shear is low, as illustrated by deposition peak b on histogram 5-27 and deposition area B in figure 5-25. A low shear region, about 250 ft from the release area, results in the deposition peak c on histogram 5-27 and deposition area C in figure 5-25.

5.5 Analysis of SSR and SSS Boundary Conditions

Further bed shear stress boundary condition analysis was performed for this study. Physical properties of Bliss Rapids snails were used for the discrete phase model.

A histogram for deposition percentage as a function of travel distance was plotted under SSR and SSS boundary conditions in figure 5-28. A similar deposition pattern was obtained for the two boundary conditions, but the general curve shape was obtained from

the SSS condition was shifted backward in space slightly. This is due to the fact that particles can be resuspended and travel a greater distance.

Figure 5-29 shows the average travel distance of snails for the three boundaries studied: trap, SSR, and SSS. An average travel distance of 108.60 ft (33.11 m) was obtained under the Fluent default trap boundary condition. An approximately further 8.2 ft (2.5 m), 7.55% in average particle distance traveled was obtained using SSR. Still another 8.2 ft (2.5 m), 7.02% in average travel is added using SSS.

Particle travel distance depends on bed shear stress distribution. Selection of the critical bed shear stress value is thus a key factor for the SSR and SSS boundary conditions. Sensitivity of the selected critical bed shear stress value is shown by the histogram in figure 5-30. It illustrates deposition percentage as a function of particle travelling distance with critical bed shears of 0.06, 0.13 and 0.25 lb/ft^2. Results show that travel distance is sensitive to the selected critical bed shear stress value. This is especially the case when the bed shear stress range is large and unevenly distributed over the river bed.

Figure 5-31 shows the average distance traveled for the three selected critical bed shear stress value utilized in the sensitivity analysis. An average of 8.7% difference in travel distance was obtained by doubling and halving the selected critical shear stress. Particle behaviors under larger critical shear stress resemble those predicted with the Fluent default trap condition. Particles under smaller critical shear stress behave more like those modeled by the Fluent reflect boundary condition.

Simulation results for SSR and SSS boundary conditions show discrete phase particles redistributed spatially over the river bottom based on bed shear stress. However, the average travel distance predictions are within the range of previous measurements by McDonald et al., with differences less than 10%. These results validate this new boundary condition for simulating interactions between aquatic organisms and the river

bed. Therefore, the results indicate it is seems appropriate to utilize this new boundary condition to simulate the interaction between aquatic organisms and river bed.

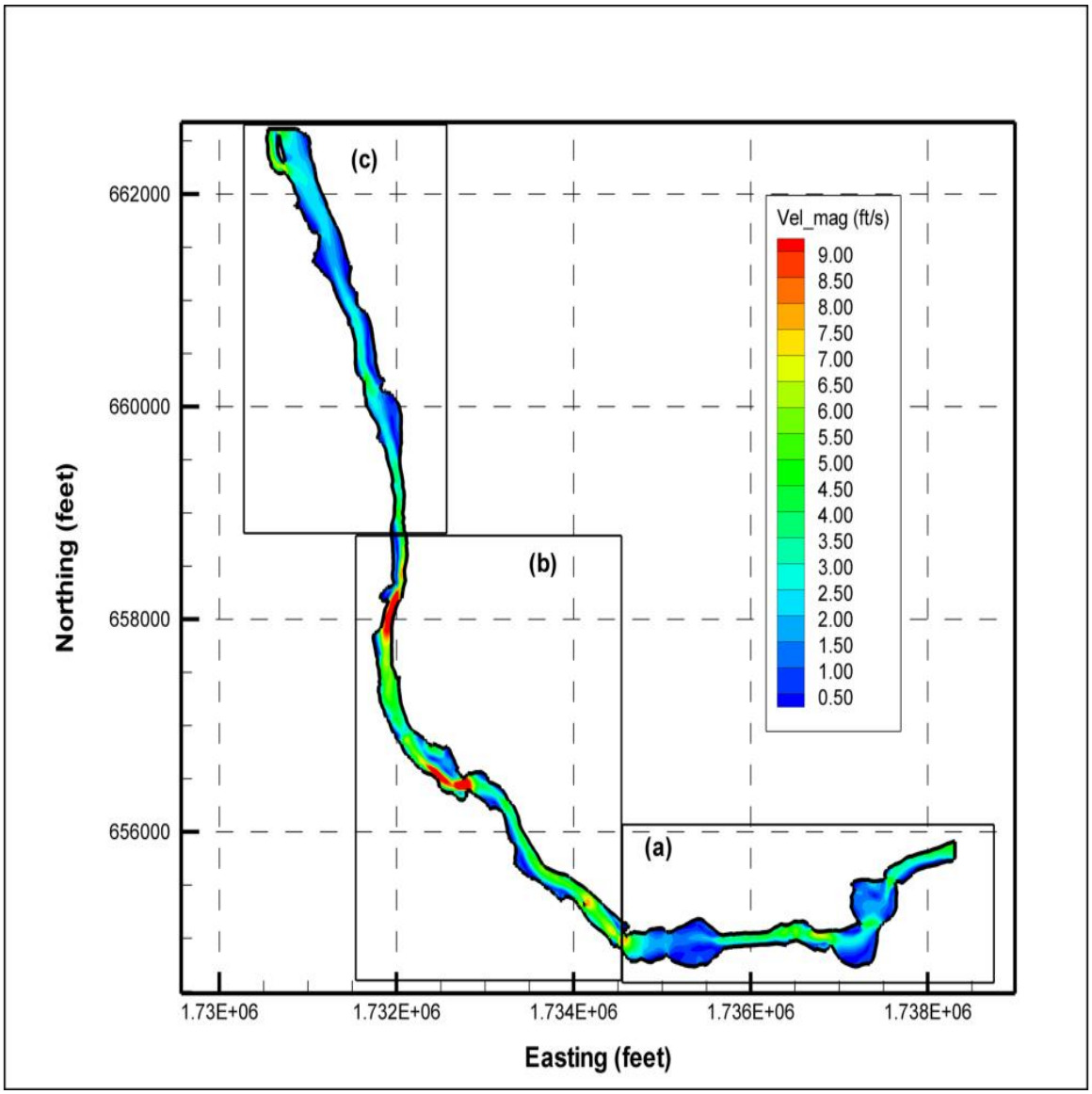

Figure 5-1: Velocity contours at the free surface for low flow condition

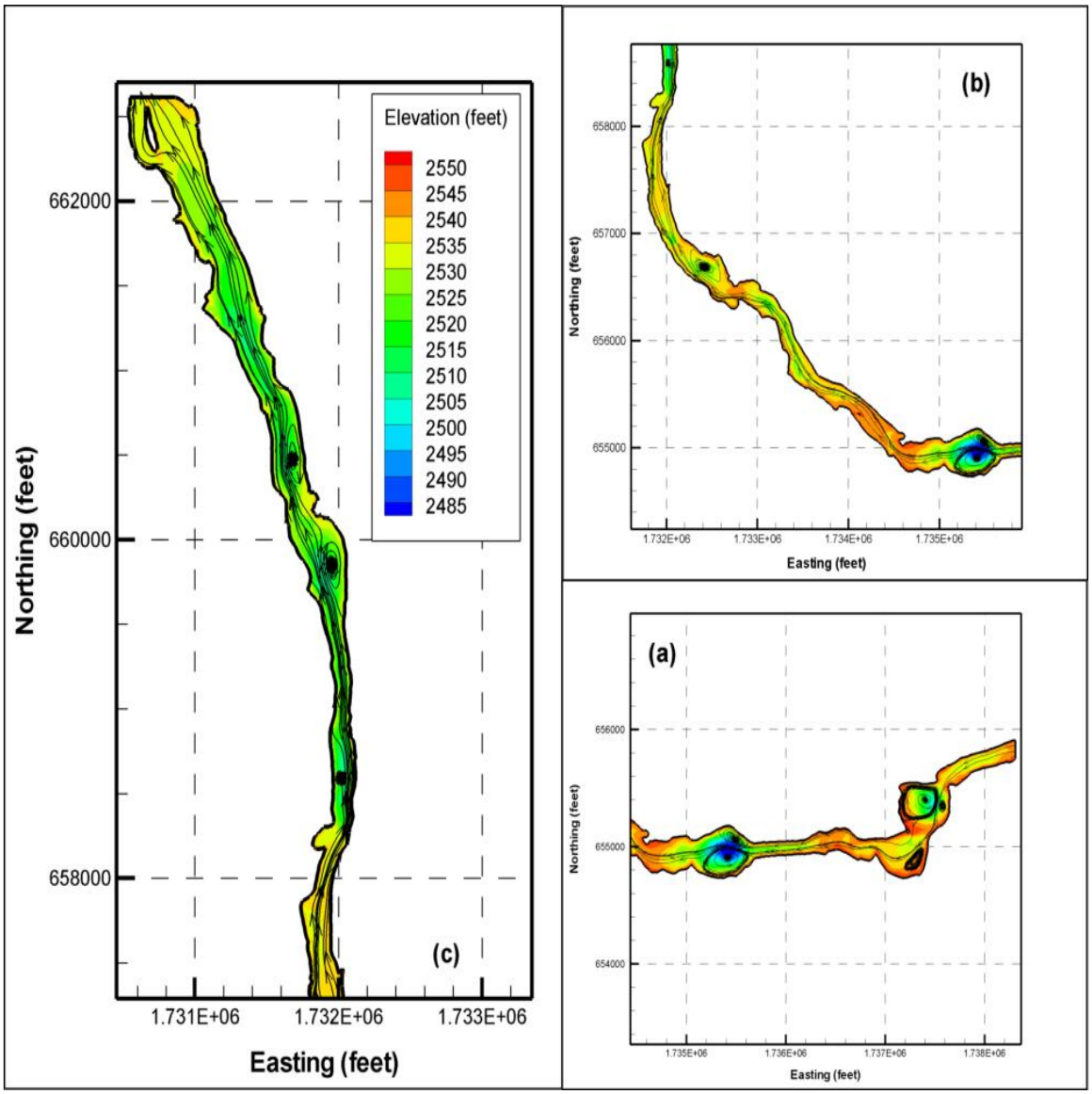

Figure 5-2: Streamlines at the free surface for low flow condition

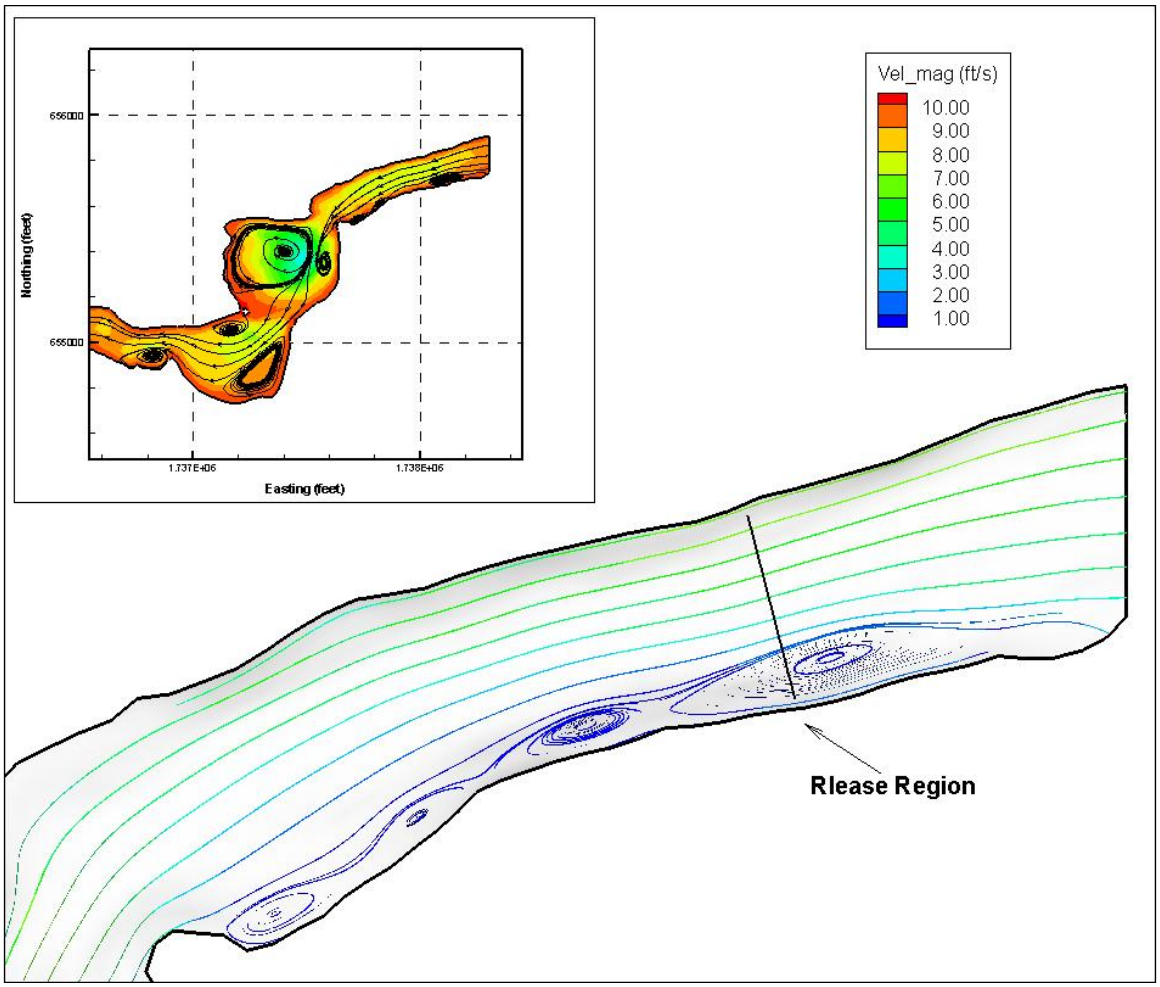

Figure 5-3: Streamlines colored by velocity magnitude near the particle release region for low flow condition

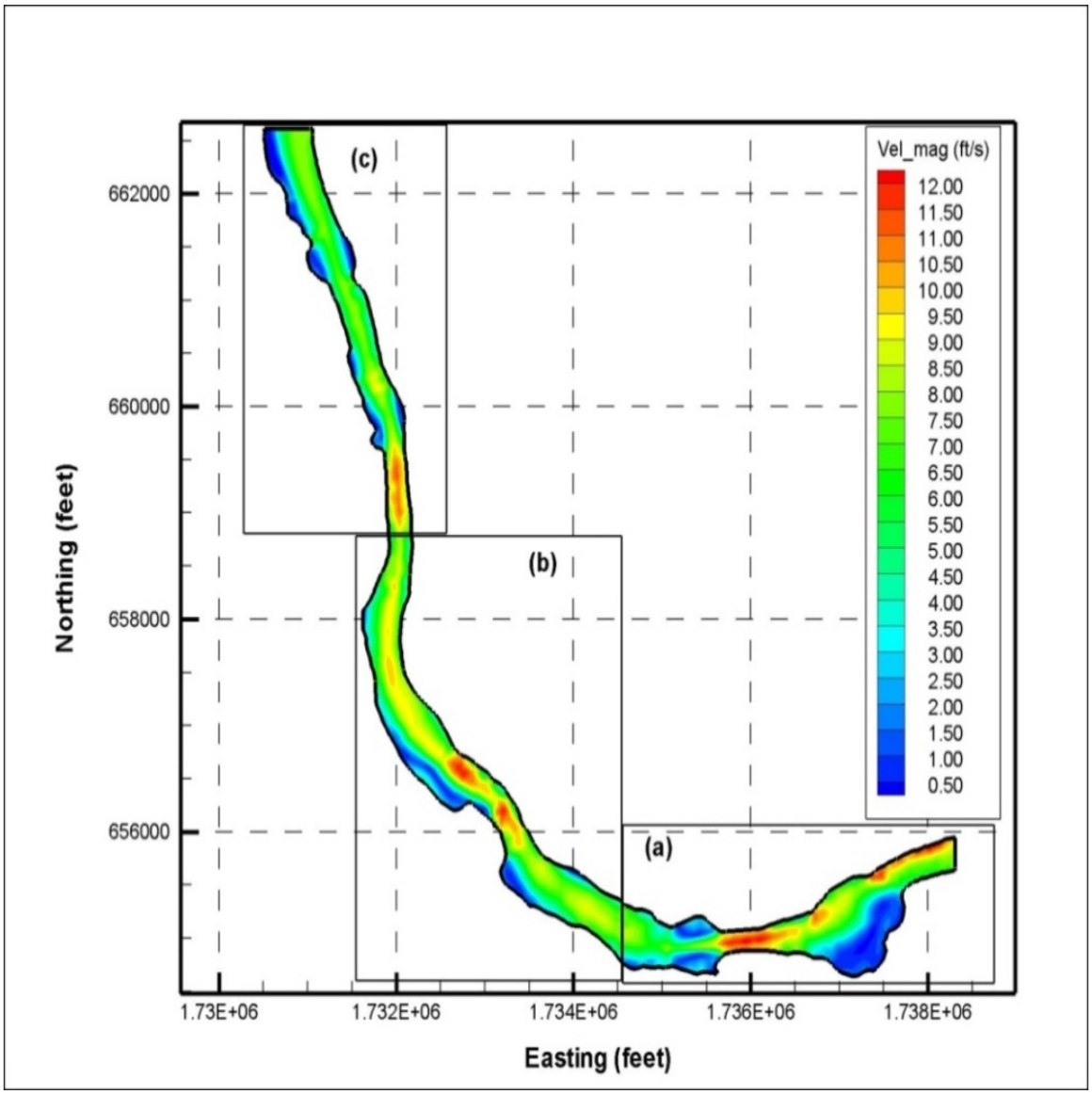

Figure 5-4: Velocity contours at the free surface for high flow condition

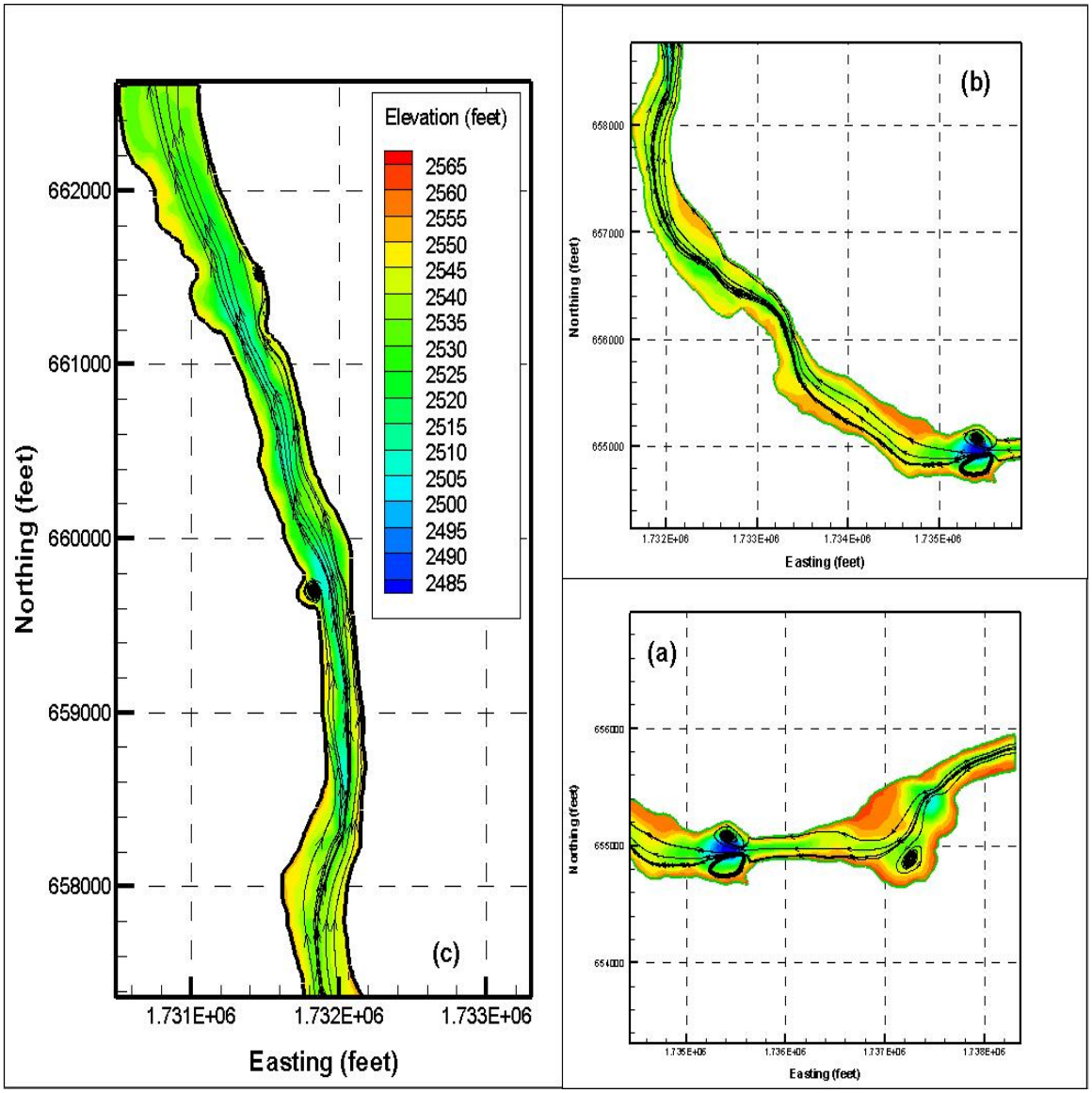

Figure 5-5: Streamlines at the free surface for high flow condition

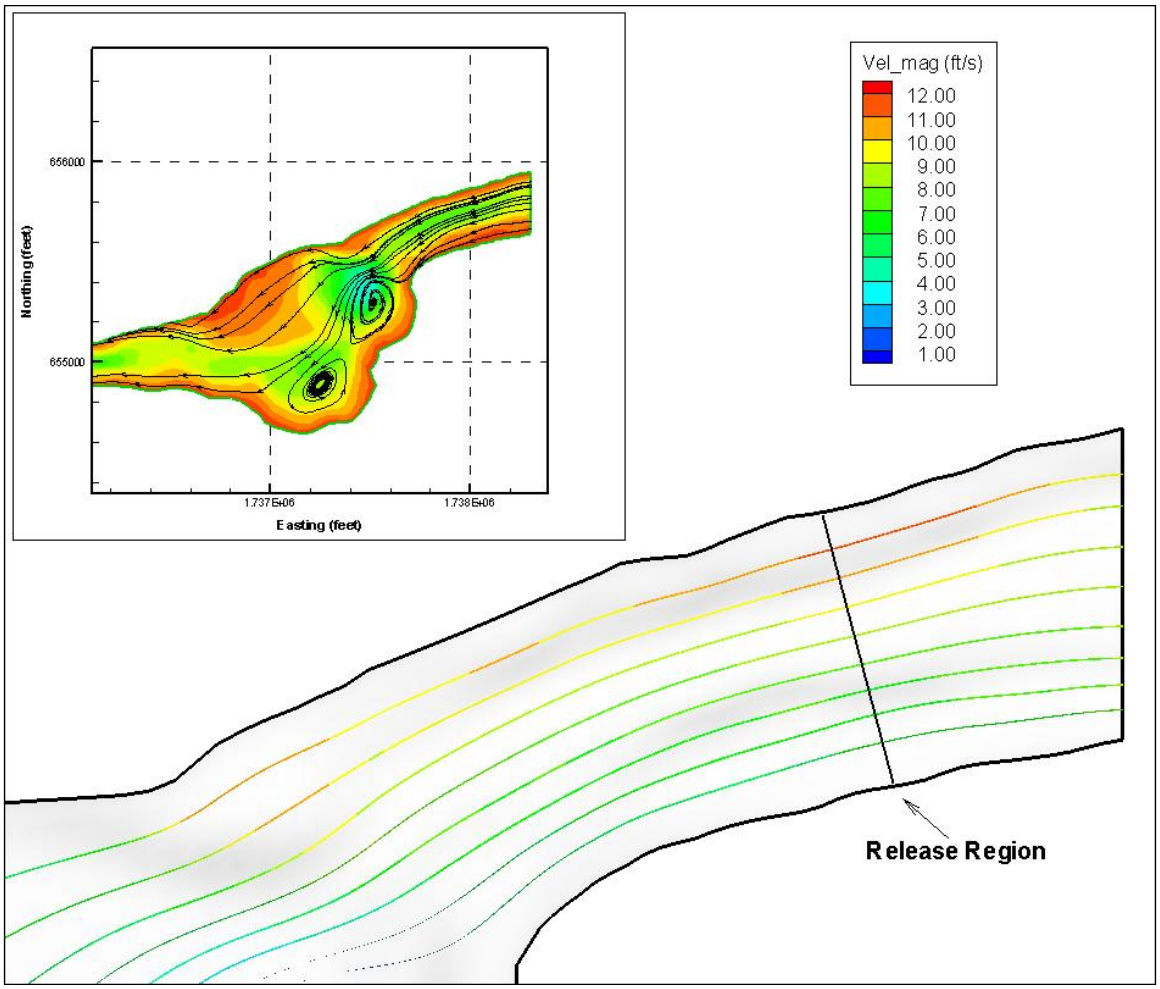

Figure 5-6: Streamlines colored by velocity magnitude near the particle release region for high flow condition

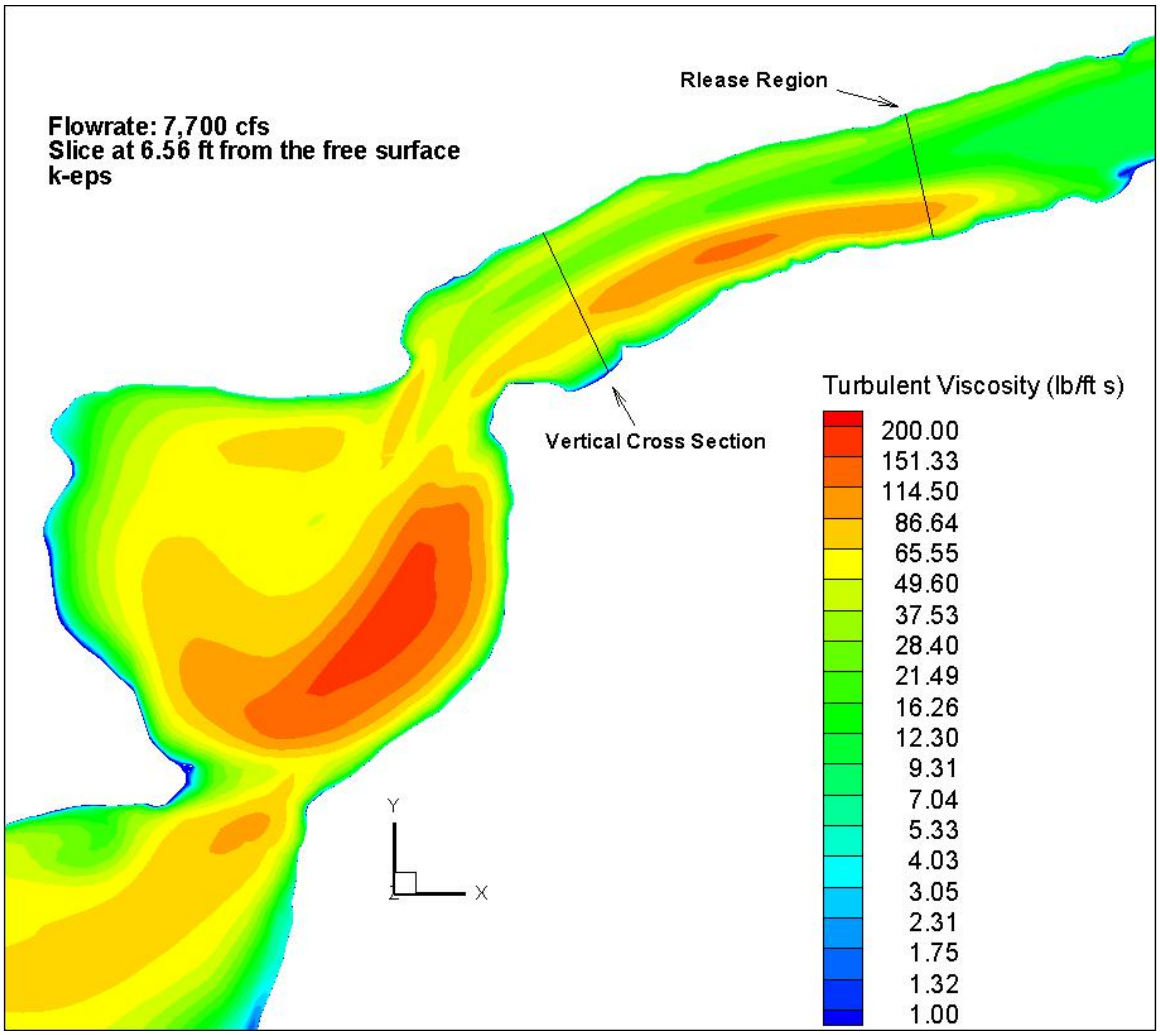

Figure 5-7: Turbulent Viscosity contours located at depth of 6.56 ft with k-epsilon model for low flow condition

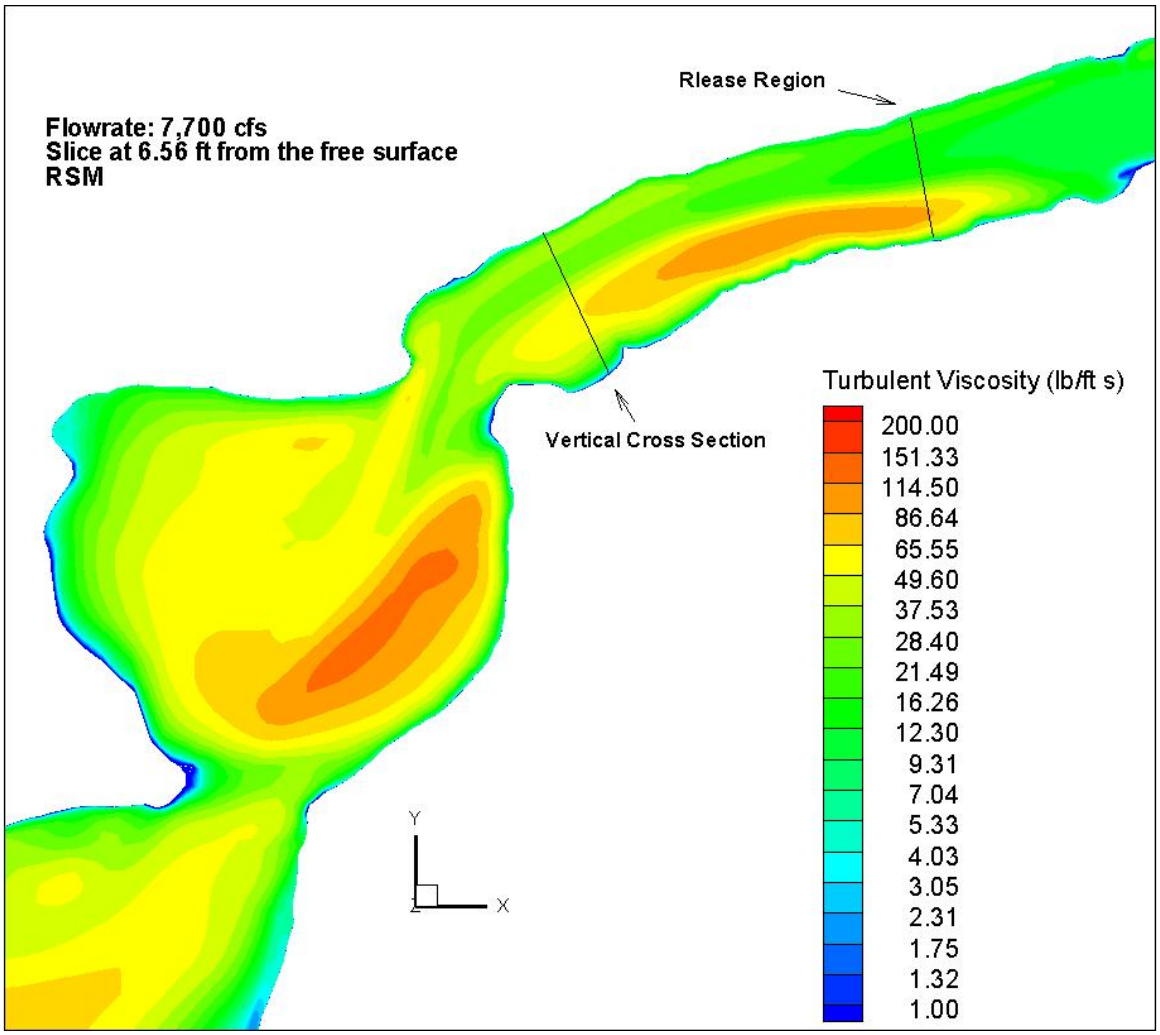

Figure 5-8: Turbulent Viscosity contours located at depth of 6.56 ft with RSM for low flow condition

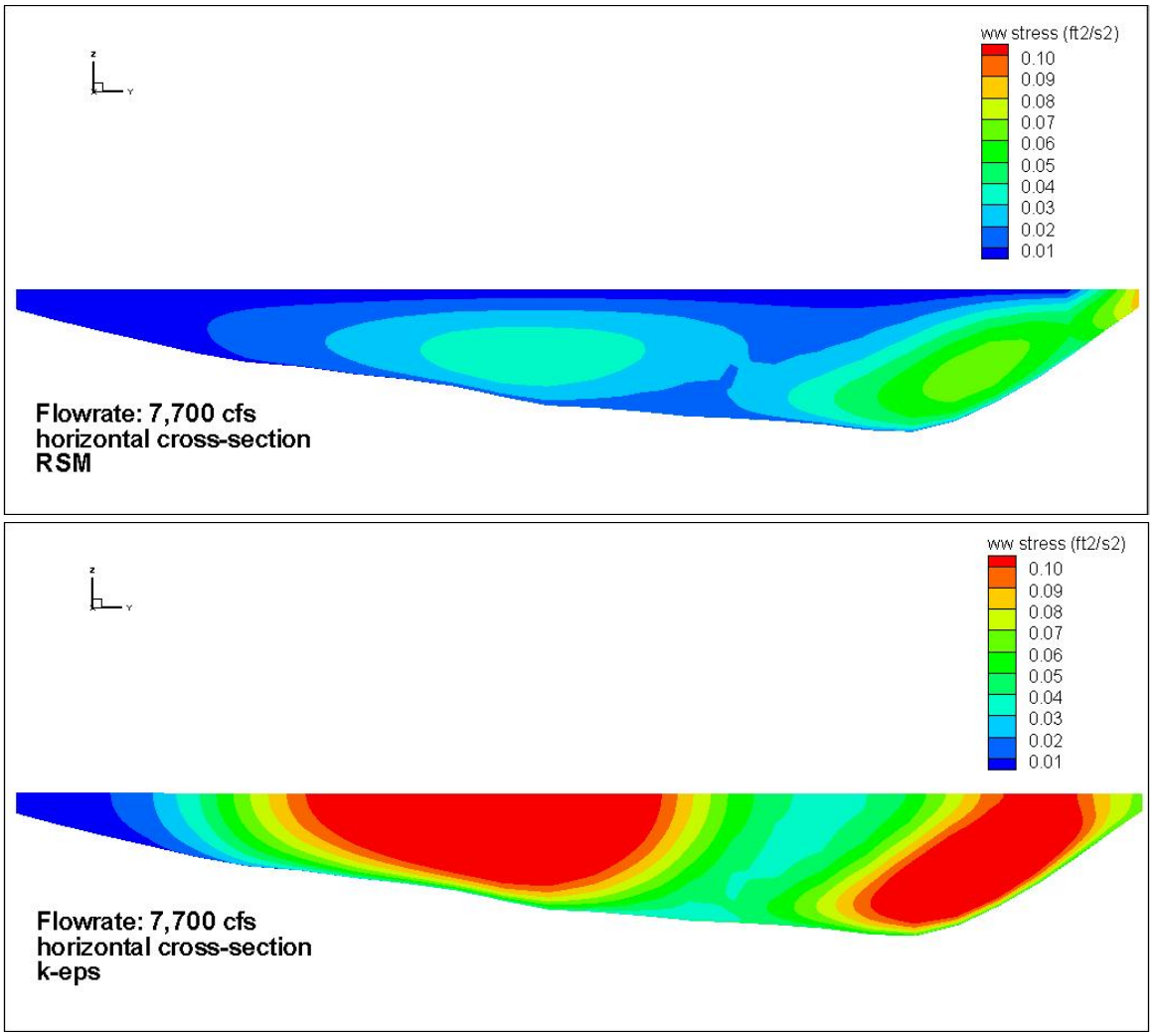

Figure 5-9: Vertical cross section of ww Reynolds stresses contours with k-epsilon model and RSM for low flow condition. The cross section located 60 ft from the inflow domain

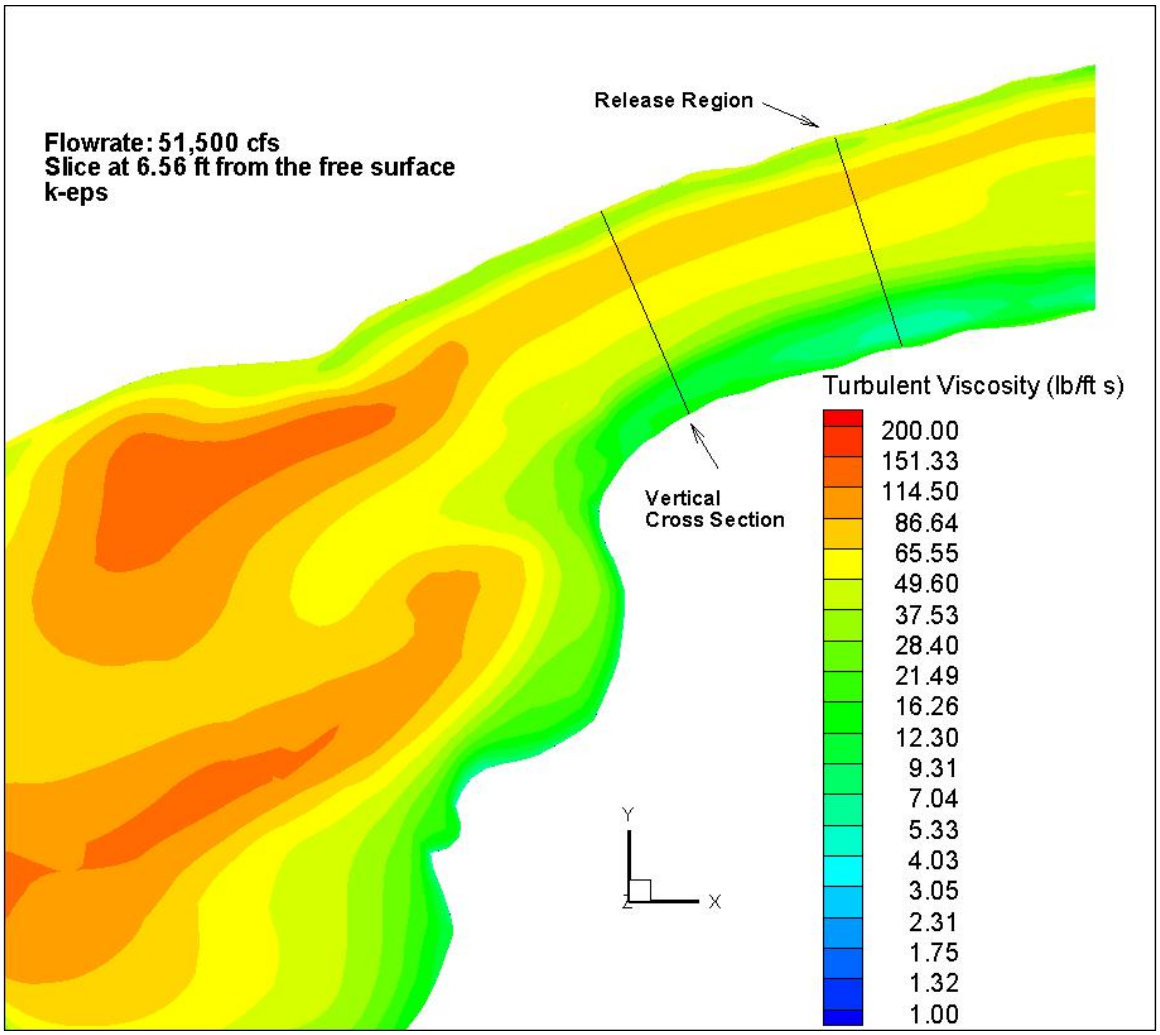

Figure 5-10: Turbulent Viscosity contours located at depth of 6.56 ft with k-epsilon model for high flow condition

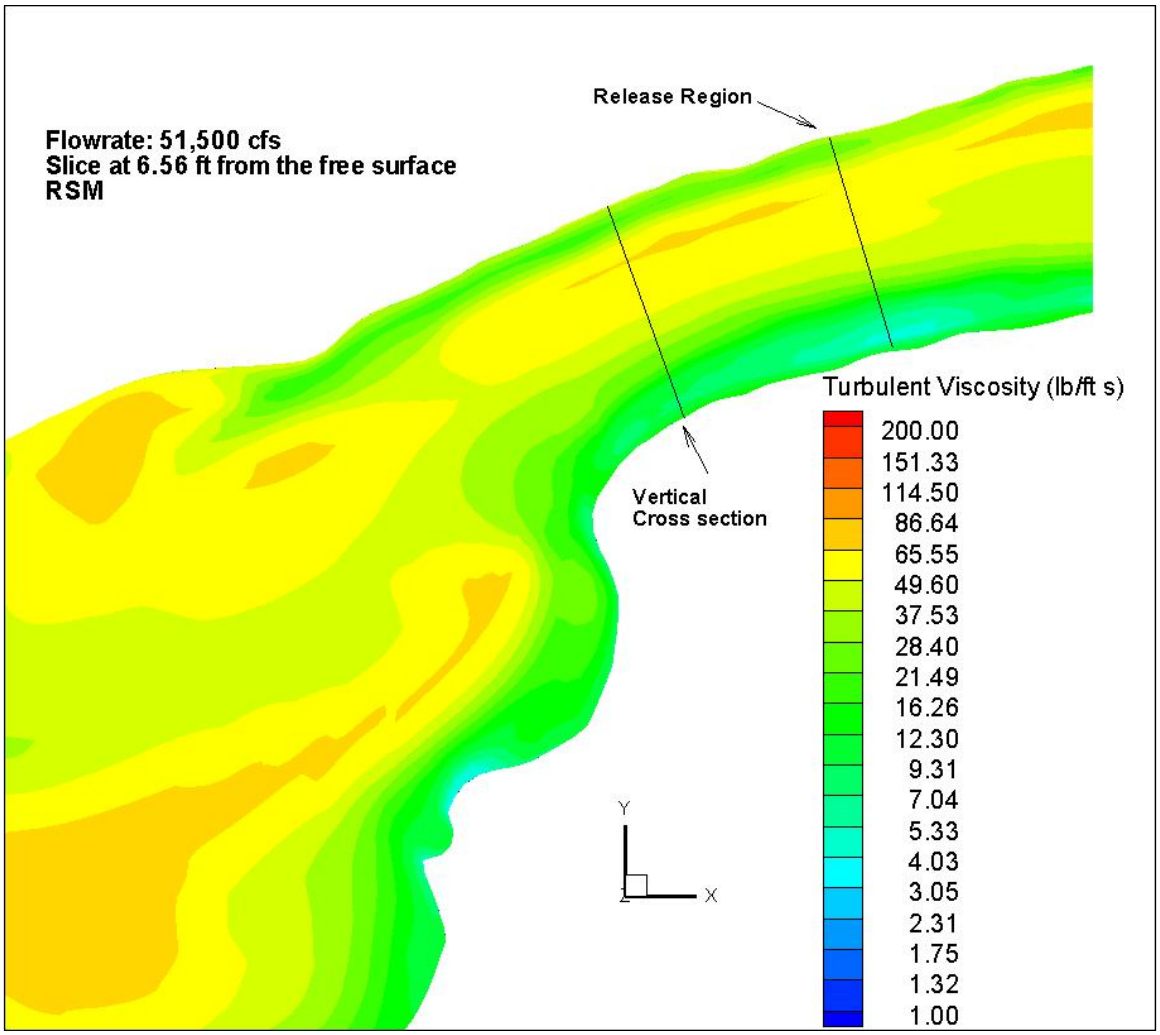

Figure 5-11: Turbulent Viscosity contours located at depth of 6.56 ft with RSM for high flow condition

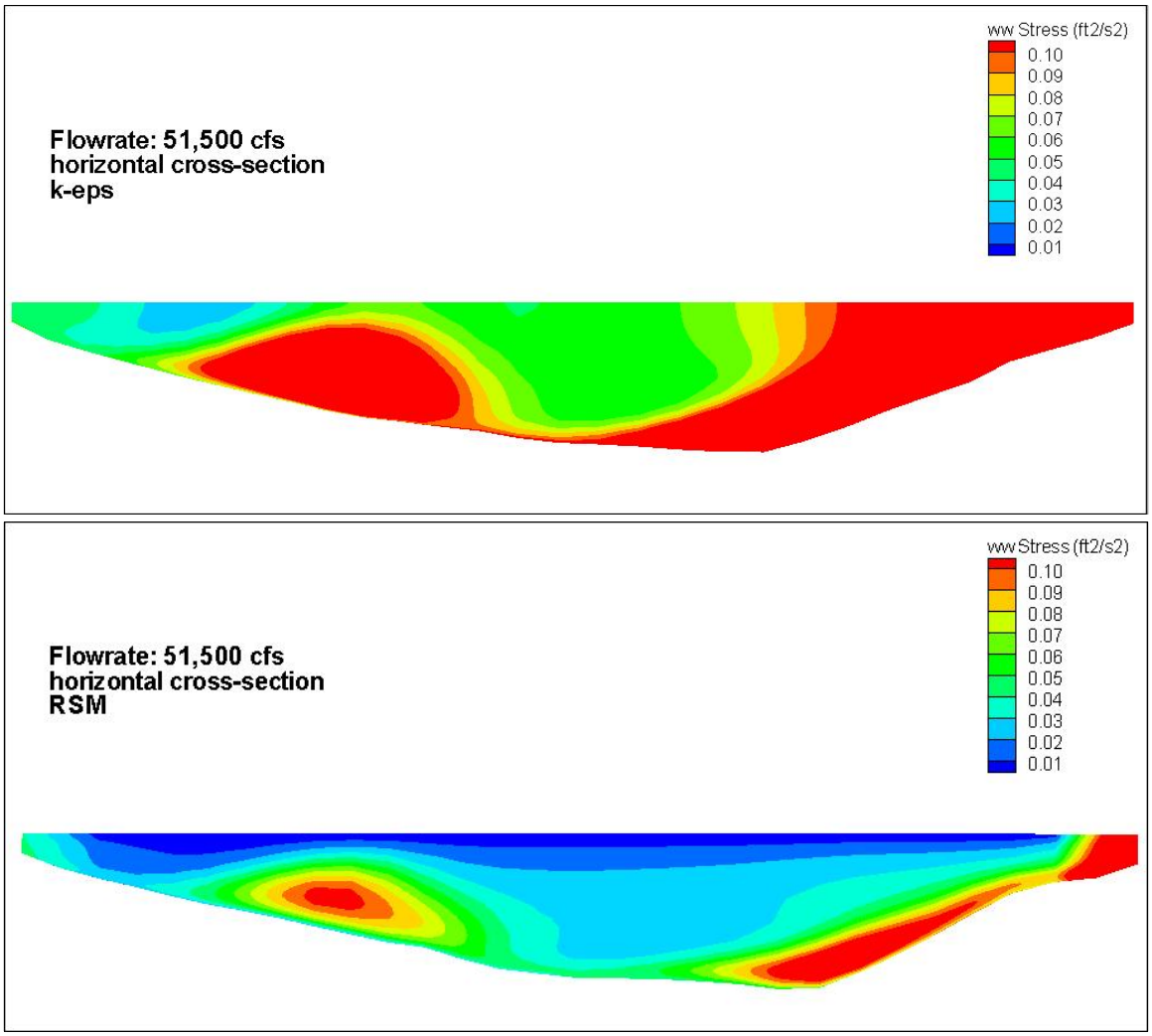

Figure 5-12: Vertical cross section of ww Reynolds stresses contours with k-epsilon model and RSM for high flow condition. The cross section located 60 ft from the inflow domain

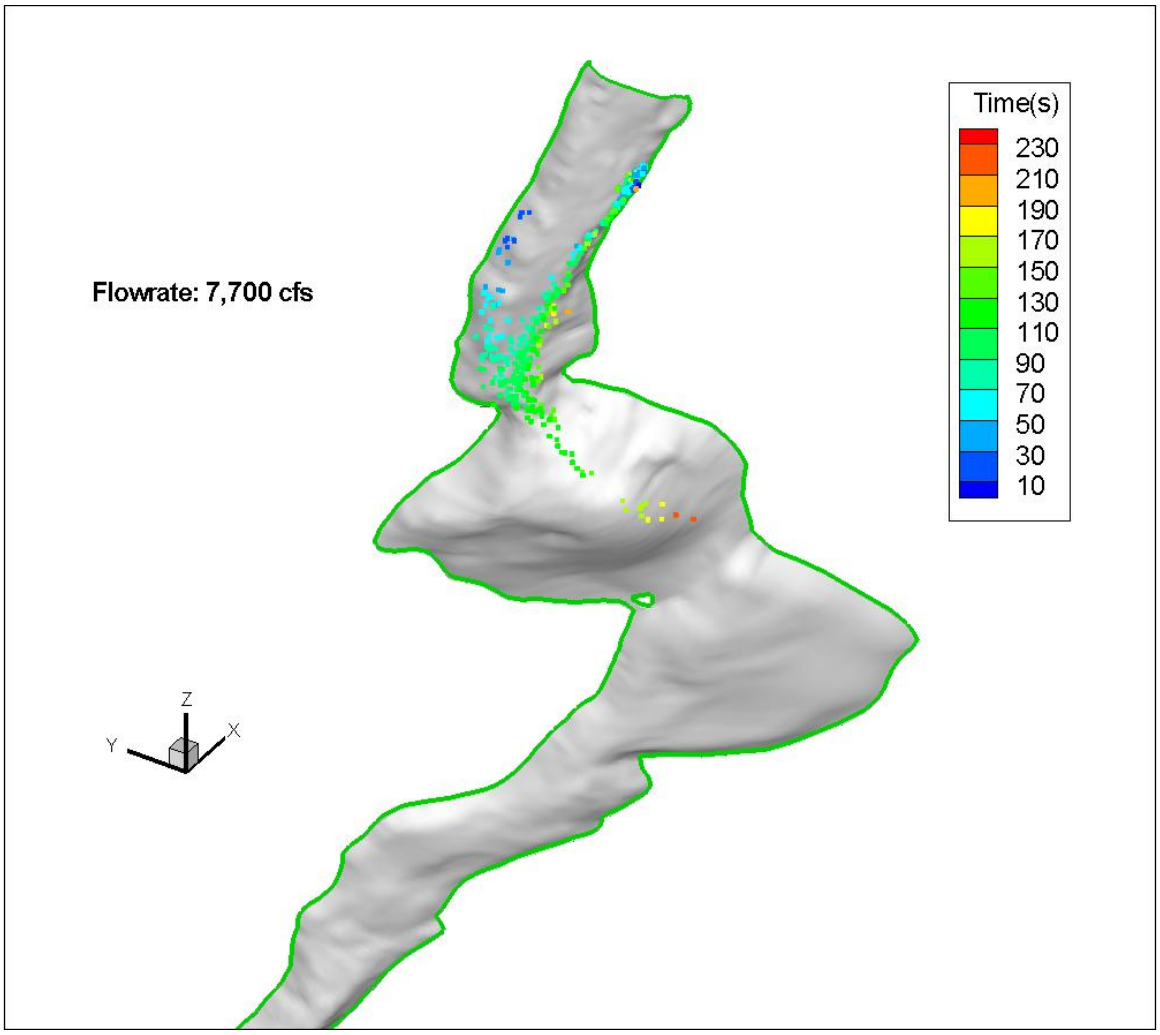

Figure 5-13: Spatial distributions of fish eggs for low flow condition. Particle colored by residence time

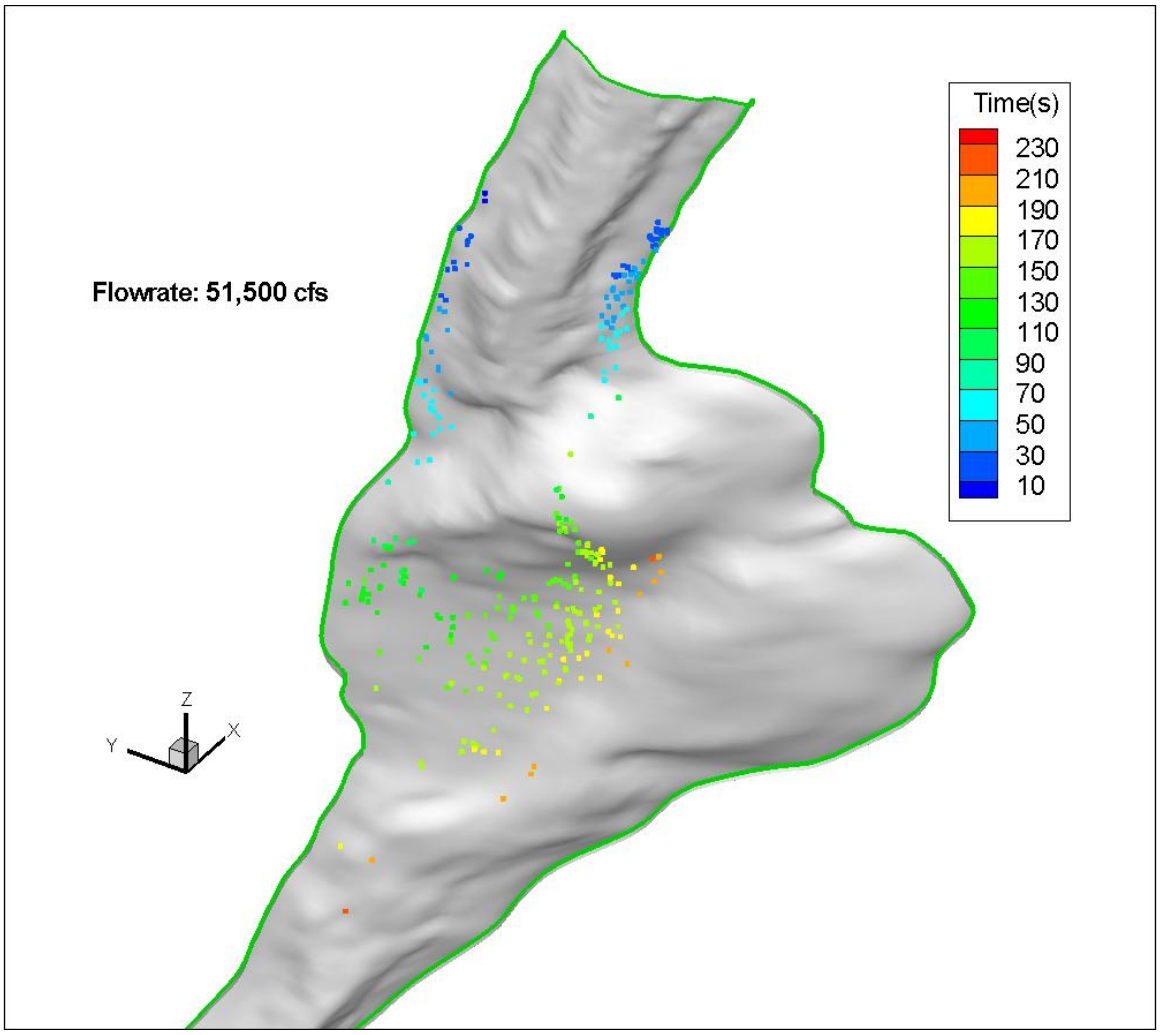

Figure 5-14: Spatial distributions of fish eggs for high flow condition. Particle colored by residence time

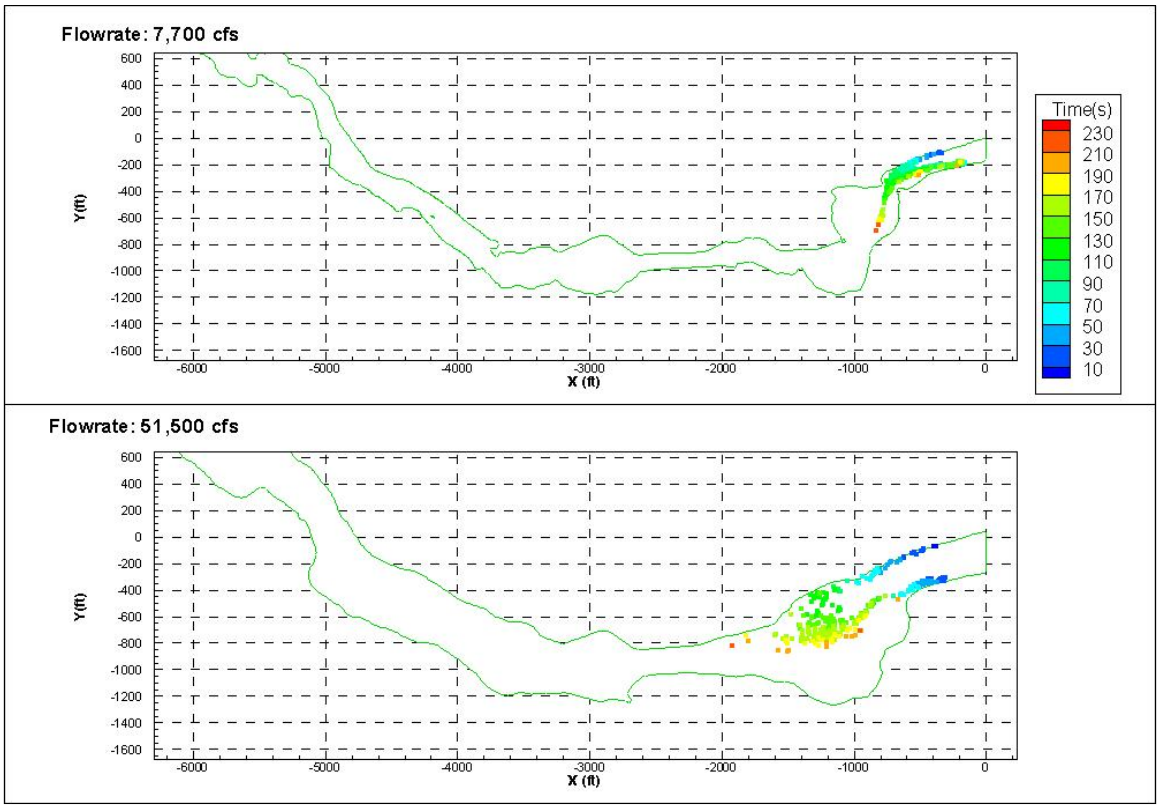

Figure 5-15: Spatial distributions of fish eggs with k-epsilon turbulence model for two flow conditions. Particle colored by residence time.

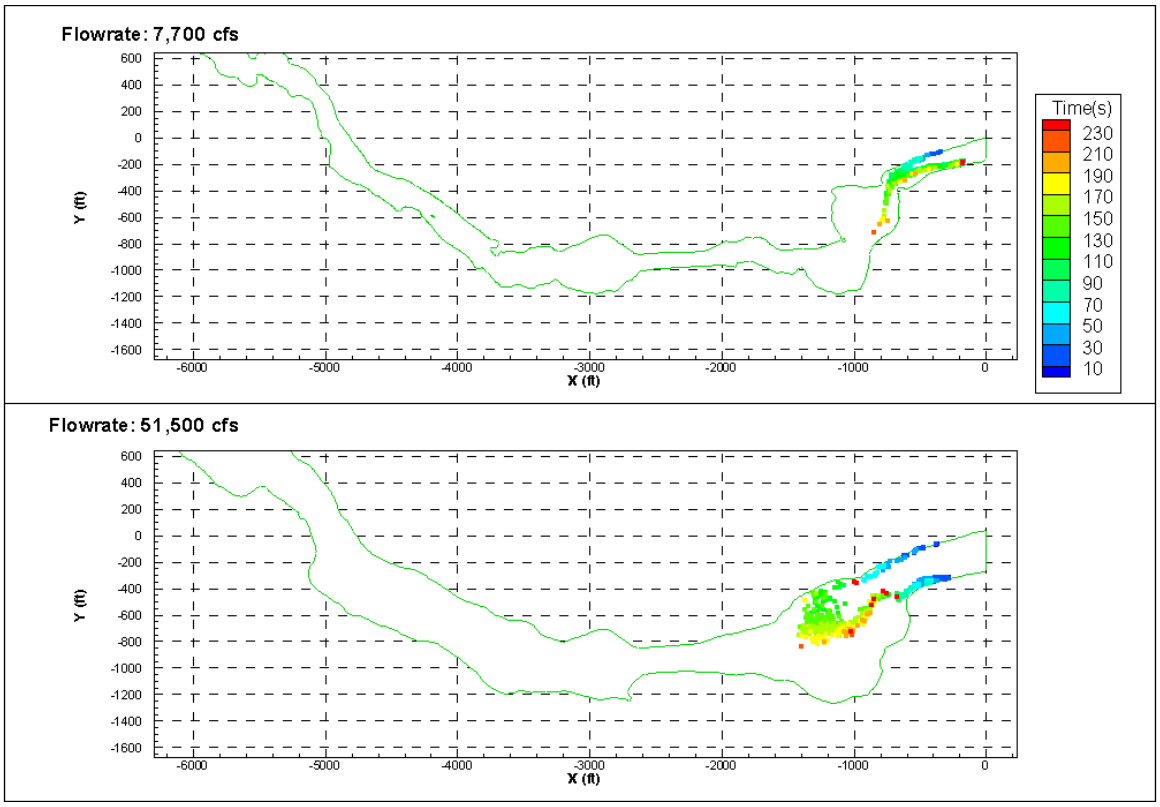

Figure 5-16: Spatial distributions of fish eggs with RSM for two flow conditions. Particle colored by residence time.

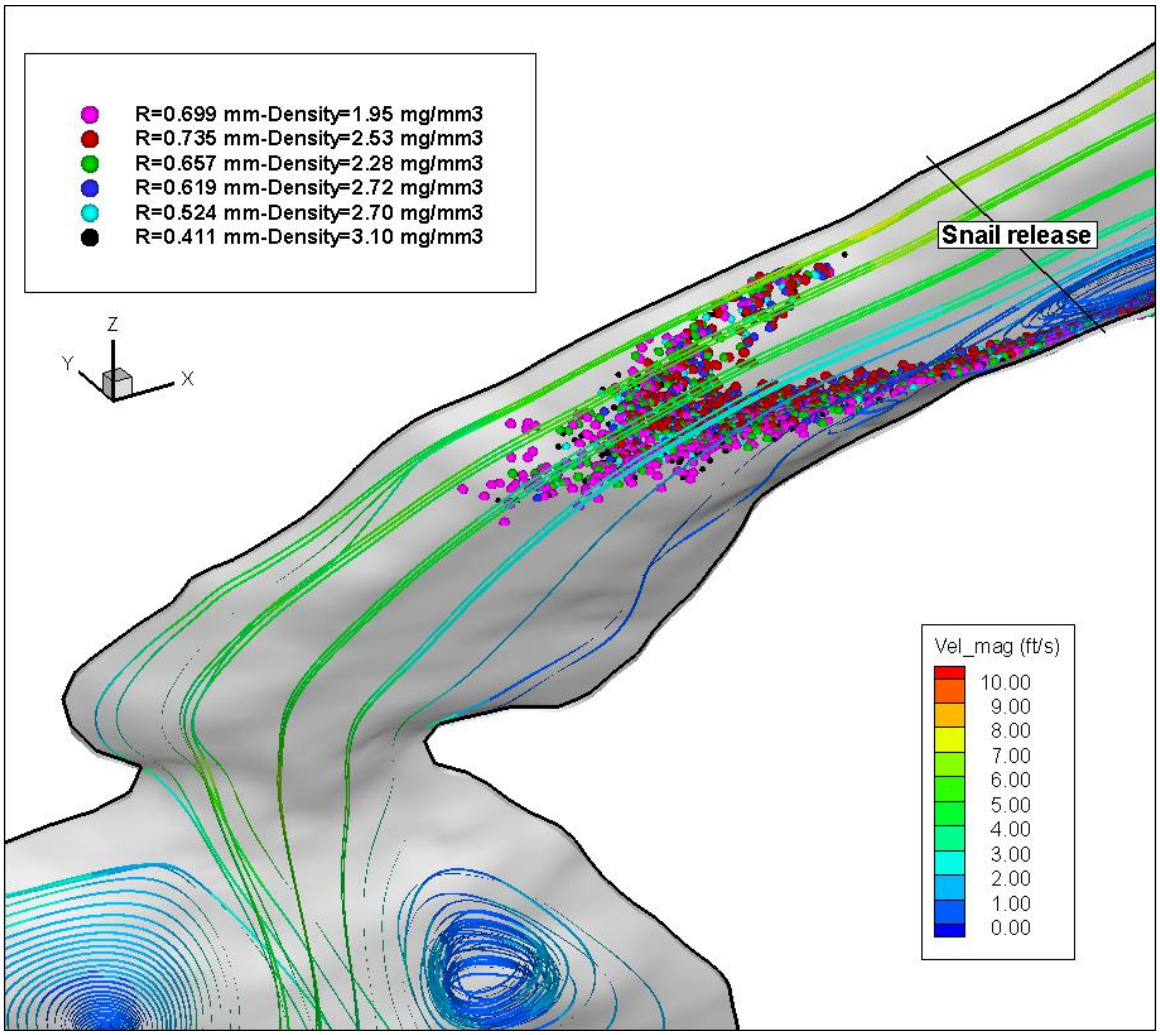

Figure 5-17: Streamlines colored by velocity magnitude with snails' distribution near the particle deposited region for low flow condition. Particles colored and scaled by size

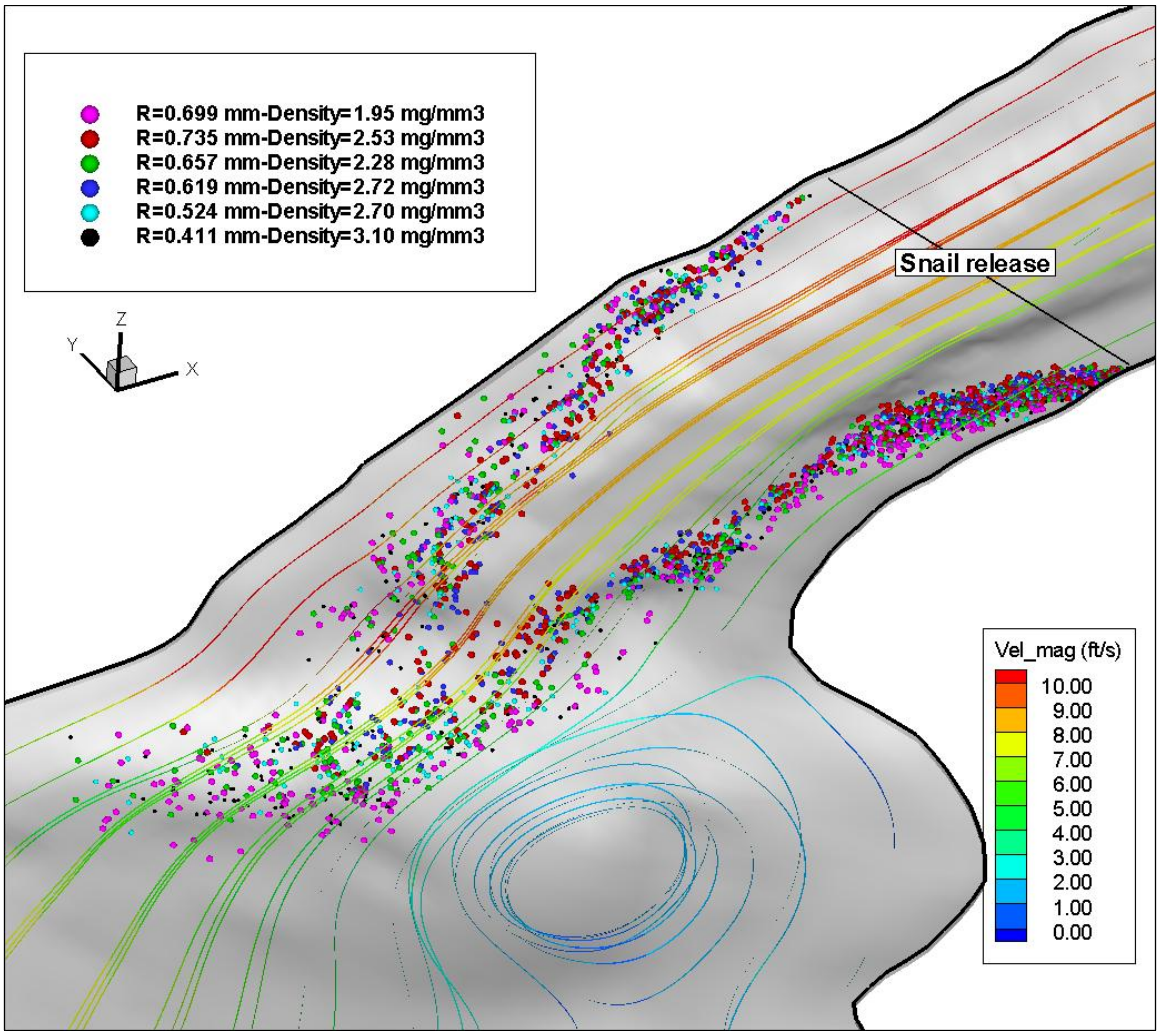

Figure 5-18: Streamlines colored by velocity magnitude with snails' distribution near the particle deposited region for high flow condition. Particles colored and scaled by size

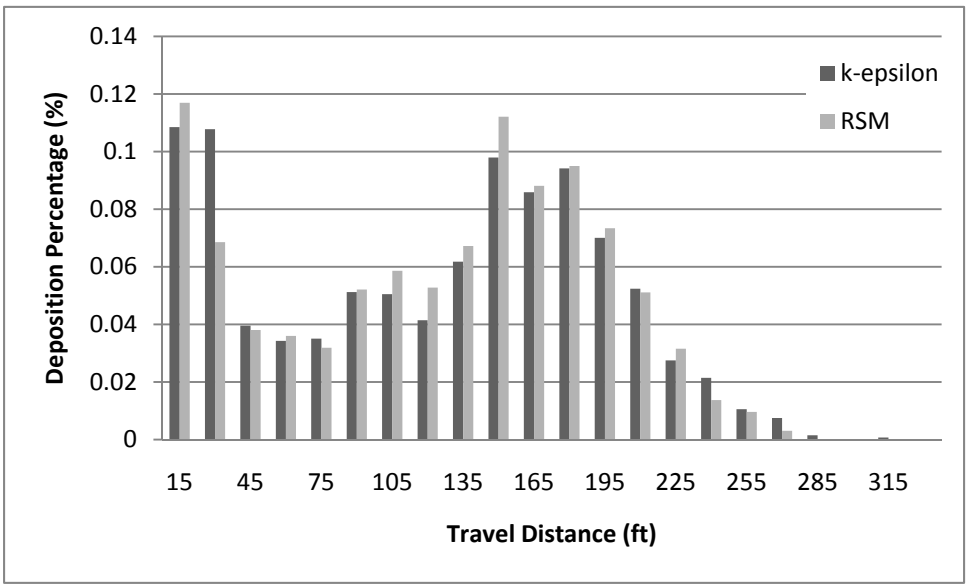

Figure 5-19: Histograms for snails with k-epsilon and RSM for low flow condition

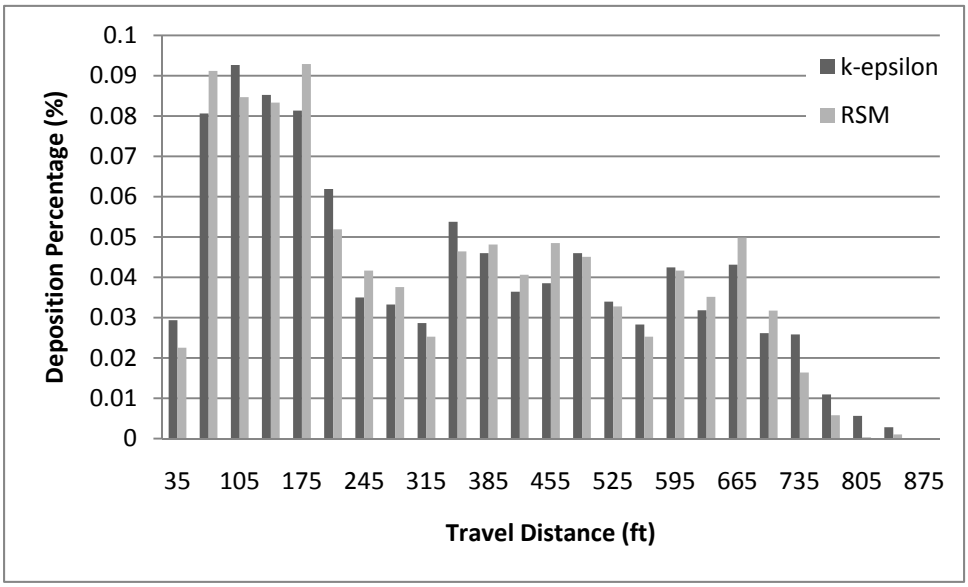

Figure 5-20 Histograms for snails with k-epsilon and RSM for high flow condition

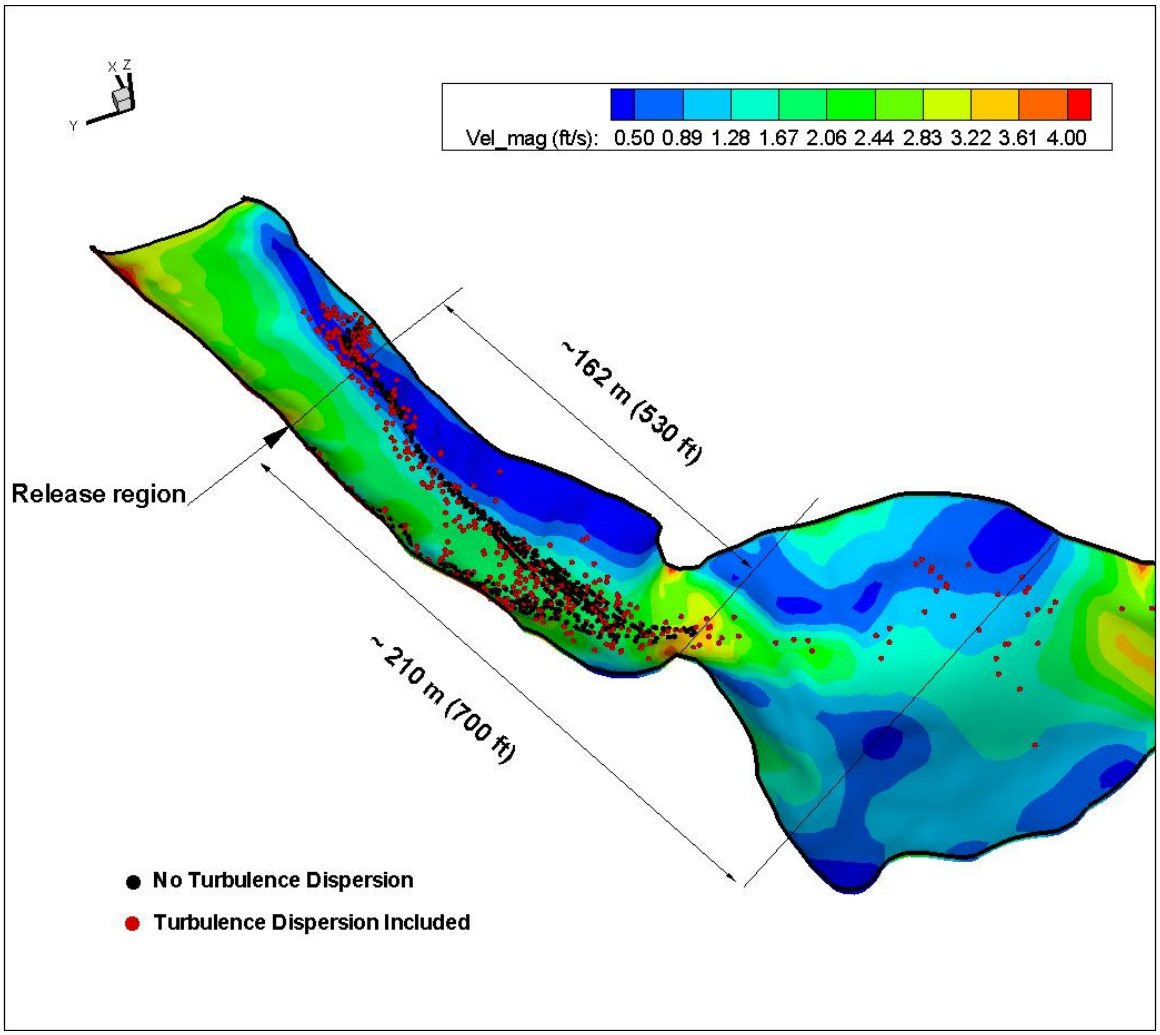

Figure 5-21: Spatial distributions of fish eggs for low flow condition. Red particle represented with RWM and black particle represented without RWM

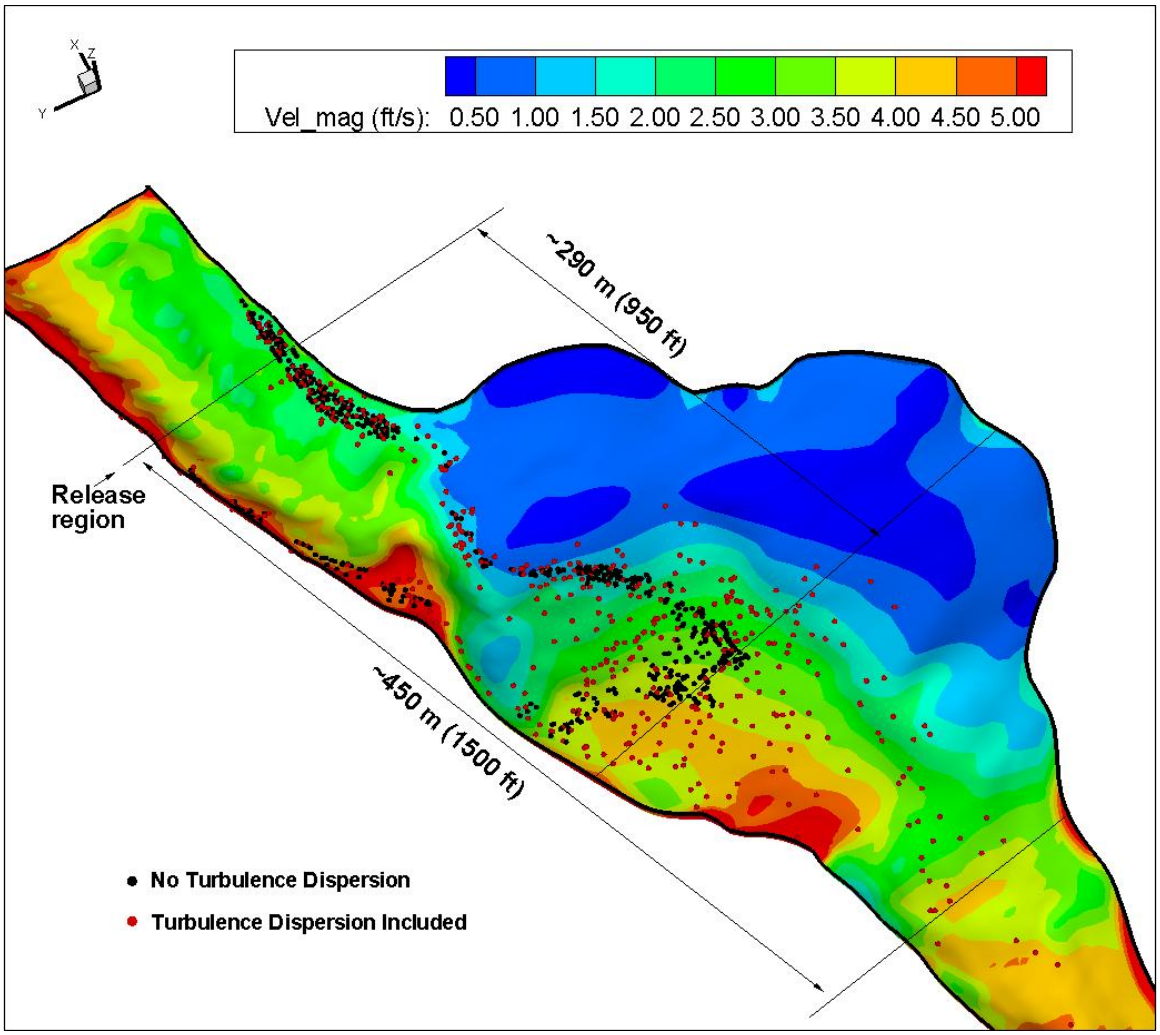

Figure 5-22: Spatial distributions of fish eggs for high flow condition. Red particle represented with RWM and black particle represented without RWM

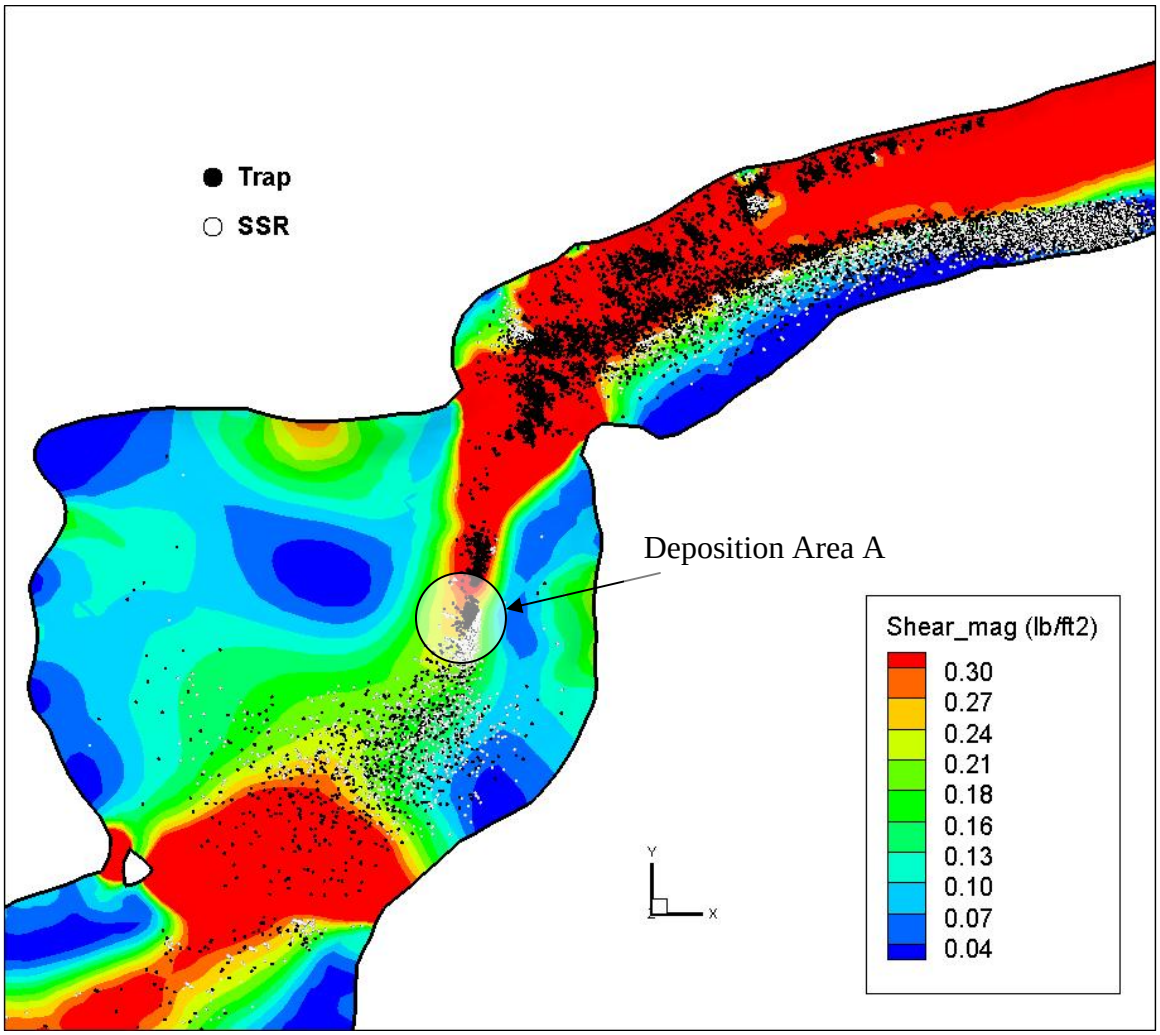

Figure 5-23: Spatial distributions of fish eggs with trap and SSR boundary condition for low flow condition. Contours color by bed shear stress

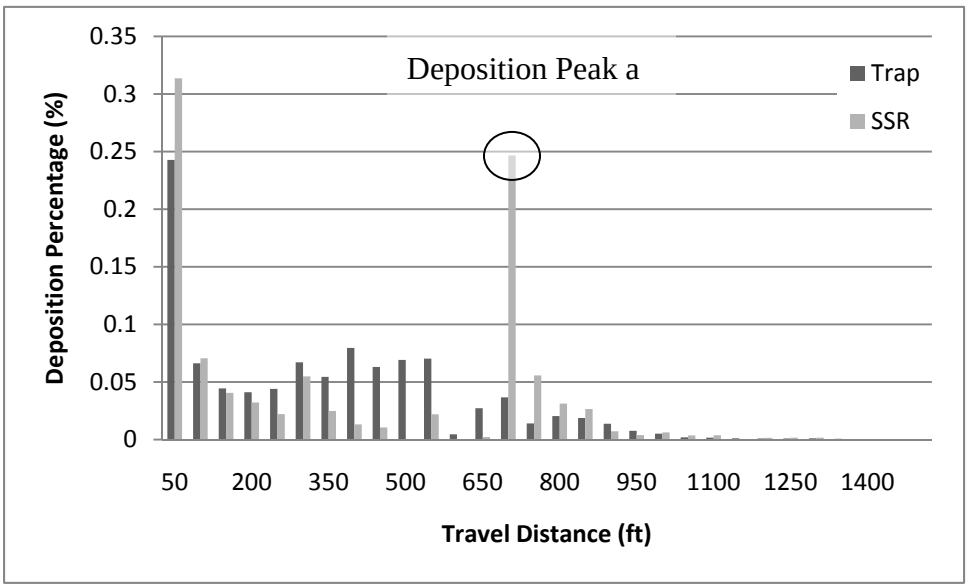

Figure 5-24: Histograms for fish eggs with trap and SSR boundary condition for low flow condition

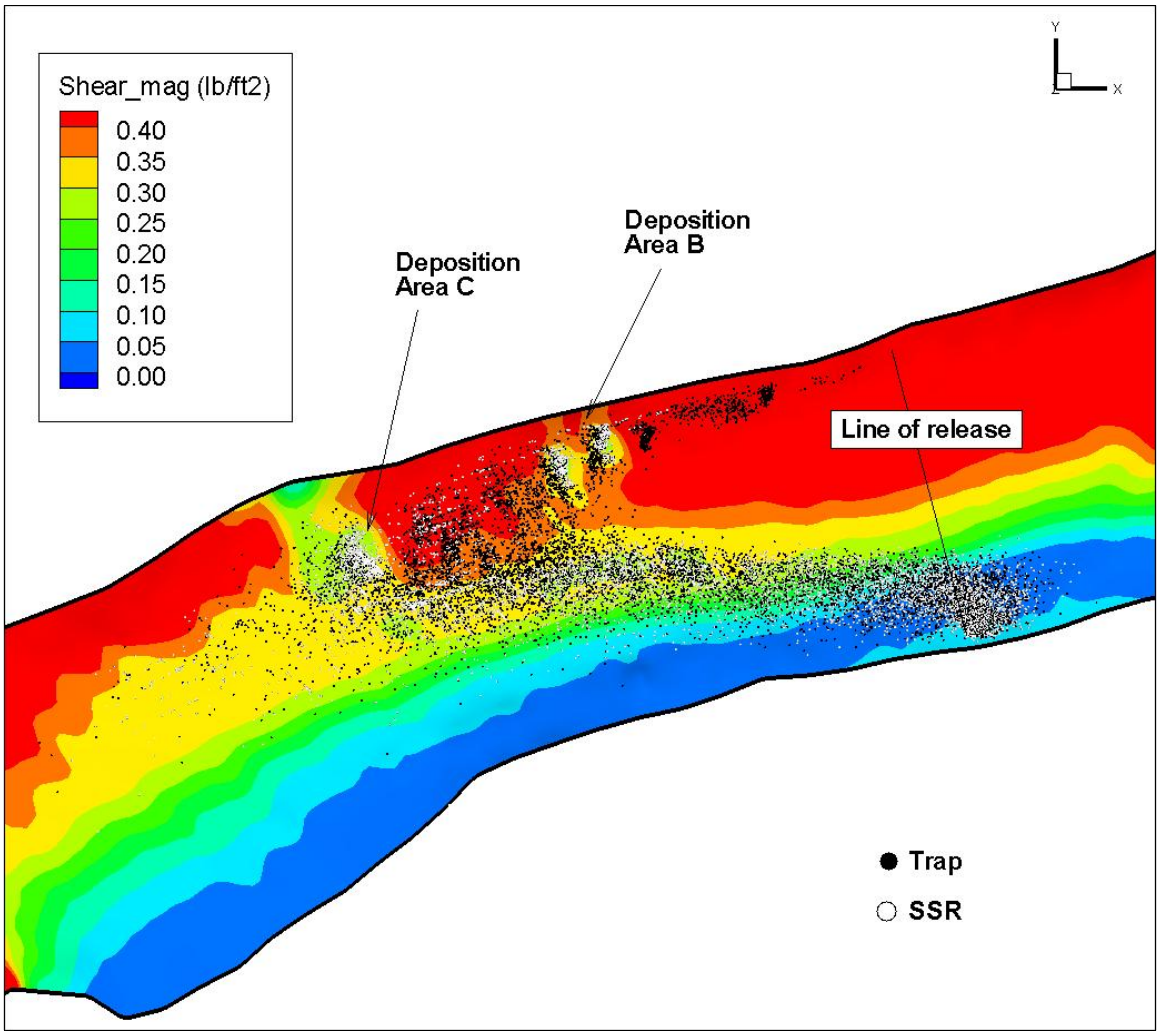

Figure 5-25: Spatial distributions of snails with trap and SSR boundary condition for low flow condition. Contours color by bed shear stress

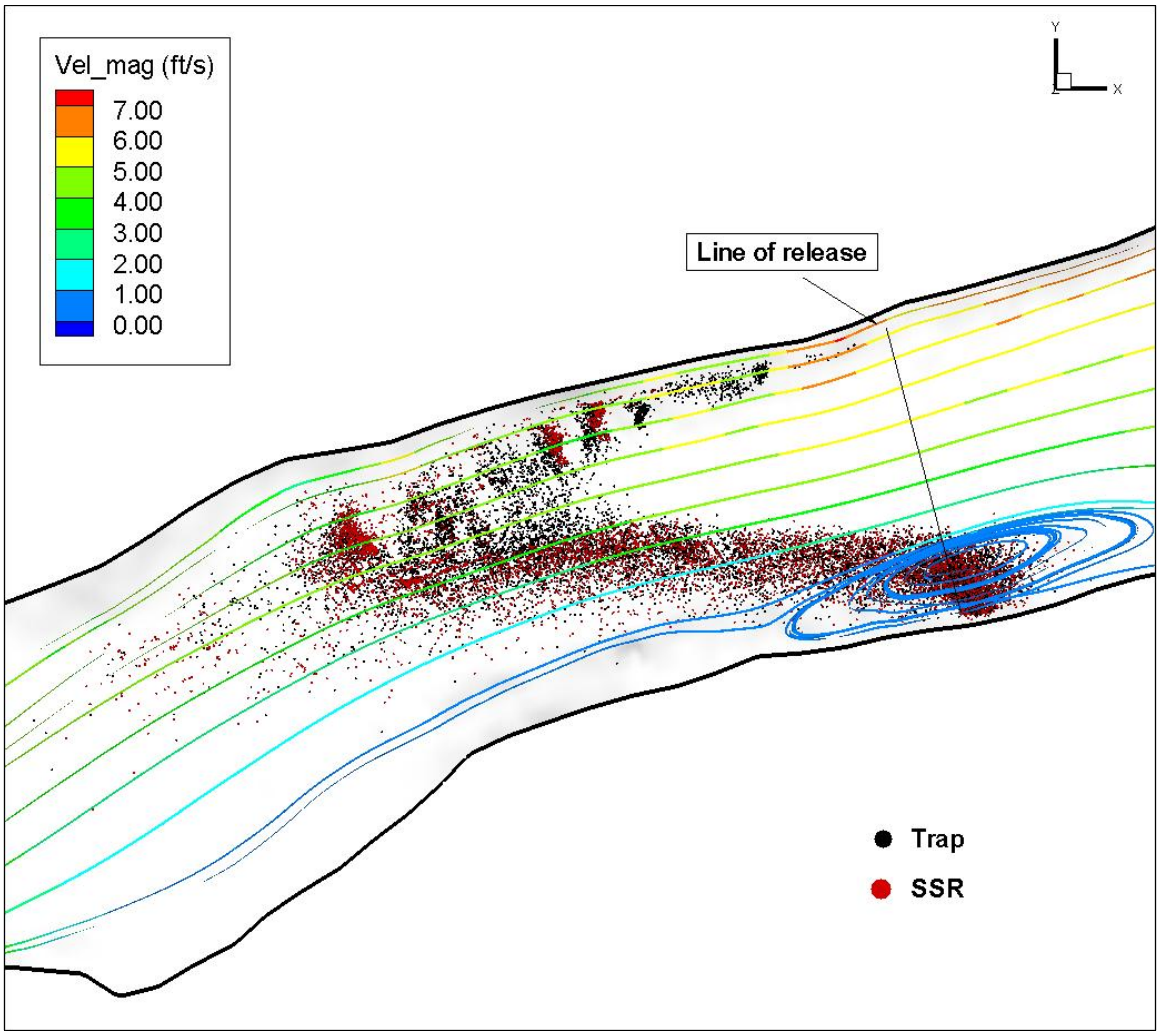

Figure 5-26: Streamlines colored by velocity magnitude with snail distributions near the particle deposited region for low flow condition. Particles colored by different boundary conditions

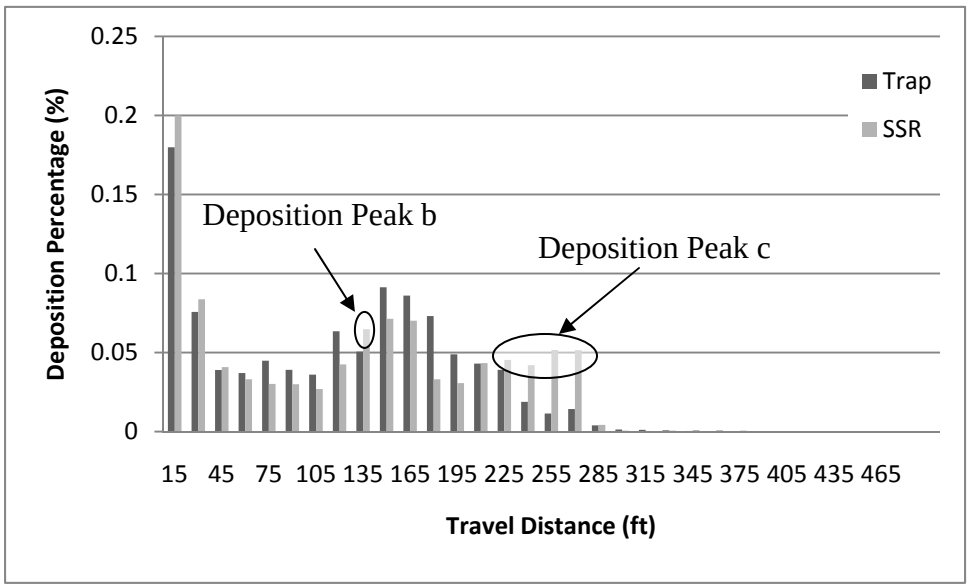

Figure 5-27: Histograms for snails with trap and SSR boundary condition for low flow condition

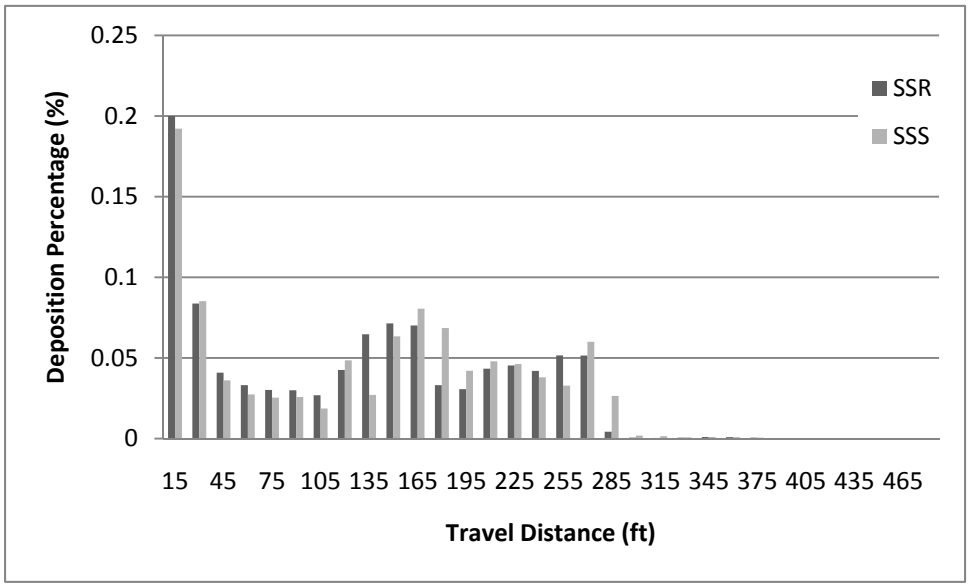

Figure 5-28: Histograms for snails with SSR and SSS boundary condition for low flow condition

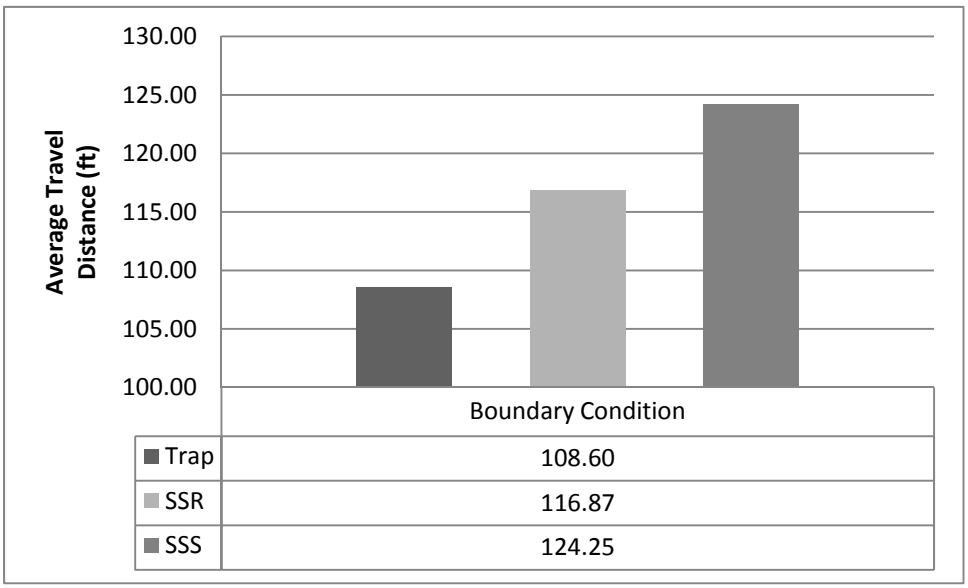

Figure 5-29: Average travel distance for snails with SSR and SSS boundary condition for low flow condition

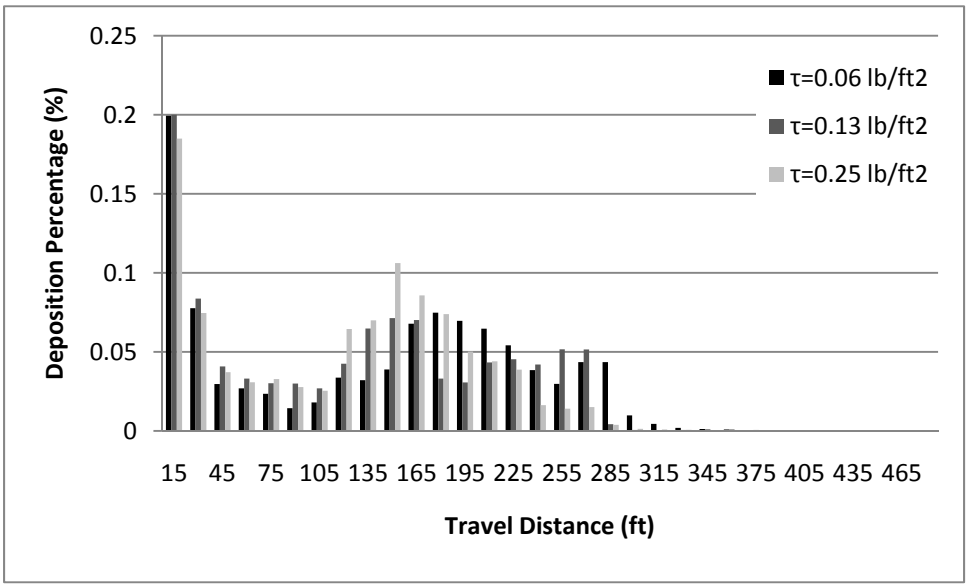

Figure 5-30: Histograms for snails with Critical Shear Stress 0.06, 0.13 and 0.25 lb/ft^2 for low flow condition

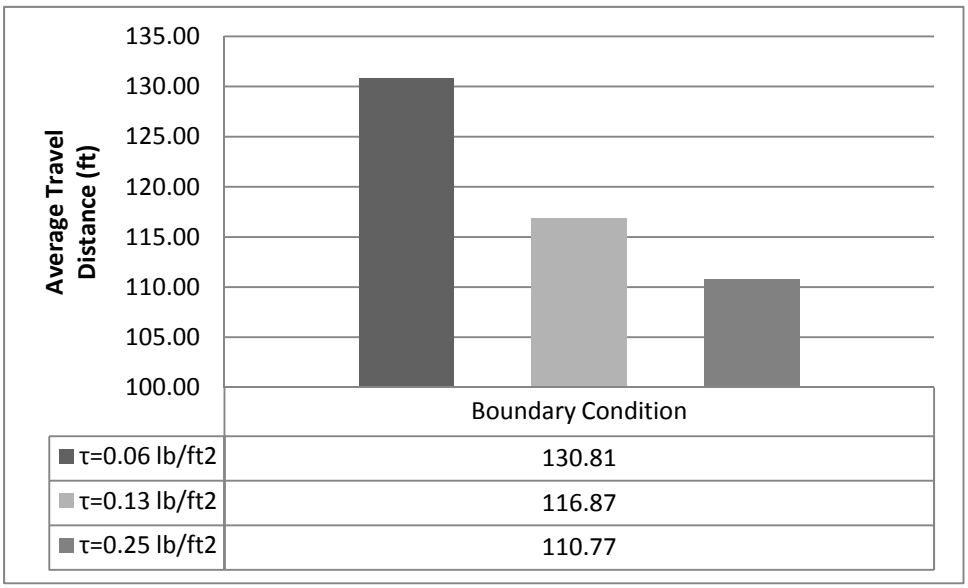

Figure 5-31: Average travel distance for snails with Critical Shear Stress 0.06, 0.13 and 0.25 lb/ft^2 for low flow condition

CHAPTER VI

SUMMARY AND RECOMMENDATIONS FOR FUTURE RESEARCH

6.1 Summary

A 3D CFD Euler-Lagrange model was developed to study hydrodynamics and aquatic organism distributions for average and 100 year flow conditions for a reach of the Mid-Snake River.

Flow field data from two distinct turbulence models were used to study model effects on aquatic organism distribution predictions. RSM simulation results indicated less overall turbulent viscosity than the k-epsilon model. Particle trajectories and distributions were calculated as a function of turbulence. Shorter average distances traveled were predicted by the RSM than by the k-epsilon model. RSM is considered more accurate in predicting particle trajectories and distributions over a river reach.

Interactions between White Sturgeon eggs/Bliss Rapids snails and river beds were studied and incorporated into the model. Previous sedimentation studies utilized boundary conditions based on critical bed shear stress to control particle deposition. Criteria for determining eventual deposition in those cases were directly related to a threshold critical value. A particle was trapped, and trajectory calculations terminated, if the local bed shear stress falls below the critical bed shear stress. If not, the particle was reflected back into the flow. Particles were not able to resuspend after being trapped. Laboratory and field observations of the sedimentation process suggest that deposition to be relatively random when local shear stresses are near the critical value. Turbulence can resuspend particles into the flow after their initial deposit. New boundary conditions were implemented, with a linear relationship incorporate local shear stress and deposition percentage, to account for this phenomenon. Particles deposited proportional to the local shear stress can be brought back into the flow after deposition. Results show the new boundary conditions redistribute particles with a high deposition percentage in low shear

stress regions and vice versa. Particles under this condition travel farther than those modeled by the traditional trap condition due to their capacity to be reflected back into the flow field after first contact with the river bed if local flow velocities are sufficiently high.

Sensitivity to the determined critical bed shear stress value was subsequently studied. Results show spatial distribution to be sensitive to the selected critical bed shear stress value. An average of 8.7% difference in travel distance was obtained by doubling and halving the selected critical shear stress. Further experimental data for White Sturgeon eggs and Bliss Rapids snails is needed to complete and validate this new proposed boundary condition.

The CFD model presented here can be used as predictive tool permitting evaluation of the effects of Bliss Dam operational conditions on Bliss Dam aquatic organism distributions.

6.2 Recommendations for Future Work

Recommendations for enhancing the present work are discussed in this section.

- Further research is required to identify relevant parameter values and relationships for SSR and SSS boundary conditions.
- Numerical model validation for this study can be achieved by implementing a discrete phase model with the new boundary conditions on a domain with known particle spatial distribution information.
- Relationships between aquatic organism depositions and local shear stresses should be determined using fish egg and snail deposition data obtained from experiments.
- Variation of aquatic organism release regions and distributions over the river reach should be used to analyze their influences to the final settling area.

- Additional flow conditions should be used to study distributions under different spawning season parameters.

REFERENCES

Adamsson, A., Stovin, V., and Bergdahl, L. (2003). "Bed Shear Stress Boundary Condition for Storage Tank Sedimentation." *J. Envi. Eng*., 129(7), 651-658.

Anderson, J. D. (1996). "Basic philosophy of CFD." In J. F. Wendt (Ed.), *Computational Fluid Dynamics: An Introduction* (2nd ed.). Berlin,, Heidelberg: Springer-Verlag.

Bakhtyar, R., Yeganeh-Bakhtiary, A., Barry, D. A., & Ghaheri, A. (2009). "Two-phase hydrodynamic and sediment transport modeling." *Water Resources* (In Press).

Barton, G.J., McDonald, R.R., Nelson, J.M., Donato, M., Van Metre, P., and Mahler, B., (2006). "Altered dynamics of Kootenai River white sturgeon spawning habitat and flow modeling." CD-ROM Proceedings of the Joint 8th Federal Interagency Sedimentation and 3rd Federal Interagency Hydrologic Modeling Conference, Reno, Nevada, April 2-6, 2006, ISBN 0-9779007-1-1.

Barton, G.J., McDonald, R.R., Nelson, J.M., and Dinehart, R.L. (2005) "Simulation of flow and sediment mobility using a multidimensional flow model for the white sturgeon critical-habitat reach, Kootenai River near Bonners Ferry, Idaho," U.S. Geological Survey Scientific Investigations Report, 100 pp.

Bates, D. (2008, March 19). Mid-Snake River Spring and Tributary Study Plan-Bliss Rapids Snail . Retrieved April 17, 2009

Bonneville Power Administration. (2009). *Power benefits of the lower Snake River dams - FACT SHEET*. Retrieved May 17, 2009

Booker, D. J., Dunbar, M. J., & Ibbotson, A. (2004). "Predicting juvenile salmonid drift-feeding habitat quality using a three-dimensional hydraulic-bioenergetic model." *Ecological Modelling*, 177, 157-177.

Clark, W. H., M. A. Stephenson, B. M. Bean, and A. J. Foster. (2007). "Mid-Snake River snail sampling study year 2006 progress report: settlement agreement information needs." Idaho Power Company, Boise, ID. 52 p., plus 19 appendices.

Cochnauer, T.G., Lukens, J.R. and Partridge, F.E., (1985). "Status of white sturgeon, Acipenser transmontanus, in Idaho." In: Binkowski, F.P. and Doroshov, S.I., Editors, 1985. North American Sturgeons, Dr W. Junk, Publishers, Dordrecht, The Netherlands, pp. 127–133.

Daraio, J. A., Morales-Chaves, Y., Mynett, A., & Weber, L. (2006). "Ecohydraulics in the Mississippi River: Freshwater Mussel Dynamics Model." Paper presented at 3rd Biennial meeting of the nternational Environmental Modelling and Software Society, Burlington, Vermont.

Drew D.A. and Passman S.L. (1998). *Theory of Multicomponent fluids, Applied Mathematical Sciences* volume 135, Springer, New York

Dufresne, M., Vazquez, J., Terfous, A., Ghenaim, A., and Poulet, J. B. (2008). "Experimental Investigation and CFD Modelling of Flow, Sedimentation, and Solids Separation in a Combined Sewer Detention Tank." *J. Comp. Fluid*, 38, 1042-1049.

FLUENT (2006). Fluent user's guide-version 6.3, Fluenr Inc., Lebanon, NH.

German, J., & Kant, H. (1998). "FEM-analys av strömningsförhållanden i en dagvattendamm (FEM-analysis of the hydraulic conditions in a stormwater detention pond)." *Vatten*, No. 54, 183-190.

Goodwin, Andrew R., John M. Nestler, James J. Anderson, Larry J. Weber et al.. (2006), "Forecasting 3-D fish movement behavior using a Eulerian-Lagrangian-agent method (ELAM)." *Ecological Modelling*, 192, 197-223.

Groll, R. and Tropea, C. (2005), "On Euler/Euler Modeling of Turbulent Particle Diffusion in Dispersed Two-Phase Flows" Paper presented at ERCOFTAC International Symposium on Engineering Turbulence Modelling and Measurements(ETMM6), Sardinia, Italy.

Haider A. and Levenspiel O. (1989). "Drag Coefficient and Terminal Velocity of Spherical and Nonspherical Particles." *Powder Technology*, 58, 63-70.

Ingham, D.B. and Ma L (2005), "Fundamental equations for CFD river flow simulations." In: Bates PD, Lane SN, Ferguson RI (eds) *Computational fluid dynamics. Applications in environmental hydraulics*. Wiley, Chichester, p 534 ISBN 978-0-470-84359-8

Jager, H. I., Lepla, K., Chandler, J., Bates, P., & Van Winkle, W. (2000). Population viability analysis of white sturgeon and other riverine fishes. *Environmental Science & Policy*, 3(1), 483-489.

Jakobsen, H. A., Lindborg, H., & Dorao, C. A. (2005). :Modeling of Bubble Column Reactors: Progress and Limitations." *Ind. Eng. Chem*, 44, 5107-5151.

Kang, H., & Choi, S. (2006). "Turbulence modeling of compound open-channel flows with and without vegetation on the floodplain using the Reynolds stress model." *Advances in Water Resources*, 29, 1650-1664.

Larinier, M. (2000). Dams and Fish Migration. World Commission on Dams, *26*.

Launder, B.E., Reece, G.J. and Rodi, W. (1975). "Progress in the Development of a Reynolds-Stress Turbulence Closure." *J. Fluid Mech.*, 68(3), 537-566.

Ma, L., Ashworth, P. J., Best, J. L., Elliott, L., Ingham, D. B., & Whitcombe, L. J. (2002). "Computational f luid dynamics and the physical modelling of an upland urban river." *Geomorphology*, 44, 375-391.

Meselhe, E.A. and Odgaard, A.J. (1998), "3D Numerical Flow Model for Fish Diversion Studies at Wanapum Dam", *Journal of Hydraulic Engineering*, December 1998, pp. 1203-1214.

Modenesi, K., Furlan, L. T., Tomaz, E., Guirardello, R., & Núnez, J. R. (2004). "A CFD model for pollutant dispersion in rivers." *Braz. J. Chem. Eng*, 21(4), 557-568.

Morsi, S. A., and Alexander, A. J. (1972). "An Investigation of Particle Trajectories in Two- Phase Flow Systems" Journal Fluid Mech., 55(2), 193-208.

Paragamian, V. L., Kruse, G., & Wakkinen, V. (2001). "Spawning Habitat of Kootenai River White Sturgeon, Post-Libby Dam." *North American Journal of Fisheries Management*, 21, 22-23.

Richard, D. C. (2004). "Competition between the threatened Bliss Rapids snail, Taylorconcha serpenticola (Hershler et al.) and the invasive, aquatic snail Potamopyrgus antipodarum (Gray)." Doctoral dissertation. Montana State University. Bozeman. 156. pages.

Stovin, V. R. (1996). "The Prediction of Sediment Deposition in Storage Chambers Based on Laboratory Observations and Numerical Simulation." PhD thesis, Univ. of Sheffield, UK.

Stovin, V. R., and Saul, A. J. (2000). "Computational Fluid Dynamics and the Design of Sewage Storage Chambers." *J. CIWEM*, 14(2), 103-110.

Suzzi, D., Radl, S., & Khinast, J. (2009). "Validation of Euler-Euler and Euler-Lagrange Approaches in the Simulation of Bubble Columns." Paper presented at the 9th International Conference on Chemical & Process Engineering, Rome, Italy.

The Idaho Water Resource Board. (1996). *Idaho State Water Plan.* Boise, Idaho.

Turan, C., Politano, M. S., Carrica, P. M., & Weber, L. (2007). "Water Entrainment due to Spillway Surface Jets." International Journal of Computational Fluid Dynamics, 21(3-4), 137-153.

Vanoni, V. A. (1977). Sedimentation Engineering, American Society of Civil Engineers, New York, NY.

Wright, N. G., Crossley, A. J., Morvan, H. P., & Stoesser, T. (2004). "Detailed validation of CFD for flows in straight channels." River Flow, 2, 1041-1048.

Wyland , J. (2008, September 15). Idaho Power Company Protects the Lifeblood of the State. V1 Magazine.

Zhou, Q. and Leschziner, M. A., (1991). Technical Report, 8th Turbulent Shear Flows Symp., Munch.